# Exploration and Mapping of Spatio-Temporal Pedestrian Flow Patterns for Mobile Robots

UNIVERSITY OF
LINCOLN

Sergio Molina Mellado

School of Computer Science

College of Science

University of Lincoln

A thesis submitted for the degree of
Doctor of Philosophy

*Supervisor* Prof. Tom Duckett
*Second Supervisor* Dr. Grzegorz Cielniak

March 2021

Failure is an option here. If things are not failing, you are not innovating enough.

---

Elon Musk

**Declaration**

The work in this Ph.D. thesis is based on research carried out at the Lincoln Centre for Autonomous Systems at the University of Lincoln in United Kingdom. No part of this thesis has been submitted elsewhere for any other degree or qualification and it is all my own work unless referenced to the contrary in the text.

**Ethical considerations**

The work presented in this thesis comply with the Ethical Approval Forms EA1 and EA2 from the University of Lincoln submitted and approved at the beginning of the research activities.

# Abstract

Socially compliant robot navigation is one of the key aspects for long-term acceptance of mobile robots in human-populated environments. One of the current barriers for this acceptance is that many navigation methods are based only on reactive behaviours, which can lead to frequent re-plannings, causing an erratic or aggressive robot behaviour. Instead, giving the ability to model and predict in advance how the people are likely to behave, from a long-term perspective, is an important enabler for safe and efficient navigation. For example, a robot may use its knowledge of the expected human motion to go with the main direction of flow to minimise the possibility of collisions or trajectory re-plannings.

In order to provide robots with knowledge of the expected activity patterns of people at different places and times, the first main contribution of this thesis is the introduction of a Spatio-Temporal Flow map (STeF-map). This is a time-dependent probabilistic map able to model and predict the flow patterns of people in the environment. The proposed representation models the likelihood of motion directions on a grid-based map by a set of harmonic functions, which efficiently capture long-term variations of crowd movements over time. The experimental evaluation shows that the proposed model enables a better human motion prediction than spatial-only approaches and an increased capacity for socially compliant robot navigation.

Obtaining this knowledge from a mobile robot platform is, however, not a trivial task, as usually they can only observe a fraction of the environment at a time, while the activity patterns of people may also change at different times. Therefore, the second main contribution is the investigation of a new methodology for mobile robot exploration to maximise the knowledge of human activity patterns, by deciding where and when to collect observations based on an exploration policy driven by the entropy levels in a spatio-temporal map. The evaluation is performed by simulating mobile robot exploration using real sensory data from three long-term pedestrian datasets, and the results show that for certain scenarios, the proposed exploration

system can learn STeF-maps more quickly and better predict the flow patterns than uninformed strategies.

# Acknowledgements

I still remember when my dad started to build, during the time when building things by issues was popular, the first robot I was in touch with. I am not very sure, but I believe the main purpose of that robot was to follow a line on the floor. I was around 10 year old, and that thing was amazing for me. I remember keep asking my dad when we would be able to continue with the robot building. At that time and still now, I don't really get building thing by issues, I'm too impatient. I think we never fully completed the building, but given my persistence, I was lucky to be given as presents in the following years a walking robot, the popular LEGO Mindstorms and the Robonova-I. Robots that probably have taken me to the thesis that I am presenting. For all this and much more, I want to thank above all my family for being always next to me, helping with my decisions, whatever I do and wherever I go.

I would like to also thank my friends from the *Jacksons*, *Llamalencs* and *Cuajas* for making me feel like I never left in all the trips I have done to Reus. And the new friends from Lincoln for the new adventures lived.

I want to thank Prof. Tom Duckett, Dr. Grzegorz Cielniak and Prof. Marc Hanheide for guiding me during my doctorate, opening new doors and new possibilities, and all the colleagues from L-CAS to make the work in the office more fun and entertaining.

Finally I want to make a special mention to Emma, to be with me the last three years listening to my bad jokes, sharing experiences, trips and making difficult moments more easy to overcome.

This thesis was supported within H2020-ICT by the EC under grant number 732737 (ILIAD)

# Català - Agraïments

Encara me'n recordo de quan el meu pare va començar a fer, durant l'època en la qual fer les coses per fascicles estava de moda, el que seria el meu primer contacte amb un robot. No ho recordo massa bé però crec que la funció principal d'aquell robot era la de seguir una línia a terra. Jo, petit, probablement al voltant dels deu anys, aquella cosa em fascinava, i constantment li deia al meu pare que quan podíem continuar amb la construcció del robot. En aquella època i encara ara, el tema dels fascicles no li veig massa sentit, soc massa impacient. Crec que no el vam acabar de construir mai, però donada la meva insistència vaig tenir la sort que em regalessin durant els següents anys un robot caminador, el conegut LEGO Mindstorms i el Robonova-I. Robots, sense els quals probablement no estaria presentant aquesta tesi. Per això i molt més, vull donar les gràcies per damunt de tot a la meva família per sempre estar al meu costat, ajudant-me en totes les meves decisions, fes el que fes i anés on anés.

M'agradaria també agrair a tots els meus amics dels *Jacksons*, *Llamalencs* i *Cuajas* per fer-me sentir en els meus viatges i estades a Reus com si no hagués marxat mai. I als nous companys de Lincoln, per les noves aventures viscudes.

Vull donar les gràcies al Prof. Tom Duckett, Dr. Grzegorz Cielniak i Prof. Marc Hanheide per guiar-me durant els meus estudis del doctorat, obrint-me noves portes i possibilitats. I als companys del L-CAS per fer el treball a l'oficina més divertit i entretingut.

I finalment vull fer una menció especial a l'Emma, per acompanyar-me durant els últims tres anys escoltant les meves bromes dolentes, compartint experiencies, viatges i fent que moments difícils siguin més fàcils.

# Table of Contents

# List of Figures

# List of Tables

# Acronyms

**CLiFF-map** Circular Linear Flow Field map. 64, 74, 75, 79, 80, 83

**DGM** Directional Grid Map. 64, 69, 74, 75, 79

**EM** Expectation Maximisation. 69

**FreMEn** Frequency Map Enhancement. 40, 41

**GNT** Gap Navigation Tree. 23

**LSTM** Long Short-term Memory. 14, 65, 71, 74, 76, 79

**MDP** Markov Decision Problem. 16, 24

**RMSE** Root Mean Squared Error. 78

**SSC** Social Service Cost. 83

**STeF-map** Spatio-Temporal Flow map. 4, 5, 7, 17, 38, 47, 48, 50, 58, 62–64, 74, 75, 77–80, 83, 86, 87, 91, 99–101, 109–111, 113, 114

**SWGMM** Semi-Wrapped Gaussian Mixture model. 71

**SWND** Semi-Wrapped normal distribution. 70

**WHyTe** Warped Hyper-time Space. 64, 74, 76, 78–80, 83

# Chapter 1

# Introduction

## 1.1 Context

Robot technology has improved tremendously over the last decade and continues to improve further. Consequently, autonomous robot systems have been able to operate in increasingly complex environments and for longer periods of time. This includes, for example, the introduction of mobile robots into environments shared with humans, such as hotels, warehouse or shopping centres, to operate as guides and human collaborators, and in tasks such as surveillance and patrolling. Considering these scenarios described, the mobile robot should operate with a certain degree of autonomy, since one of the aims is to actually use a robot instead of a person in tasks that are more repetitive or "dirty, dull and dangerous". However, achieving reliable robot long-term autonomy in human-shared scenarios leads to many challenges arising from the different robotic system components, such as localisation, navigation, mapping, knowledge acquisition and representation (Kunze et al., 2018). Many of these challenges come from the fact that in long-term operation, the introduction of the time dimension in the system plays a key role.

## 1.2 Motivation

As pointed out in Kucner, 2018, navigation around people is one of the key aspects for long-term acceptance of mobile robots in human-populated environments. One of the current barriers for this acceptance is that many navigation methods are based only on reactive behaviours, where the robot tracks the people in its vicinity and replans its trajectory accordingly. The work in Sun et al., 2018 reported that the errors of the state-of-the-art methods for prediction of human motion exceed 0.4

m for predictions horizons of 1 s, which can lead to frequent re-planning, causing an erratic or aggressive robot behaviour. Instead, giving the robot the ability to model and predict in advance how the people are likely to behave from a long-term perspective, is an important factor for safer and more efficient navigation (Jumel et al., 2017; Palmieri et al., 2017).

Works like Senanayake et al., 2018; Kucner et al., 2017 aim to model the pedestrian motion in the environment. But despite being focused on modelling human motion they do not take into account the fact that the motion directions can fluctuate over time, resulting in a potential loss in model accuracy in the long-term and, as a consequence, less socially compliant robot navigation. We, people, tend to follow certain routines in our lives. We wake up more or less at the same time, we commute to work at the same time (Figure 1.1), we have two days off a week (usually Saturday and Sunday), we have holidays at a similar time every year, etc. So, understanding the existence of these patterns due to nature of the human activities, it is possible to encode temporal fluctuations in dynamic environments to improve the robustness of robotic capabilities like mapping, localisation or navigation (Krajník et al., 2017).

Figure 1.1: People commuting in Canary Wharf (London). Photo from Manning, 2018.

However, obtaining an applicable spatio-temporal model of the environment is not a

straightforward task from a mobile robot's point-of-view, due to visibility and time constraints. The robot's view is constrained by sensor limitations and occlusions, and the robot usually has to perform other tasks, limiting the time available for data gathering. Hence, a mobile robot requires an exploratory strategy, which comprises a planned sequence of data observations with the primary aim of building a model of an environment to overcome the aforementioned constraints. Traditional exploration strategies assume a static scenario, i.e. the states measured do not change over time. Their aim is to build a spatial model that covers the operational environment as quickly as possible. If the flow of people remains constant (static in time), this would mean visiting the locations which have never been visited before. However, when modelling human motion, the environment tends to change over time, e.g. with different flow patterns at different times of the day (Molina et al., 2018). Thus, apart from deciding where to explore, the exploration strategy must also consider the temporal dimension (i.e. when to explore) in order to obtain the maximum information from each observation. By learning and refining its knowledge of human motion patterns over time, the robot should be able to operate more reliably in challenging environments shared with humans.

Taking into account the aforementioned concepts, the questions that this thesis tries to answer are:

- How to incorporate long-term temporal dependencies in human motion behaviour?
- How to efficiently build and refine a spatio-temporal human motion model taking into account the constraints present in a mobile robot?

### 1.2.1 Case scenario

Let us take for example the case of a pallet truck or forklift, like the ones shown in Figure 1.2, operating in a warehouse environment. By learning typical motion patterns in the environment where the system is deployed, it can better blend in with current operations. For example, if the system observes that a certain aisle is often traversed by other operators from north to south at a particular time of

day or during a specific warehouse operation, the motion planner may prefer to use the neighbouring aisle for the pallet truck, at least when it needs to go in the opposite direction of the main stream. A further application would be to enable the robots to anticipate and actively avoid areas of high traffic learned from long-term experience as a pro-active approach to safety. Information about typical motion patterns (the quantity or frequency of changes, and the types of motions) can also help the localisation system: knowing that a certain area is very dynamic, the sensor models used for localisation and mapping can be updated accordingly.

Figure 1.2: Pallet trucks in the National Centre for Food Manufacturing in Holbeach, United Kingdom (Left). Forklift operating in the Orkla facilities in Örebro, Sweden (Right).

## 1.3 Contributions

This sections lists the novel contributions to the field of spatio-temporal modelling and exploration of human motion. They are the following:

- a spatio-temporal flow map (STeF-map) representation, which models the likelihood of motion direction on a grid-based map by a set of harmonic functions that capture long-term changes of crowd movements over time;
- a metric to compare spatio-temporal human motion models with the ground truth;
- a comparison between STeF-map and other state-of-the-art human motion models;

- a new methodology for mobile robot exploration to maximise the knowledge of human activity patterns, by deciding where and when to collect observations based on cell entropy levels;
- a study comparing multiple spatio-temporal robotic exploration policies, evaluating their performance in building and refining a time-dependent probabilistic model of human activity patterns; and
- two new long-term datasets containing 14 and 22 days of observed pedestrian motions.

## 1.4 Publications

Parts of this thesis have previously appeared in the following publications. In all the articles for which I am the first author, I have performed the relevant implementation and testing, as well as the major part of analysing and reporting the obtained results.

- **Molina, S.**, Cielniak, G., Krajnik, T., Duckett, T., (2017), Modelling and predicting rhythmic flow patterns in dynamic environments, in 'UK-RAS Network Conference 2017'.

  This extended abstract presents a proof of concept of the spatio-temporal model described in Chapter 4.

- **Molina, S.**, Cielniak, G., Krajnik, T., Duckett, T., (2018), Modelling and predicting rhythmic flow patterns in dynamic environments, in 'Annual Conference Towards Autonomous Robotic Systems (*TAROS*)', pages 135-146.

  This conference paper describes the STeF-map representation extending the concept in Molina et al., 2017 and introduces the first of the two long-term pedestrian datasets recorded (dataset described in Chapter 3). This work corresponds to Chapter 4 in this thesis. However the work carried out in Chapter 4 extends the original in several ways: the description of the model is explained more in depth, a new dataset has been added in the experimental part, the

evaluation section has been further extended with a new methodology and a new evaluation metric is introduced.

- **Molina, S.**, Cielniak, G., Duckett, T., (2019), Go with the flow: Exploration and mapping of pedestrian flow patterns from partial observations, in '2019 International Conference on Robotics and Automation (*ICRA*)', pages 9725-9731.

  This conference paper introduces the spatio-temporal mobile robot exploration framework which is extended in Chapter 6 to overcome certain assumptions and simplifications present in this work.

- **Molina, S.**, Cielniak, G., Duckett, T., (2020), Robotic exploration for learning human motion patterns , in 'submitted to Transactions on Robotics (*T-RO*)'.

  This journal extends the spatio-temporal exploration framework first presented in Molina et al., 2019 and introduces the second of the two long-term pedestrian datasets recorded (dataset described in Chapter 3). This work corresponds to Chapter 6 in the thesis.

- Vintr, T, **Molina, S.**, Senanayake, R., Broughton, G., Yan, Z., Ulrich, J., Kucner, T., Swaminathan, C., Majer, F., Stachova, M ., Lilienthal, A., Krajnik, T., (2019), Time-varying pedestrian flow models for service robots, in '2019 European Conference on Mobile Robots (*ECMR*)', pages 1-7.

  This joint work presents a comparison between state-of-the-art human motion models for predicting future people behaviour. My contribution includes providing the dataset for the comparison, supporting the methodology and evaluation definition, the introduction of the $\chi^2$ evaluation metric, computing the scores for all the compared models with regard to the aforementioned metric and reporting the results. This work corresponds to Section 5.2 in Chapter 5.

- Krajnik, T., Vintr, T., **Molina, S.**, Pulido Fentanes, J., Cielniak, G., Martinez Mozos, O., Broughton, G., Duckett, T., (2019), Warped hypertime rep-

resentations for long-term autonomy of mobile robots, in 'IEEE Robotics and Automation Letters', vol.4, pages 3310-3317.

This journal paper presents a novel method for introducing time into discrete and continuous spatial representation by modelling long-term pseudo-periodic variations of events. My contribution was to provide a pedestrian dataset for one of the experiments and assist in the conceptual idea. This work corresponds to Section 5.1.1 in Chapter 5 where the model is briefly defined.

- Vintr, T., Yan, Z., Eyisoy, K., Kubi, F., Blaha, J., Ulrich, J., Swaminathan, C., **Molina, S.**, Kucner, T., Magnusson, M., Cielniak, G., Faigl, J., Duckett, T., Lilienthal, A., Krajnik, T., (2020), Natural Criteria for Comparison of Pedestrian Flow Forecasting Models, in 'IEEE International Conference on Intelligent Robots and Systems (*IROS*)'.

  This collaboration work introduces a methodology to compare multiple human motion models from a robot navigation social cost perspective. My contribution was to compute the STeF-map model from the data recorded in the location where the experiments were performed. This work corresponds to Section 5.3 in Chapter 5.

- Vintr, T., **Molina, S.**, Senanayake, R., Broughton, G., Yan, Z., Ulrich, J., Kucner, T., Swaminathan, C., Majer, F., Stachova, M ., Lilienthal, A., Krajnik, T., (2019), Spatio-temporal representation of time-varying pedestrian flows, in '2019 *ICRA* Workshop in Long-term Human Motion Prediction'.

  This workshop abstract was mainly aimed to give dissemination of the warped hypertime representation in Krajnik et al., 2019 and the multi-model comparison in Vintr et al., 2019. My contribution was assisting in the writing. This work is not part of the thesis.

- Sun, L., Yan, Z., **Molina, S.**, Hanheide, M., Duckett, T., (2018) 3DOF pedestrian trajectory prediction learned from long-term autonomous mobile robot deployment data, in '2018 IEEE International Conference on Robotics and Automation (*ICRA*)', pages 1-7.

The paper presents a novel 3DOF pedestrian trajectory prediction approach for autonomous mobile service robots. This is based on Temporal 3DOF-Pose Long-Short-Term Memory trained using long-term data from real-world robot deployments and aims to learn context-dependent human activities. My contribution was to elaborate a set of figures to illustrate the data used and some of the results. This paper is not part of the thesis.

# Chapter 2

# Related Work

Typically, in order to allow a robot to autonomously build a model of its operational environment, it is provided with two alternating processes: mapping/modelling, in which the robot integrates the gathered human data into the model, and planning, during which the robot chooses the actions that would best contribute to the model improvement. This combination of the two processes is what is commonly known as an exploration strategy.

Traditional exploration strategies are based on policies that assume the environment to be constant in time; therefore the exploration task concludes when all locations have been explored at least once. However, because the human flows tend to change over time, due to the nature of human activities, visiting the locations once will not be enough, and a static model will not capture the dynamics of real human environments. For these reasons, mobile robot exploration should use models that allow to represent time-varying environments and planning policies that can determine not only where to explore, but also *when* to do it in order to build, maintain and refine the accuracy of the model over time. This chapter thus presents a review of both human motion models and exploration strategies for mobile robots. The discussion is focused on the challenges arising from the inclusion of the temporal dimension in both aspects.

## 2.1 Human motion models

In the literature, many authors have presented approaches on how to model the behaviour of people in a given space. Some of them focus on learning the so-called human density affordance maps, which define the probability of finding a person in certain regions of the environment. In the work by Limosani et al., 2015, for example,

the authors create the affordance maps by clustering and overlapping the data from 2D laser scans from multiple robot data-gathering runs. Zapf et al., 2019 exploit a Gaussian Process regression model to predict human density in the surrounding unobserved locations of the environment. In Tipaldi et al., 2011 the probability of activity events is modelled by a Poisson process, which is also exploited by a motion planning algorithm to find a person as quickly as possible. And Saarinen et al., 2012 propose to use Poisson processes to learn online the transition parameters of an independent Markov chain with two states to model a cell (free and occupied).

However, allowing the robot to learn the human density variation in the environment may not always be the best approach for ensuring socially compliant navigation. Let us take the example in Figure 2.1 of a robot that has to navigate from point A to point B. In this case, even if the robot knows that left side should contain fewer people, the fact that robot has to move against the main direction of human motion would mean multiple avoidance manoeuvres. The robot would eventually reach the goal, but it would be more likely to collide with a person, be delayed by the multiple path re-plannings and annoy the people walking, and so, in summary, will be less socially compliant. Allowing the robot to learn the human flow patterns means that in an optimal situation the robot should choose the right side of the environment to navigate even though the people density is higher. Doing so, the robot follows the flow and does not have to handle encounters with opposing orientation of motion.

Learning the expected motion of people in an environment is key for safer and more efficient mobile robot navigation, hence many authors focus on modelling human motion behaviour (Camara et al., 2020a; Camara et al., 2020b). Based on the modelling approach, the models presented can be classified into three main categories (Rudenko et al., 2019):

- Physics-based methods which define an explicit dynamical model based on Newton's laws of motion.
- Pattern-based methods which learn motion patterns from data of observed agent trajectories.

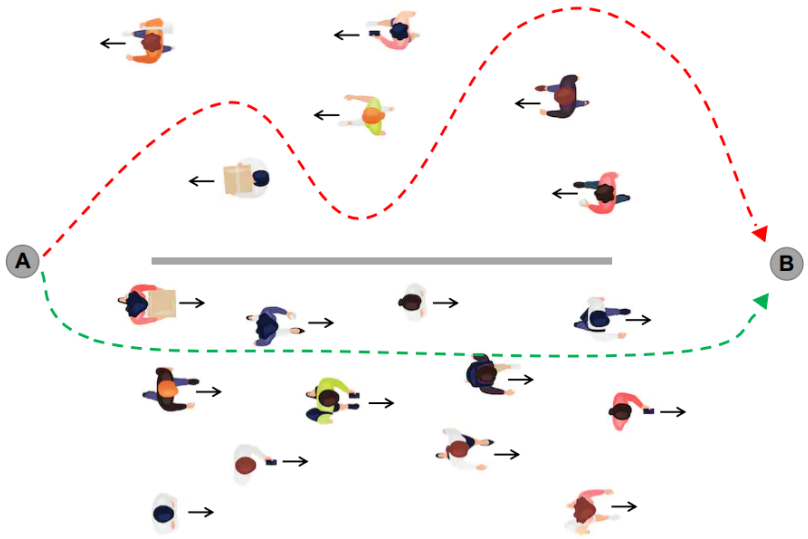


Figure 2.1: Scenario where a mobile robot has to go from point A to point B. The red path shows a situation where the robot plans to go on the left side because the intensity is lower. The green path takes into account the information about the people flow, resulting in a more social compliant trajectory.

- Planning-based methods which reason about the motion intent of rational agents.

### 2.1.1 Physics-based methods

In this case motion is predicted by forward simulating a set of explicitly defined dynamics equations that follow a physics-inspired model. The most simple models are based on kinematics models without considering forces that govern the motion. Examples include the constant velocity model, constant acceleration, the coordinated turn model that assumes constant turn rate and speed, or the more general curvilinear motion model by Best et al., 1997. These simple methods are used by many authors for their simplicity and acceptable performance, such as in Elnagar, 2001 for Kalman-filter-based prediction of dynamic obstacles using a constant acceleration model, or Barth et al., 2008 using the coordinated turn model for one-step ahead prediction in an Extended Kalman Filter.

Other approaches extend the physics-based models to account for information coming from static environmental cues such as a map. To this end, Coscia et al., 2018 proposes a grid-based discretisation, while Aoude et al., 2011 presents a more general

graph-based method. Coscia et al., 2018 uses polar grids, centered at the currently predicted agent position to represent three different local influences to the constant velocity model, which are prior motion knowledge, semantic map label and direction to goal. Instead, Aoude et al., 2011 uses a metric map to grow a tree of possible future trajectories to check and avoid the static obstacles.

The aforementioned works consider only a single target agent and neglect local interactions between other agents in the environment, hence other authors add social awareness, i.e. adding dynamic cues on top of the static ones. One of the most popular is the social force model by Helbing et al., 1995 which defines attractive forces coming from the agent's goal and repulsive forces coming from other agents or obstacles (Figure 2.2). This has been used, for example, to extend the physical model and improve the short-term tracking prediction for 2D laser data in Luber et al., 2010. Also it has been extended by embedding social relationships in a linear combination of predefined basic social effects such as attraction, repulsion or non-interaction (X. Yan et al., 2014). Other agent interaction models compute joint motion predictions based on the expected point of closest approach between pedestrians. Firstly introduced by Pellegrini et al., 2009 as Linear Trajectory Avoidance, this method firstly computes the expected closest point between a set of agents and then uses that point as a driving force to perform avoidance actions. Based on this same approach, Yamaguchi et al., 2011 formulates a human motion prediction approach as an energy minimisation problem, where the energy function is defined by multiple characteristics of a person motion such as damping, speed, directions, group belonging or collision avoidance.

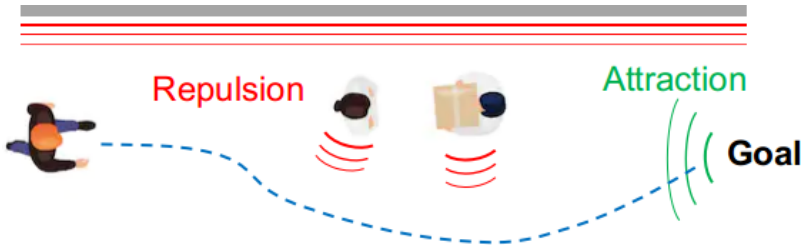


Figure 2.2: Potential field model with static and dynamic environmental cues.

### 2.1.2 Pattern-based methods

In contrast to the physics-based approaches, these methods learn human motion behaviour by fitting different function approximators to the data. Some authors focus on learning local motion patterns, such as probabilities of transitions between cells on a grid map, which are applied for prediction only in a particular environment. Early examples of local motion patterns include the work by Kruse et al., 1998. Kruse et al., 1998 presents two models, a statistical grid representation containing information regarding the frequency and direction of obstacle motions, and a stochastic trajectory prediction model which makes use of Poisson processes to determine the occurrence rate. More recently, Thompson et al., 2009 expand the local motion patterns model by accounting for transitions several steps in the future. Their method maps the motion state of the person to a series of local envelopes defining the motion intent estimation, which are biased by way points in the map describing functional places such as an entrance, desktop, exit or room. Kucner et al., 2013 proposes a Conditional Transition Map which is a grid-based representation that associates a probability distribution for an object exiting the cell given its entry direction. In Z. Wang et al., 2015 for each cell in the grid, they formulate the local dynamics using a variant of the left-to-right Hidden Markov model which explicitly models the exiting directions form the current cell (Figure 2.3). The dependency of this process is based on the entry direction captured by employing an Input-Output Hidden Markov model and is also conditioned by the place where the whole person trajectory originated in the environment. Ballan et al., 2016 proposes a Dynamic

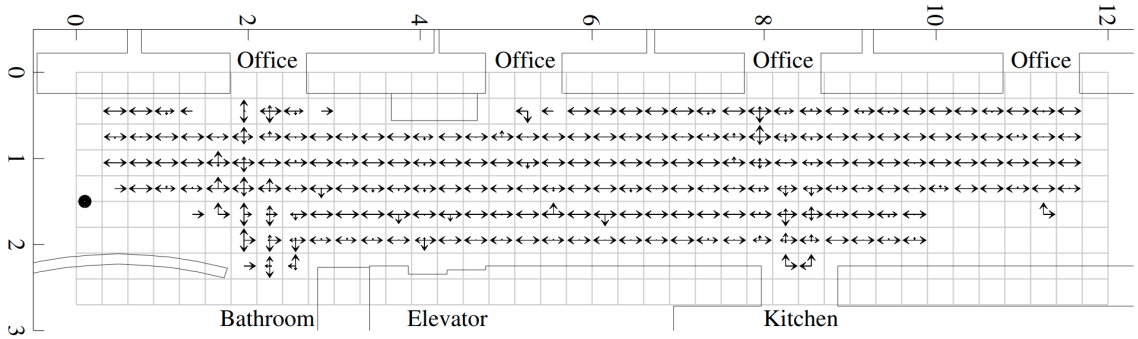


Figure 2.3: Local-based discrete transition map. Taken from Z. Wang et al., 2015

.

Bayesian Network method to predict human trajectories in a given environment by transferring functional properties of a navigation map (e.g direction and speed of the targets, crossing frequency for each patch, identification of routing points, etc.) that is learned from the training set.

Opposed to the discrete transition patterns aforementioned, other authors model the transition dynamics as a continuous function of the agent's motion state. Joseph et al., 2011 models the multi-modal mobility patterns as a mixture of Gaussian processes with a Dirichlet process prior over mixture weights. Kucner et al., 2017 models a multi-modal distribution with a Semi Wrapped Gaussian Mixture Model in the joint velocity-orientation space. And Senanayake et al., 2018 proposes a directional grid map to represent the location-wide long-term angular motion of the environment based on a multi-modal mixture of von Mises distributions that models the likely direction of movement in certain parts of the environment.

Moreover, recently with the quickly increasing growth of neural networks in the field, there have been many methods using Long Short-term Memory (LSTM) networks aiming at human motion prediction (Alahi et al., 2016; Bartoli et al., 2018; Sun et al., 2018). Alahi et al., 2016 was the first one to propose a social-LSTM to predict joint trajectories in continuous spaces. Each person is modeled by an individual LSTM. Since humans are influenced by nearby people, LSTMs are connected in the social pooling system, sharing information from the hidden state of the LSTMs with the neighbouring pedestrians. The work of Bartoli et al., 2018 extends the Social-LSTM explicitly modeling human-space interactions by defining a context-aware pooling layer, which considers the static objects in the neighbourhood of a person. And Sun et al., 2018 uses an LSTM to learn environment- and time-specific human activity patterns in the target environment from long-term observations (Figure 2.4) .

Alternatively, instead of focusing on the local transition methods, other authors focus on directly learning a distribution of full trajectories that the observed agents may follow in the future. Basic approaches are based on clustering the observed people trajectories over time to generalise the main trajectory patterns. For example, Bennewitz et al., 2002; Bennewitz et al., 2005; Cielniak et al., 2003 cluster

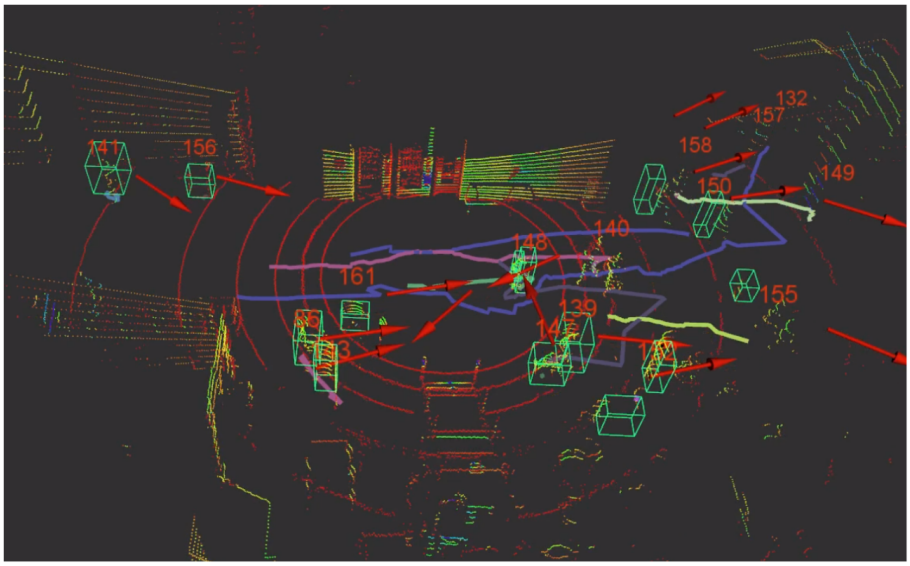


Figure 2.4: Screen-shot of the 3DOF pedestrian trajectory prediction in a 3D lidar scan. The detected people are enclosed in green bounding boxes with unique ID. The colored lines represent the observed people trajectories. The red arrows indicate the predicted poses 1.2s in the future. Taken from Sun et al., 2018.

recorded trajectories into global motion patterns using the expectation maximisation algorithm and build a Hidden Markov Model for each cluster found. Then the prediction task consists of comparing the current observed motion with the already learnt clusters and finding the one that best fits the data. Tay et al., 2008 use instead Gaussian processes and Gaussian Mixtures to represent the cluster centroids in order to predict the motion of a dynamic object in known scenes. Xiao et al., 2015 adds semantic labelling to the set of sample trajectories like wandering or stopping, and Luber et al., 2012 extends the model by explicitly modelling the pairwise interaction between two observed agents during the recorded trajectories.

### 2.1.3 Planning-based methods

Unlike the previous two categories, the methods that fall into this category incorporate the concept of a rational agent when modelling the human motion. By placing an assumption of rationality on the human, the models used to represent human motion must take into account the impact of current actions on the future as part of its model. Several methods use optimal motion and path planning techniques. For example, Xie et al., 2013 uses a Dijkstra-based planner to predict human transitions

in a generated attractive/repulsive energy field. Gong et al., 2011 uses instead an A* algorithm for generating the path hypothesis, and Vasishta et al., 2017 extends the A* algorithm over a potential cost-map built from semantic properties of the environment. Other methods model the probabilities of future motion based on cost-to-go value estimates. Karasev et al., 2016 predicts the long-term motion of pedestrians using jump-Markov processes. A Markov Decision Process (MDP) policy is in charge of describing the motion behaviour while the goal variable governs the jumps. The work by Rudenko et al., 2018 extends the MDP prediction approach by incorporating other agents in the model using the physics-based social forces model (Figure 2.5). More recently Muench et al., 2019 also extends the MDP predictor, but in this case the authors propose to learn an additional interaction-aware Q-function with imitation learning.

Figure 2.5: Trajectory prediction results for four people in the environment. The current position of each person is indicated by a yellow circle and the white path represents the ground truth trajectory. Taken from Rudenko et al., 2018.

### 2.1.4 Limitations and challenges

**Temporal representation** Despite the fact that the methodologies presented in this section focus on modelling and predicting human motion, they do not take into account temporal variations in their approaches. This means that it does not matter if the trajectory, person detection or cell transition has been acquired at 3 am or 3 pm, the input for training the model is the same. Instead the input data tends to be accumulated over time rather than using time as a new dimension or feature. As

a consequence, the predictions of the aforementioned models are neither affected by the querying time. A prediction given for 3 am will be the same as the one for 3 pm. In the long-term, and depending on how dynamic the environment is, not taking into account the time can lead to a decrease in the accuracy of the model predictions.

Therefore, some authors have worked on approaches to encode time in environmental models. Dayoub et al., 2008 presents a method for creating an adaptive map using the human-based concepts of long-term and short-term memory, identifying which map features should be placed in the long-term map so they are not forgotten. In a similar approach, Biber et al., 2009 extends the trade-off between adaptation to new patterns and preservation of old ones, to represent the environment using multiple timescales where each one defines a different fading rate. A different method is presented by Tipaldi et al., 2013, where each cell of an occupancy map is modeled using a Hidden Markov Model defining the state transition probability between the two states of 'free' or 'occupied'. In Churchill et al., 2013 images are accumulated from scenes at different times of the day where the robot fails to localise, in order to store the temporal variations of the different locations. Finally, Krajník et al., 2017 proposes to represent the discrete dynamic environment states by their frequency spectra. The spectral model can represent arbitrary timescales and the transformation of the spectra in the time domain allows the predictions of future environmental states. This same concept is used in Jovan et al., 2016 with periodic Poisson processes that characterise the time behaviour of different rooms in a building, which helps to better capture the nature of temporal people activities. Recently the spectral model has been extended to the continuous space using Gaussian Mixture models in Krajnik et al., 2018. This approach has been further applied to motion directions in a grid map to obtain the STeF-map representation developed in this PhD thesis.

**Data sparsity** Due to the sensors' field of view and temporal limitations present when working with mobile robots, the models need to have the ability to be built from sparse data in space/time and update the model as the robot is gathering new information. However, most of the models do not take that into account, as the model creation and updating can be computationally expensive and tedious. Works

like Wada et al., 2012; Kucner et al., 2017 aim to solve this issue in the spatial domain. Wada et al., 2012 focuses on developing an incremental human motion map by a human walking area interpolating algorithm and map update algorithm. Kucner et al., 2017 present and compare two non-parametric random kernel data imputation allowing to build dense maps from sparsely distribution measurements.

Others authors like Chinellato et al., 2017; Machado dos Santos et al., 2017 focus on addressing the temporal domain. Chinellato et al., 2017 solves the temporal incremental building of a von Mises Mixture model to represent multi-modal distributions of human activity in a time cyclic domain from data streams. And Machado dos Santos et al., 2017 extends the approach presented by Krajník et al., 2017 to a non-regular basis updating by maintaining a predefined frequency spectrum, instead of calculating a continuous one in every update.

## 2.2 Robotic exploration

### 2.2.1 Spatial exploration

The goal of an exploration algorithm is to increase a robot's knowledge of its workspace by selecting appropriate control actions which will lead the robot to visit previously unseen areas. The exploration algorithms can be classified depending on whether the robot makes use of the map knowledge gathered from past observations or not. Figure 2.6 shows an overview of the categorisation mentioned (Machado dos Santos et al., 2017; Shade, 2011) and the subcategories that will be explained in this subsection.

#### Non-map driven strategies

Non-map based strategies completely ignore the previously data gathered about the environment to plan future actions, hence they do not guarantee the completeness of the model in a timely and efficient manner (Sim et al., 2003). These strategies are normally used by robots with low computation power or that are very limited from a perception point-of-view. They can be based on random movements around the scen-

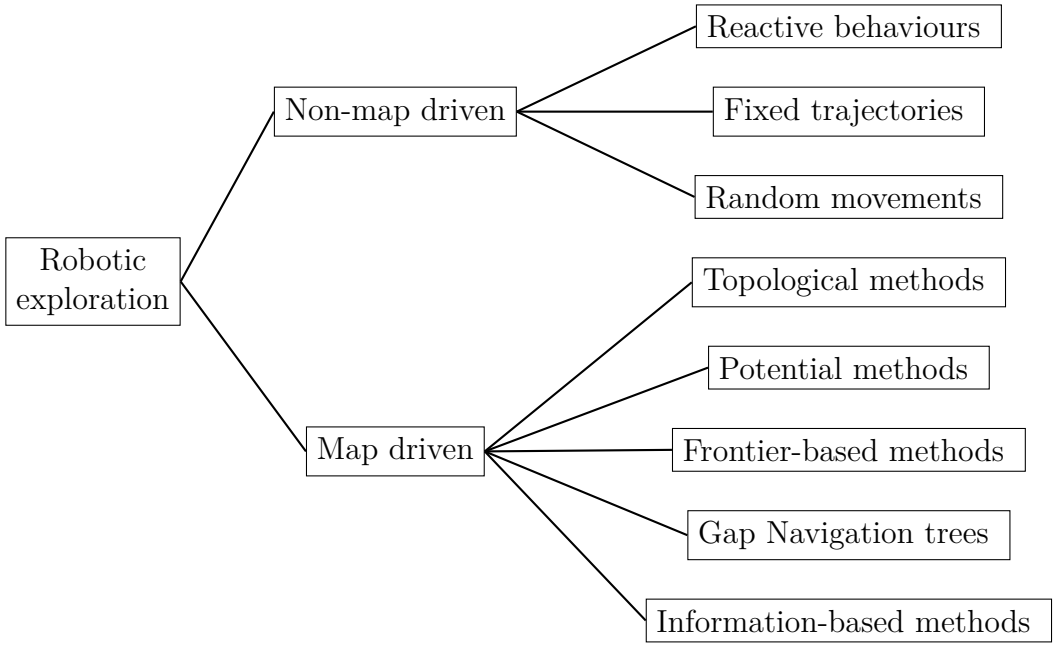


Figure 2.6: Overview of mobile robot exploration strategies.

ario or following certain fixed trajectories like performing concentric circles/spirals. These trajectories can also be combined with the addition of certain reactive behaviours to external stimuli, like whiskers to perform wall following (Jung et al., 1996) or a bumper triggering collisions (Kumar et al., 2016) as in autonomous house vacuum cleaners.

### Map driven strategies

On the other hand, map-driven strategies use the previous knowledge of the world to identify which are the unknown areas that remain to be explored, ensuring map completeness in a shorter time.

**Topological methods** Topological exploration describes an exploration method in which a robot constructs a connected graph of its environment. Early works such as Dudek et al., 1978 describes a robot exploring a graph-like world, without any assumption on distance or orientation metric. Or Duckett et al., 1999, that proposes to use a neural network to predict the new nodes which correspond to new places the robot has to explore. More recently, a topological approach has been used to explore mines (Morris et al., 2005), where each node of the graph corresponds to identified

intersections in the mine corridor. In Fraundorfer et al., 2007, images taken by the robot are associated to new nodes in the topological graph, to provide a more reliable localisation and navigation. Or in the work by Fermin-Leon et al., 2017 where the authors exploit Constrained Depth-First Search-based graph traversal algorithms to efficiently explore the navigation area.

**Potential methods** Potential methods are widely-used approaches in the field of robotic path-planning (Barraquand et al., 1992; Hwang et al., 1992; Y. Wang et al., 2000; Ge et al., 2002; Daily et al., 2008). They are based on assigning a high potential to the robot starting position and a low potential to the goal, so the path between the two points can be found by gradient descent through the resulting field. This approach can be extended for the exploration domain to make the robot explore unknown areas of the map, corresponding to the lower potential. However, one of the problems of using potential fields for exploration are the local minima where the robot can get "trapped" during the navigation. Silva Jr et al., 2002 has demonstrated a successful exploration with a sonar sensor using potential fields. They make use of a harmonic function relying on Dirichlet boundary conditions to avoid the generation of local minima. A similar strategy is proposed by Shade, 2011, which again exploits the properties of harmonic solutions but with Laplace's equation to find the scalar potential field. Vallvé et al., 2014 approach instead, creates a potential information

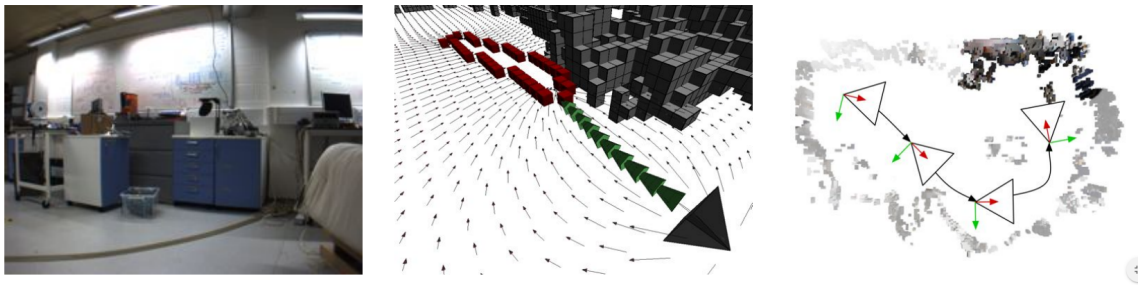

Figure 2.7: Representative images from a potential-based exploration of a lab environment. The middle column shows the gradient of the harmonic function that forms the potential field, and the stream line chosen for exploration. Taken from Shade, 2011.

field calculating the entropy decrease in the robot configuration space.

The aforementioned potential methods are presented having in mind only one robot

exploring at the same time. Works like Juliá et al., 2008; Renzaglia et al., 2010 extend the potential field to multi-robot systems. Juliá et al., 2008 uses attractive forces for areas of interest while using repulsive forces to enforce the dispersion of the robot and the avoidance of obstacles. Renzaglia et al., 2010 tackles the problem of local minima with several robots by assigning a robot leader with different control laws.

**Frontier-based methods** As the name suggests, these exploration approaches are based on frontiers. First defined in Yamauchi, 1998, a frontier is a boundary between the known and unknown parts of the environment. These boundaries are commonly represented in an occupancy grid map, which is a discretisation of the environment into regular volumetric elements usually referred as voxels or cells. The main idea is then to create a plan so that the robot visits these boundaries to remove them, expecting that the robot, using its sensors, expands the map beyond the boundaries (Figure 2.8).

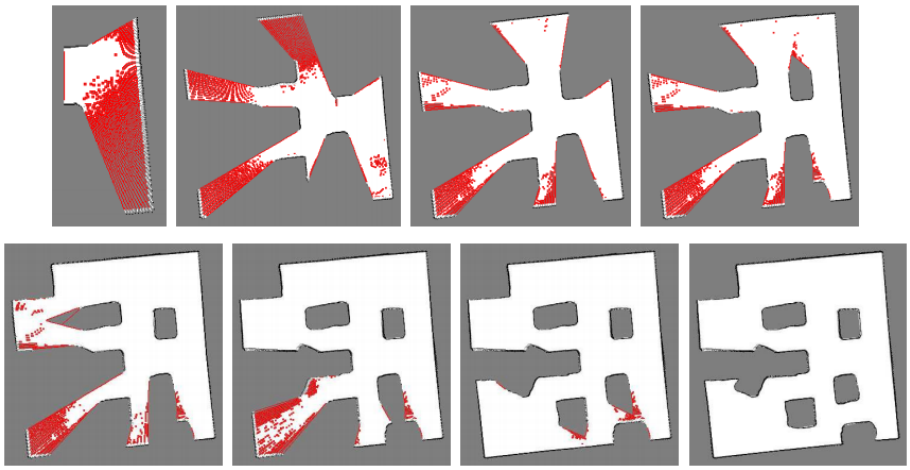

Figure 2.8: From left to right and top to bottom: frontier cells in the progress of exploration and incremental map construction (free space: white, unknown regions: gray, frontiers: red/dark grey). Taken from Holz et al., 2010.

The same definition of frontier has remained, but different authors have proposed different strategies to define the order in which to visit the frontiers. Yamauchi, 1998 follows a method which consists in identifying the frontier voxel which is the closest to the robot position. The robot is then instructed to reach that frontier, perform a sensor scan and continue to the next closest frontier repeating the process until

no frontiers remain. Studying how to optimise frontier-based strategies has been a widely researched topic in the community since this first approach. Holz et al., 2010 detects a problem in the previous strategy, which is that the closest frontier can lie outside of the room that is currently being explored, leading the robot to explore the same room twice with unnecessarily long trajectories. To solve this problem, they apply segmentation to areas in the map, achieving a lower travel distance needed for full coverage. Mei et al., 2006 instead optimises trajectories that require lower energy to accomplish by the robot, reducing in that way the repeated coverage issue. In Wirth et al., 2007, apart from the distance to the frontier, they propose to use the distance to the closest object in an attempt to improve efficiency and safety in Search and Rescue scenarios. Other strategies focus on improving the robustness of the robot navigation by minimising the localisation error (Tao et al., 2007) and ensuring safe way-finding to the frontier (Wettach et al., 2010).

The scalability of this approach due to its ability to distribute the frontiers among multiple robots is one of the main advantages. Hence other authors focus on exploiting the frontier-based methods for multi-robot systems (Yamauchi, 1998; Burgard et al., 2000; Simmons et al., 2000; D. Fox et al., 2006; Wurm et al., 2008; Benkrid et al., 2019). Burgard et al., 2000 takes into account the cost of reaching a target point and its utility for the robot task assignment. Simmons et al., 2000 tries to maximise the overall utility by minimising the potential for overlap in information gain among the multiple robots. In D. Fox et al., 2006, the authors explore the topic of improving the consistency of the maps created by multi-robot systems by actively seeking to verify their relative position and maximise efficiency. Wurm et al., 2008 uses structure segmentation besides the frontiers, to better assign the robots the regions to explore. And Benkrid et al., 2019 employs an energy consumption heuristic for the coordination.

**Gap Navigation Trees** Gap Navigation Tree (GNT), introduced by Tovar et al., 2004; LaValle, 2006, is a data structure designed to maintain a graph of gaps. A gap is defined as a depth discontinuity with respect to the heading of the robot, see Figure 2.9. Using this gap representation the authors in Landa et al., 2007 present

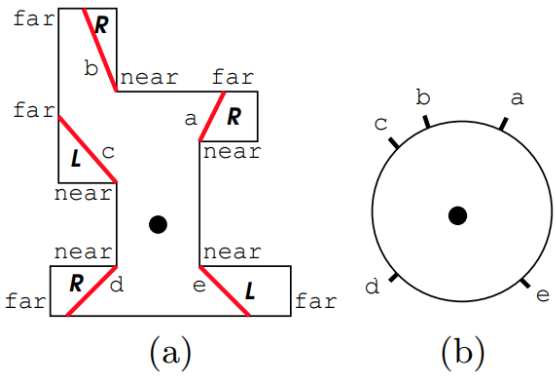


Figure 2.9: The robot's view of the environment. The position of the robot is shown with a black disk. (a) The environment and the respective labelling of the gaps detected. (b) Angular position of the gaps detected in the visibility region. Taken from Tovar et al., 2004.

an exploration algorithm based on eliminating these gaps using visibility maps. The GNT approach has a lot of similarities with the frontier-based approaches. However, GNT was created with the aim of achieving exploration while using the minimum amount of information possible. For example, exploring a large environment with the occupancy grid map used in frontier-based exploration has a high memory cost, especially when dealing with 3D environments.

**Information-based methods** In information-based approaches the goal of the exploration is two-fold; to create a complete map of the environment, while maximising the amount of new information the robot can collect for each measurement. These strategies are usually based on the entropy concept, which defines the information of a measurable variable. Going to the areas where the information gain is higher means a bigger decrease in the entropy, and hence a reduction of the uncertainty of the map (Figure 2.10). This usually translates to an increased quality and accuracy of the maps obtained.

For example, Bourgault et al., 2002 maximises the expected Shannon information gain, while minimising the uncertainty of the robot localisation, to obtain more accurate maps from laser scans. In similar works, Carrillo et al., 2015; Carrillo et al., 2018 also add Renyi's definition of entropy together with the Shannon one to jointly consider the uncertainty of the robot and the map. Sujan et al., 2006 also

exploits the Shannon's information theory, but the information gain is calculated from sub-regions of a 2D panoramic image of the environment, with the aim to build a graph-based representation. The work by C. Fox, 2013 presents a comparison between a simple wall-following rule and full Bayesian utility maximisation via entropy-based exploration, showing that wall-following tends to approximate optimal action selection for a certain class of scenarios. Always going to the selected pose which is expected to yield maximum information can result in the robot travelling long distances to reach that area, resulting in wasted time and traversals across previously seen areas. Thus, González-Banos et al., 2002; Amigoni et al., 2010 present systems that optimise the estimated time to reach a certain location and the amount of information expected to be gathered there.

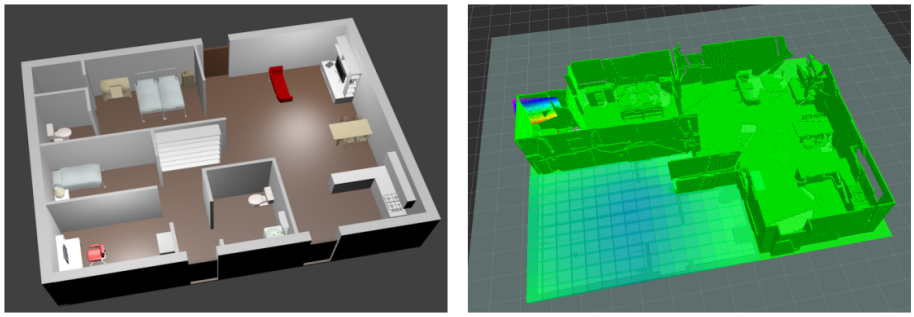

Figure 2.10: Left: render of a domestic environment. Right: outcome of an entropy-based exploration strategy. Blue cells indicate higher expected information gain. Taken from Machado dos Santos et al., 2017

In other approaches like Zreda et al., 2012; Fentanes et al., 2018, they exploit the utilisation of the Poisson uncertainty to drive the observation and mapping of soil moisture by counting neutrons using a cosmic-ray sensor. Or Lauri et al., 2016 that explores the problem of exploring a partially known environment, using a partially observable MDP with an information-theoretic objective function that is shown to improve performance over frontier exploration.

The same as in the frontier-based methods, information-based ones can be also extended for multi-robot applications. For example, Baglietto et al., 2002 defines an heuristic that exploits the concepts of both information-gain and frontier-based approaches for assigning the goals to the multi-agent system, assuming a constant communication between the agents for coordination purposes. Or Burgard et al.,

2005, where the goal assignation is based on the trade-off between the cost to reach the desired location and the expected information-gain. Other strategies rely on semantic information to coordinate the multiple robots and reduce the redundant coverage (Stachniss et al., 2006).

### 2.2.2 Introducing the time domain

In an attempt to increase the accuracy of the environmental representation, authors have proposed approaches that explicitly model temporal changes in dynamics environments (see Section 2.1.4). These time-dependant representations allow to improve the robot's localisation accuracy (Dayoub et al., 2008; Biber et al., 2009; Tipaldi et al., 2013), navigation(Churchill et al., 2013; Neubert et al., 2015), path planning (Fentanes et al., 2015) and robotic search (Krajnik et al., 2015). These approaches are aimed at enabling robotic systems to perform autonomously for longer operation times, i.e. improving their long-term autonomy (Hawes et al., 2017).

However, with the introduction of time in the models, there is a need for exploration strategies which work in synergy with the models they have to build. Long-running robots need to consider environment mapping as a never-ending process (Kunze et al., 2018), therefore, the mapping strategies not only have to decide "where" to go (spatial exploration), but also consider how the environment evolves over time and decide "when" to go there (spatio-temporal exploration).

The strategies presented in the previous section do not consider or attempt to maintain the map after its initial acquisition. Once the environment map is completed with a certain level of accuracy, they stop the mapping process. From a long-term perspective (days, months or years) the model will lose accuracy as new changes appear in the environment. To deal with this problem, another branch of algorithms aim to create models of the environment which allow the robot to reason about the best times and locations to make observations of specific phenomena. In Singh et al., 2010; Marchant et al., 2012 the decision making for environmental surveillance and monitoring is based on Gaussian Processes, which allow the robot to learn the spatio-temporal patterns in the environment. S. Martin et al., 2014 study how a

localised and energy-constrained robot can maximise its time in the field by taking paths and tours that minimise its energy expenditure. And more recently, Santos et al., 2017 present a method for life-long spatio-temporal exploration of dynamic environments, using the entropy of binary states predictions in an occupancy map to create a scheduler that determines which areas and times to explore for each day. The scheduler assumes that exploring the environment for mapping purposes is not the main task of the robot, so only a fraction of the total navigation time can be devoted to it. To this end, the robot must maximise the information gain from each measurement in each location and time with the available time given.

## 2.3 Summary

Related work on human motion mapping and exploration strategies has been presented in this chapter.

Allowing the robot to understand how the people move is key for safer and more efficient mobile robot navigation around people. Hence, the field exploring ways to model human motion has been increasing in the last fews years (Rudenko et al., 2019) as robots are introduced into environments shared with humans. With the improvements in both the hardware and software of robotic systems, mobile robots are able to operate for increasingly longer periods of time. This raises new challenges, because models that are valid at the beginning of the operation time may decrease in accuracy as time passes due to the environmental changes. As a consequence, the robot localisation system could fail, or the navigation could become less socially compliant. To overcome the long-term environmental modelling problem, some authors present approaches to store and learn the changes in dynamic environments. These models, though, are mainly focused on representing the temporal dynamics of the environment structure, treating the people as "noise" to be filtered out rather than as important actors in the environment that the robot should be able to predict and take into account. Hence, one of the aims of this thesis is to tackle this gap in the literature, in an attempt to provide a spatio-temporal human motion model that is capable of learning the temporal human activities.

In the robot deployment phase, one of the key system components is an exploration strategy with the aim of creating a spatial model that covers the operational environment. Traditional exploration strategies assume a static scenario, i.e. the states measured do not change over time. If the flow of people remains constant (static in time), this would mean visiting the locations which have never been visited before. But as mentioned before, in long-term deployments this tends not to be true (Hawes et al., 2017; Biswas et al., 2016). Therefore, apart from deciding where to explore, the exploration strategy must also consider the temporal dimension (i.e. when to explore) in order to obtain the maximum information from each human motion observation. By learning and refining its knowledge of human motion patterns over time, the robot should be able to operate more reliably in challenging environments shared with humans.

# Chapter 3

# Long-term pedestrian datasets

Datasets play a fundamental role in many research projects, as they allow us to test methodologies more quickly and more repeatably than having to rely on robot data acquired in real time. However, finding an available dataset that is suitable for a given task is not always straightforward, especially in the robotics domain, as their acquisition and annotation can be costly tasks.

All the contributions presented in this thesis make use of long-term pedestrian datasets to perform the evaluation in the corresponding experimental sections. Hence, before starting to explain the spatio-temporal model and exploration strategy proposed in the thesis, this chapter presents a literature review on the available datasets. Moreover, the three main datasets used throughout the thesis are described. One of the datasets is taken from the literature, and two of them were recorded by the author, which are also part of the contributions to the field.

## 3.1 Pedestrian datasets in the literature

Table 3.1 provides a summary of the relevant pedestrian datasets available in the surveyed literature.

The common recording setup includes a video-camera with static top-down view of the scene, ground-based lasers and/or depth sensors, mounted on a static or moving platform. Detected agents in each frame are labelled with unique IDs, and their positions with respect to the global frame are given in $x, y$ coordinates together with the timestamp of the detection. Sometimes, this coordinate vector is augmented with orientation and velocity information. Moreover, additional social grouping information, gaze direction, motion mode or manoeuvre labels and other contextual clues can be provided. Apart from this specific form of labelling, further requirements

| Dataset | Location | Agents | Sensors | Scene description | Duration | Tracks |
|---|---|---|---|---|---|---|
| **ATC (Brscic et al., 2013)** | Indoor | People | 3D range sensors | Recordings in a shopping center, 900 $m^2$ coverage, varying density of people | 92 days | 50k per day |
| **Daimler (Schneider et al., 2013)** | Outdoor | People | Stereo camera | Recording from a moving or standing vehicle | 4 sec each track | 68 |
| **Edinburgh (Majecka, 2009)** | Outdoor | People | Camera | 1 pedestrian scene, top-down view covering $12 \times 16$ $m^2$ | 123 days | 92k |
| **ETH (Pellegrini et al., 2009)** | Outdoor | People | Camera | 2 pedestrian scenes, top-down view | 25 min | 650 |
| **Grand Central Station (Zhou et al., 2012)** | Indoor | People | Camera | Recording in the crowded New York Grand Central Station. | 33 min | - |
| **JRDB (R. Martin et al., 2019)** | Indoor/ Outdoor | People | 360° cameras, Velodynes | 54 sequences in Stanford campus, highly annotated. | 64 min | 3.5k |
| **KITTI (Geiger et al., 2012)** | Outdoor | People, cyclists, vehicles | Velodyne, 4 cameras | Recorded around the Karlsruhe city, in rural areas and on highways | 50 sequences | - |
| **L-CAS (Z. Yan et al., 2017)** | Indoor | People | Velodyne | Recording in a university building from a moving or stationary robot. | 49 min | - |
| **Stanford Drone (Robicquet et al., 2016)** | Outdoor | People, cyclists, vehicles | Camera | 8 urban scenes, top-down view, moderately crowded. | 5 h | 20k |
| **THÖR (Rudenko et al. 2020)** | Indoor | People | Motion Capture | Human-robot navigation study in a university lab | 60 min | 600 |
| **Town Center (Benfold et al., 2011)** | Outdoor | People | Camera | Pedestrians moving in moderately crowded street | 5 min | 230 |
| **TU GRAZ (Roth et al., 2009)** | Indoor | People | Camera | Pedestrians moving in corridor, top-view, very few detections | 7 days | - |
| **UCY (Lerner et al., 2007)** | Outdoor | People | Camera | 2 pedestrian scenes, 1 sparse and 1 crowded, top-down view | 16.5 min | 700 |
| **VIRAT (Oh et al., 2011)** | Outdoor | People, vehicles | Camera | 16 urban scenes, 20-50° camera angle | 25 h | - |

Table 3.1: Overview of pedestrian datasets found in the literature.

for benchmark datasets for evaluating human motion prediction include interactions between agents, varying density of people, semantic maps, and long-term continuous observations of the agents.

Regarding time duration, most of the pedestrian datasets available only provide people detections during a time span of less than 1 day, commonly in the range of several minutes. These types of datasets tend to be very useful for evaluating person detection and tracking algorithms, as they have a very accurate and exhaustive labelling. The work developed in this thesis focuses on modelling and analysing the

output of the tracking algorithms in a long-term perspective, where datasets with a shorter duration are not suitable.

From the datasets found in the literature, the only one that provides sufficient duration, a reasonable number of people occurrences and complex human flow models is the ATC dataset (Brscic et al., 2013), which is described in more depth in the following subsection.

### 3.1.1 ATC - Shopping Center Dataset

This long-term pedestrian dataset was recorded in the ATC - Shopping center in Osaka, Japan. The perception system consists of multiple 3D range sensors (36 $\times$ Panasonic D-Imager, 11 $\times$ Asus Xtion PRO and 2 $\times$ Velodyne HDL-32E), covering an area of approximately 900 $m^2$ (Figure 3.1), which is able to detect and track all the people around the place at every instant of time. The data was recorded on every Wednesday and Sunday between October $24^{th}$, 2012 and November $29^{th}$, 2013, resulting in a total of 92 days. The recording of each day provides people trajectories starting from approximately 09:00 until 21:00, so for the rest of day it is assumed that the shopping center is closed and empty. Each sensor provides people detections at frame rates going from 10 fps to 30 fps, in the format: time [ms] (unixtime + milliseconds/1000), person id, position $x$ [mm], position $y$ [mm], position $z$ (height) [mm], velocity [mm/s], angle of motion [rad], facing angle [rad]. In order to make the data more manageable, all the data was down-sampled to 2 Hz, or having a detection every 0.5 seconds, which results in having around 1 million people detections on average per day.

## 3.2 Recorded datasets

Having multiple datasets in different type of environments and conditions is always interesting, as it provides a set of cases to understand the generalisation capabilities of the methods presented. From the literature reviewed, the only dataset relevant for this work was the aforementioned ATC dataset, hence during the development of

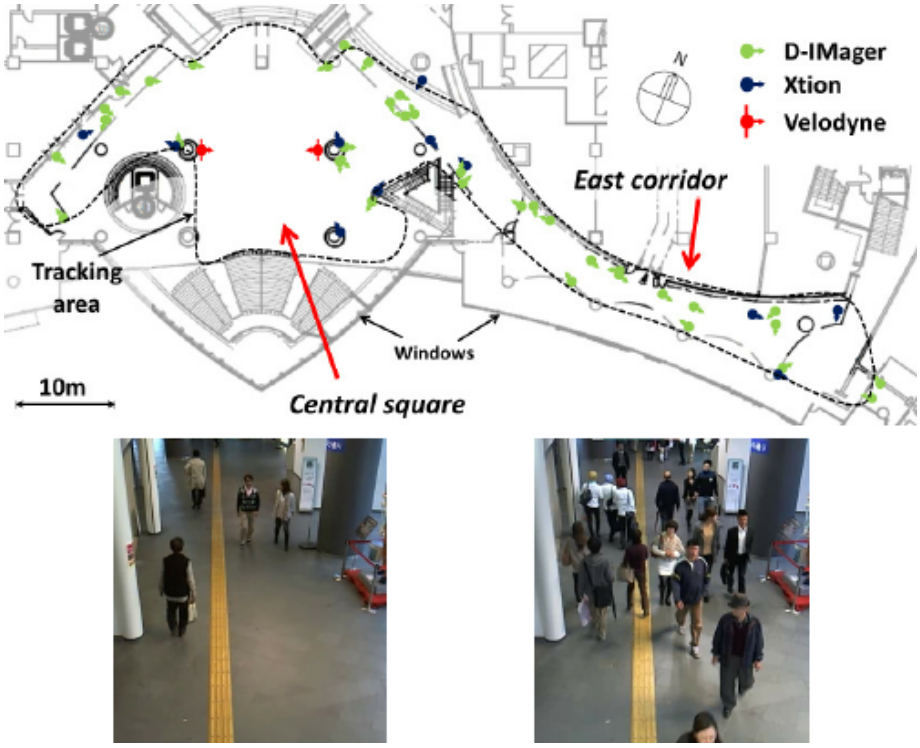


Figure 3.1: Tracking area of the sensors setup in ATC shopping center. The dashed line shows the approximate border of the area covered by the sensors. The photos below show the corridor areas in the afternoon on a typical weekday (left) and weekend (right). Taken from Brscic et al., 2013.

the experiments presented in this thesis, two additional long-term pedestrian detests were recorded.

### 3.2.1 Recording set-up

Human detection and tracking have been widely studied in recent years. Many popular approaches are based on RGB-D cameras, such as the Microsoft Kinect (*Kinect v2* 2020) or Asus Xtion (*Xtion* 2020). The performance achieved with these cameras is very good, as they contain a high density of points, but on the other hand, they are limited when it comes to field of view and range. In order to record larger areas from a stationary position, 3D lidars (such as the Velodyne VLP family) provide a useful alternative. In both datasets recorded, a Velodyne VLP-16 (*VLP-16* 2020) was used, which provides 16 scans with a 360 degrees horizontal and 30 degrees vertical field-of-view. However, one of the main challenges working with this type of sensor is the difficulty of recognising humans using only the relatively low

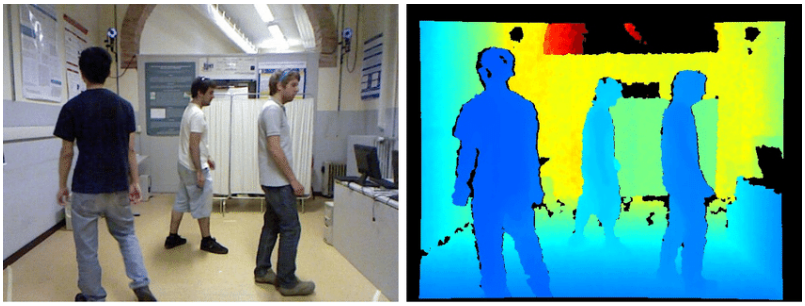

(a) RGB-D (Microsoft kinect) output. Taken from Camplani et al., 2016.

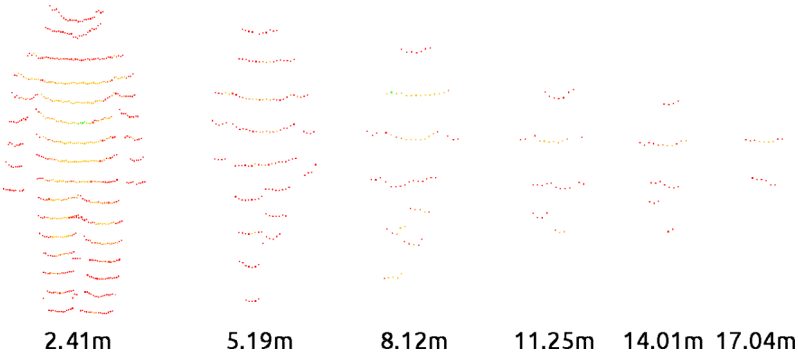


(b) 3D lidar (Velodyne VLP-16) output. Taken from Z. Yan et al., 2017.

Figure 3.2: Comparison between pedestrians seen by an RGB-D camera and a 3D lidar.

information they provide as the distance between the sensor and the pedestrian is increased. A comparison between the output of the two types of sensors can be seen in Figure 3.2. As seen in the comparison, the further the person being tracked is from the sensor, the fewer laser points are reflected from the human body shape.

### 3.2.2 Human detection and tracking

To obtain the human trajectories from the Velodyne pointclouds, a people detector and tracker developed by Z. Yan et al., 2017 was used.

The framework is based on 3 main components: a 3D lidar point cloud cluster detector, a multi-target tracker and a human classifier. The general overview of the pipeline and how the components are connected can be seen in Figure 3.3.

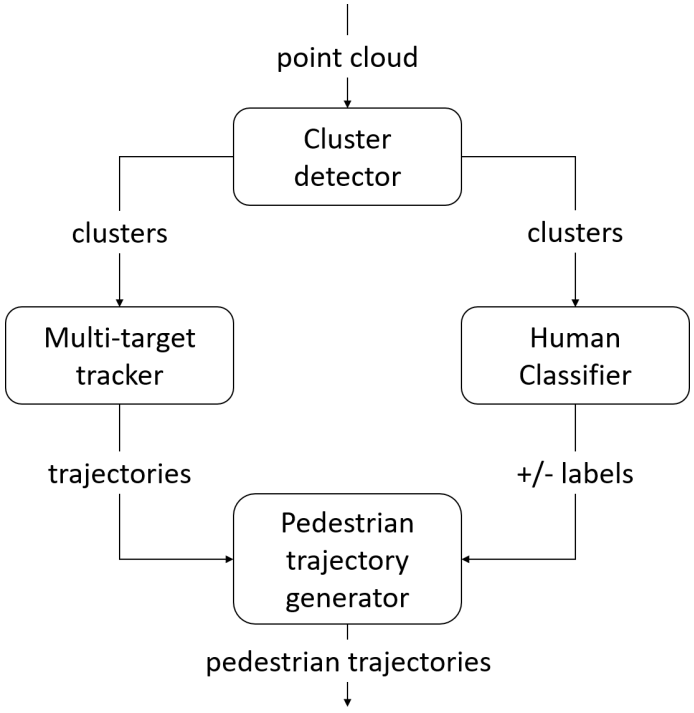


Figure 3.3: Pedestrian trajectory generator pipeline.

### Cluster detector

At each iteration, the 3D lidar point cloud received is segmented into clusters. First, the ground plane is removed, by keeping only the points above a certain height. Then, the point clusters are extracted based on the Euclidean distance between points in 3D space. Due to the increasing gaps in the laser scan with respect to a human body due to the limited vertical resolution (see Figure 3.2b), the threshold for the Euclidean clustering is adapted with the range from the sensor to the human body. The clustering performance depends on the maximum range that needs to be covered, however as shown in Figure 3.4, even with a maximum covering range of 31 meters, the clustering operating frequency is over 5 Hz, which is considered by other studies as the minimum for real-time human tracking (Bellotto et al., 2010).

### Multi-target tracker

The position and velocity of these clusters are estimated in real-time by the multi-target tracking system, which outputs the trajectories of all the clusters. For this purpose, an Unscented Kalman Filter (UKF) and Nearest Neighbour (NN) data as-

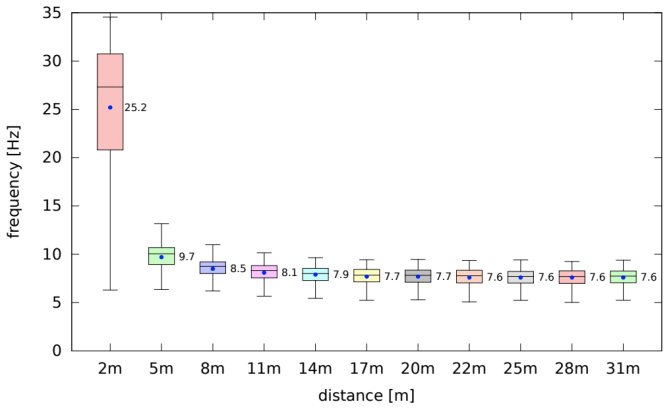


Figure 3.4: Clustering performance over a range of distance, with mean shown on the right of each box. Taken from Z. Yan et al., 2017.

sociated methods are applied (Bellotto et al., 2010). Tracking is performed assuming people move on the plane using a 2D constant velocity model.

### Human classifier

At the same time, a classifier identifies the type of cluster, i.e. human or non-human. To do so, a Support Vector Machine (Cortes et al., 1995) with six features with a total of 61 dimensions coming from the clusters found is used (LIBSVM Chang et al., 2011). In the dataset recordings, the classifier used an already pre-trained offline human model acquired with the same 3D lidar sensor. The classification performance can be seen in Figure 3.5, using the precision, recall, average precision (AveP)(Everingham et al., 2010) and F-measure (the results of the offline version are in red). The training was done using a total of 6140 single-person annotated samples, with an equal amount of randomly selected negative samples (non-human), from a dataset recorded in the main building at the University of Lincoln (Z. Yan et al., 2017; *LCAS - Software and Datasets* 2020) with the same platform used as in the Corridor dataset recordings described in Section 3.2.3. The test set consisted of 100 scans fully annotated from the aforementioned dataset distributed across 18 minutes (excluding those frames already manually annotated). These scans contain 995 single-person labels with point cluster size varying from 5 to 2250 and distance from the sensor between 0.7 and 19.9 meters. A true positive was considered such if the overlap between the ground truth and the detection was larger than 50%.

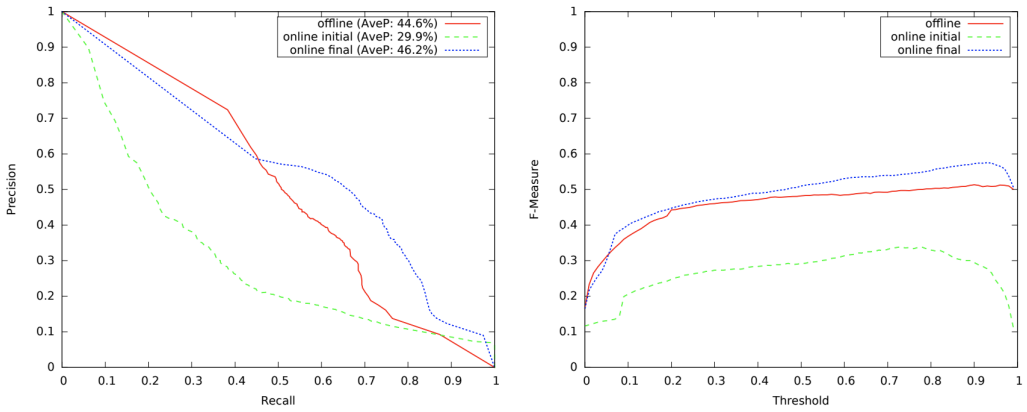


Figure 3.5: Human classifier performance. Taken from Z. Yan et al., 2017.

#### Pedestrian trajectories generation

Finally using both the inputs from the tracker and the classifier, the system is able to generate the pedestrian trajectories. An example of a subset of pedestrian trajectories of both datasets recorded can be seen in the two following subsections (Figure 3.6(c) and 3.7(b)).

### 3.2.3 Corridor dataset - University of Lincoln

The initial recorded dataset was collected at one of corridors in the Isaac Newton Building building at the University of Lincoln. The data recording was performed by a Pioneer 3-AT mobile robot equipped with the Velodyne VLP-16 at an approximate height of 0.8 meters. During the data collection, the robot remained stationary in a T-shaped junction, which allowed its sensors to scan the three connecting corridors simultaneously, covering a total area of around 75 $m^2$ (see Fig. 3.6). However, since the robot could not stay at the corridor overnight due to safety regulations, and it was needed by other researchers occasionally, the data was not collected on a full 24/7 basis. Instead, the data collection was performed during ∼10/12 hour long sessions starting before the usual working hours (usually from ∼08:00 to ∼20:00). Recharging of the batteries was performed overnight, where the building is vacant, and there are no people in the corridors. The resulting dataset is composed of 14 data-gathering sessions recorded over the span of four weeks. A typical session contains approximately 30,000 detections (at 2 Hz) of people walking in the monitored

corridors and each detection is given in the form: time (unixtime), person *id*, position $x$ [m], position $y$ [m], angle of motion [rad].

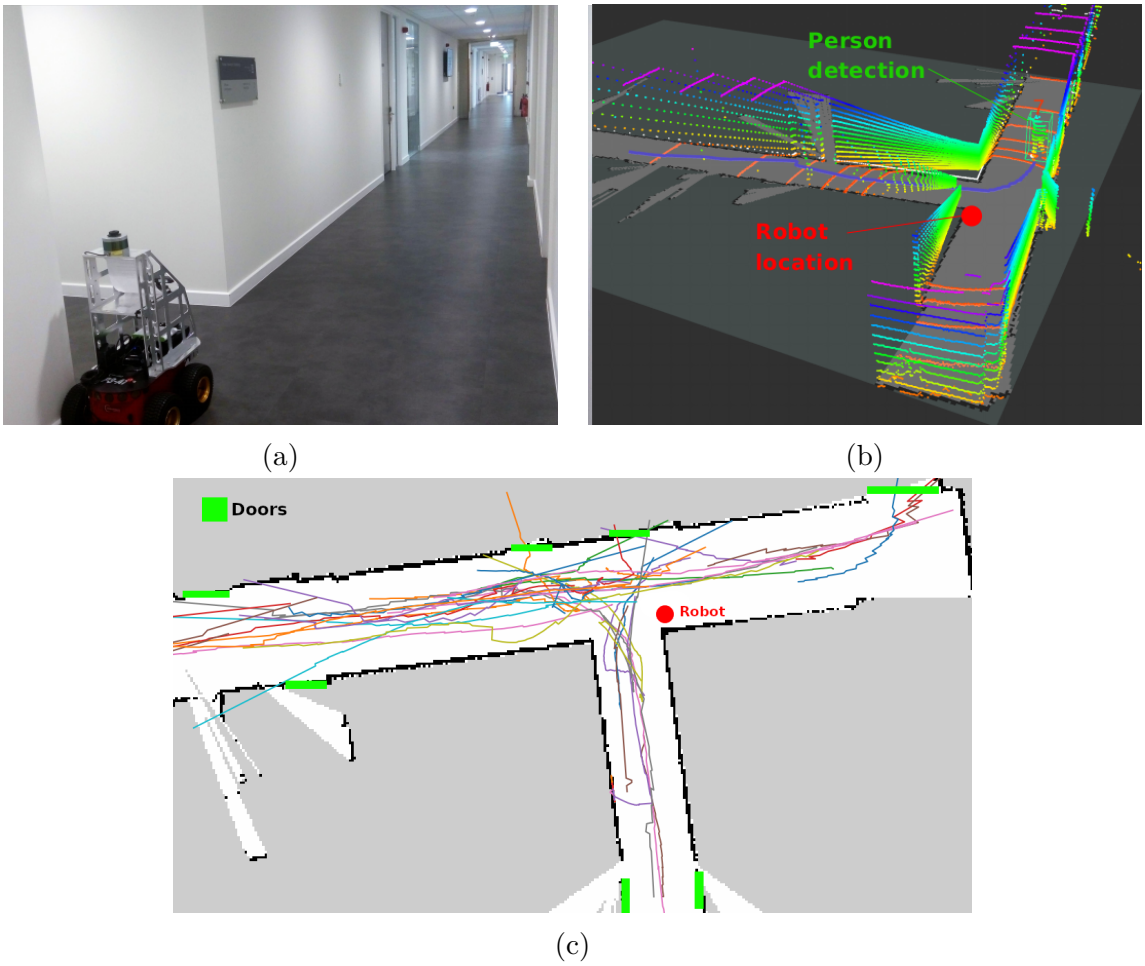


Figure 3.6: Corridor dataset: Robot location in the corridor (a), example of a person walking seen by the Velodyne scans (b), and example of a subset of the pedestrian trajectories recorded (c).

### 3.2.4 Office dataset - University of Lincoln

The second recorded dataset was also collected in the Isaac Newton Building building at the University of Lincoln, but in this case, inside one of the offices (Figure 3.7). The recordings were done again with the Velodyne VLP-16 but in this case placed on a tripod at 1.8 meters height. The sensor was placed in a position covering 2 main office entrances, an open area and the coffee area, which results in an total area covered of approximately 85 $m^2$. An overview of the whole office environment is shown in Figure 3.7 bottom. The metric map was generated using *gmapping*

2020 with a TIAGo robot (*TIAGo Robot* 2020). The final dataset contains 22 days recorded consecutively starting November the $23^{th}$ of 2018, and each day contains around 25000 entries (at 2 Hz), mainly during working hours, which are usually from 08:00 to 20:00.

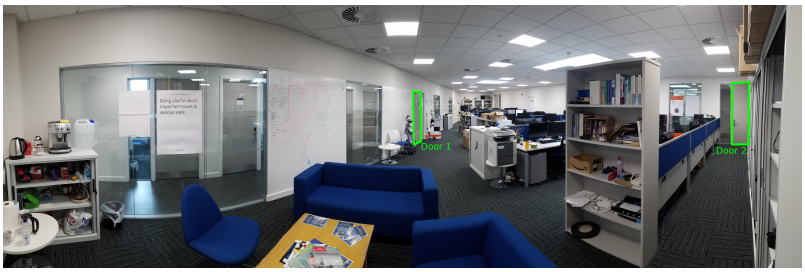

(a)

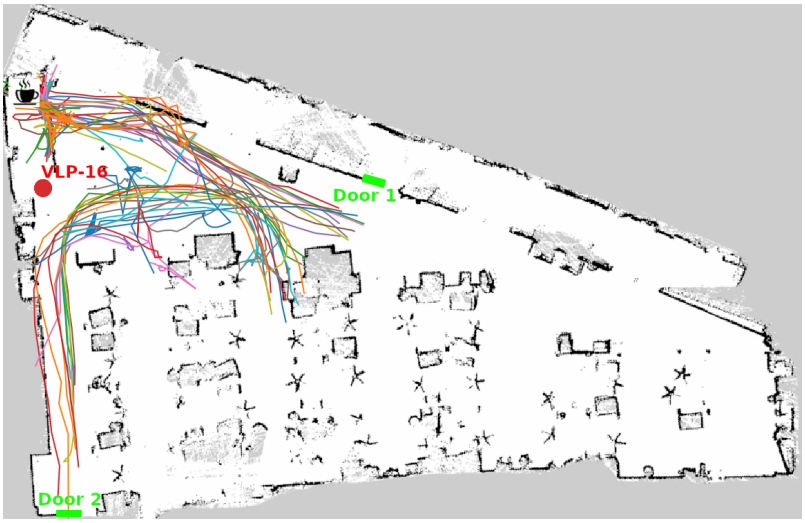


(b)

Figure 3.7: Office dataset: Panoramic view of the office from the 3D lidar position (a), and metric map of the whole office environment with the sensor location and a subset of the trajectories recorded (b).

# Chapter 4

# Spatio-Temporal Flow Map

In Section 2.1 different approaches for representing human motion in an environment were presented. The human motion model proposed in this chapter falls into the pattern-based methods (Section 2.1.2), and more specifically into the local-based approaches. However, as discussed in Section 2.1.4, previous authors have not taken into account that human activities can fluctuate over time (Brscic et al., 2013), changing the main direction of the pedestrian flows. Moreover, the previous approaches that do attempt to include the time domain in the model focus on representing the environment's structural changes rather than the dynamic activities of people.

Therefore, in order to address this gap in the field of human motion modelling, in this chapter the STeF-map is introduced as one of the main contributions of this thesis. STeF-map, which stands for Spatio-Temporal Flow Map, is a representation that models the likelihood of motion directions on a grid-based map by a set of harmonic functions. Assuming that the human motion changes follow rhythmic patterns due to the cyclic nature of everyday activities, such as the circadian rhythm, the aim of this work is to create a human motion model which is able to efficiently capture long-term (hours to weeks) variations of crowd movements over time, as well as to predict where and when these flows are happening.

This chapter is divided into 4 main sections. Section 4.1 provides a detailed description of the spatio-temporal flow model, Section 4.2 and 4.3 provide a quantitative and a qualitative evaluation of the model, respectively, using the three datasets described in Chapter 3. Finally, in Section 4.4 a summary is provided together with suggestions for future improvements to the model.

## 4.1 Spatio-Temporal Flow Map (STeF-map)

This model assumes that people detections are provided, comprising: the position in $x, y$ coordinates in a global static frame, orientation of movement $\theta$, and the timestamp $t$ of each detection. So, from the higher-level perspective of a complete robotic system, the output of the robot's person detection system would provide the input to the approach presented here.

### 4.1.1 Spatial representation

The underlying geometric space is represented by a grid, where each cell contains $k$ temporal models, corresponding to $k$ discretised orientations of people motion through the given cell over time. Since the total number of temporal models is $k \times C$ where $C$ is the total number of cells, the spatio-temporal model does not grow over time regardless of the duration of data collection. The cell size can be defined arbitrarily, however having a really fine grid could result in many cells remaining empty, depending on the number of people (or "density" of the crowd). On the other hand, defining it too coarsely could lead to an over-generalisation of the space. From the experience gained from the experiments, a cell size between 0.5 and 2 meters is recommended.

### 4.1.2 Temporal Framework

The spatio-temporal flow map proposed is built upon a spectral-based temporal representation named Frequency Map Enhancement (FreMEn) (Krajník et al., 2017), which has been already successfully applied and tested in other robotics domains such as occupancy grid mapping, localisation or navigation proving its capabilities. This model proposes to represent the uncertainty of a certain environment state (like the occupancy of cell, a door being open or closed, landmarks visible or occluded, etc.) not as a probability $p_j$, but as a probabilistic function of time $p_j(t)$. Assuming that the variations of the environment are caused by a number of unknown processes, some of which exhibit periodic patterns, the $p_j(t)$ can be represented by a combination of harmonic functions that relate to these periodic processes. To identify the parameters

of these harmonic functions, FreMEn uses the Discrete Fourier Transform (DFT) for the spectral analysis (Bracewell et al., 1986).

### Discrete Fourier Transform

The Discrete Fourier Transform (DFT) is a well-established mathematical tool widely used in the field of statistical signal processing. The DFT is the equivalent of the continuous Fourier Transform (FT) but for signals known only at $N$ instants separated by sample times $T$ (i.e. a finite sequence of data). Let $f(t)$ be a continuous signal. Let $N$ samples of $f(t)$ at sample times $t_n$ be denoted as $f(n) = f_0, f_1, ..., f_{N-1}$.

The Fourier Transform of the continuous signal $f(t)$ would be

$$F(j\omega) = \int_{\infty}^{-\infty} f(t)e^{-j\omega t}dt. \tag{4.1}$$

Taking instead the discrete sequence $f(n)$, and regarding each sample $n$ in $f(n)$ as an impulse having area $f(n)$, the integrand exists only at sample points:

$$\begin{aligned} F(j\omega) &= \int_{o}^{(N-1)T} f(n)e^{-j\omega t}dt \\ &= f(0)e^{-j0} + f(1)e^{-jwT} + ... + f(N-1)e^{-jw(N-1)T} \\ &= \sum_{k=0}^{N-1} f(n)e^{-j\omega kt}. \end{aligned} \tag{4.2}$$

This could be in principle be evaluated for any $w$, but with only $N$ data points to start with, only $N$ final outputs will be significant. Considering that the DFT treats the data as if it was periodic (i.e $f(N)$ to $f(2N-1)$ is the same as $f(0)$ to $f(N-1)$) the DFT of the sequence $f(n)$ is expressed as:

$$\mathcal{F}(f(n)) = F(k) = \sum_{n=0}^{N-1} f(n)e^{-j2\pi nk/N}. \tag{4.3}$$

So, fundamentally, the DFT transforms a finite sequence of equally-spaced samples ($f(n)$) of a function into another discrete function/sequence $F(k)$ of complex numbers, such that the absolute values and arguments of the complex number sequence correspond to the amplitudes and phase shift of the frequency components $w$, which are commonly referred to as the frequency spectrum of $f(n)$.

One of the properties of the DFT is that is invertible, and therefore, one can recover the discrete function $f(n)$ from its frequency spectrum $F(k)$ by means of the Inverse Discrete Fourier Transform (IDFT):

$$\mathcal{F}'(F(k)) = f(n) = \frac{1}{N}\sum_{k=0}^{N-1} F(k)e^{j2\pi nk/N}. \tag{4.4}$$

If one wants to analyse or alter the periodic properties of a process characterised by a discrete function $f(n)$, it is possible to calculate its frequency spectrum given by $F(k)$, perform the analysis or alteration in the frequency domain, and then transform the altered frequency spectrum $F(k)'$ back to the temporal domain. This alteration is the idea beneath the STeF-map temporal representation presented in this chapter.

**Frequency Map Enhancement**

To illustrate the principles of FreMEn, let us consider a binary state such as the occupancy of a grid cell in a map. This cell state, which can be $s = \{0, 1\}$, is assumed not to be constant, but a discrete function of time $s(t)$. Consequently the uncertainty of the state $s(t)$ is represented by its probability $p(t)$.

Measuring the temporal sequence of states $s(t)$ and treating it as a signal, its frequency spectrum $S(k)$ can be calculated by means of the DFT . Then, the $m$ most prominent (i.e. of highest absolute value) coefficients of $S(k_j)$ of the spectrum $S(k)$ are selected and stored along with their frequencies $\omega_j$ in a set $P$. The function coefficients stored in $P$ are then used to recover the $p(t)$ by means of the IDFT as

$$p(t) = \zeta(\mathcal{F}'(P(k))), \tag{4.5}$$

where $\zeta$ ($\zeta(x) = \min(\max(x, 0), 1)$) denotes a saturation function that ensures that $p(t) \in [0, 1]$.

Let us assume that

$$\begin{aligned} P(s(t) = 1) &= p(t), \\ P(s(t) = 0) &= 1 - p(t). \end{aligned} \tag{4.6}$$

The $\zeta$ function ensures that both $1 - p(t)$ and $p(t)$ are always positive, i.e.,

$$P(s(t)) \geq 0 \tag{4.7}$$

for all possible states $s(t)$. The cell is always either *free* or *occupied*, i.e. the state $s(t)$ is always 0 or 1, meaning that

$$P(\{s(t) = 0\} \cup \{s(t) = 1\}) = 1. \tag{4.8}$$

for Finally, the sum of all $P(s(t))$ for all $s(t) \in \{0, 1\}$ is

$$P(\{s(t) = 1\}) + P(\{s(t) = 0\}) = p(t) + 1 - p(t) = 1. \tag{4.9}$$

Since $P(s(t)$ satisfies Equations 4.7 - 4.9, which are Kolmogorov's axioms (Kolmogorov, 1950), we can assume that $P(s(t))$ is a probability. Thus, the function $p(t)$ recovered from the frequency spectrum of $s(t)$ by Equation 4.5 represents the probability that the cell is *occupied* at time $t$.

By thresholding the probability $p(t)$ allows to calculate an estimate $s'(t)$ of the original state $s(t)$. In order not to lose any information of the original signal, the differences between $s'(t)$ and $s(t)$ are stored in an outlier set $O$.

Thus, the model of the state consists of two finite sets $P$ and $O$. The set $P$ consists of $m$ triples $\langle abs(P_j), arg(P_j), \omega_j \rangle$, which describes the amplitude, phase shifts and frequency of the model spectra. Each chosen triple could be interpreted as the importance, time offset and periodicity of one particular periodical process influencing the state $s(t)$. The number of modelled processes $m$ chosen to reconstruct the signal is referred to as the 'order' of the spectral model. The set $O$ represents a set of time intervals, during which the state $s(t)$ did not match the state $s'(t)$ calculated from $p(t)$. Figure 4.1 provides a graphic representation of the temporal model building process for a single binary state.

### 4.1.3 Building the model

The model assumes that it is provided with people detection data, containing person position, orientation and timestamp of the detection $(x, y, \theta, t)$. At the beginning of the model construction, each cell containing $k$ bins, corresponding to the discretised orientation of people motion, is associated with a temporal model. When building the model, the $x, y$ positions are discretised and assigned to the corresponding cell

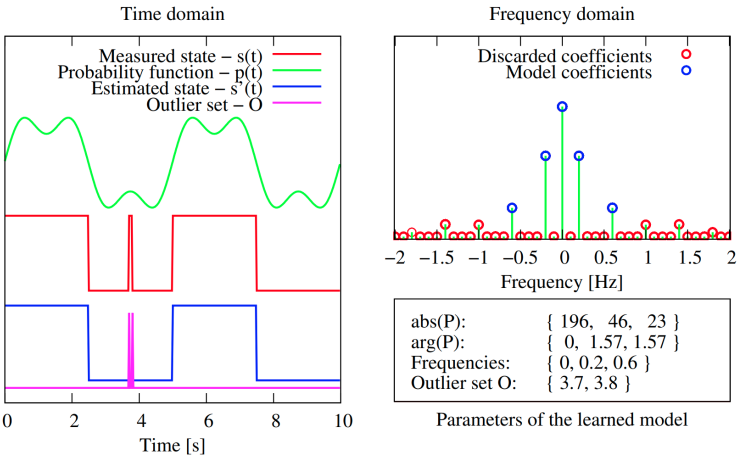


Figure 4.1: An example of a measured state and its spectral model. The left part shows the time series of the measured state $s(t)$, probability estimate $p(t)$, predicted state $s'(t)$ and outlier set $O$. The upper right part shows the absolute values of the frequency spectrum of $s(t)$ and indicates the spectral coefficients which are included in the model. The spectrum is symmetric and the spectral coefficient with frequency 0 corresponds to the mean probability of $s(t) = 1$. This model encodes two periodic processes, so the model order $m$ is 2.

and the orientation $\theta$ is assigned to one of the $k$ bins, whose value is incremented by 1. In other words, the approach counts the number of people detections occurring in each orientation bin of each cell. After a predefined interval of time, the bin values are normalised, and the values are used to update the spectra of the temporal models. In the case that during the time interval there are no people detections in a certain cell, all the bin values are set to 0, indicating that the cell was empty. After the predefined interval of time, the bin values of all cells are reset to 0 and the counting starts again.

### Updating the frequency spectrum

The Discrete Fourier Transform is applied to a discrete sequence of data $s(t)$ measured on a regular basis. This assumption of equally spaced samples allows to employ the fast Fourier Transform (FFT) algorithm to calculate the frequency spectrum in a very efficient manner (Cooley et al., 1969). However, the FFT-based model update requires recovery of the entire sequence of the observed states, which can become computationally expensive over time. Additionally, the FFT relies on the assumption that the observations of the environment states can be performed fre-

quently and on a regular basis, which is difficult to satisfy in robotic experimental settings. With this assumption the robot's activity would have to be separated into a learning phase, when it visits the different locations with a regular frequency to be able to build its environmental model, and a deployment phase when it exploits the previously built model. This means that the robot would not be able to update and adapt to variations that were not present during the learning phase, meaning that the model would become less and less reliable over time. Therefore, in order for the model to be usable in a robotic scenario, it has to allow to update the underlying dynamic models incrementally from sparse, irregular observations.

To achieve a non-uniform sampling scheme, the temporal model maintains a predefined 'sparse frequency spectrum' (Santos et al., 2017), instead of a calculating the complete one in every update. The 'sparse frequency spectrum' is defined by a set $\Gamma$ of complex numbers $\gamma_k$ for each modelled state. These correspond to the set $\Omega$ of periodicities $\omega_k$ that might be present in the modelled environment. Each time a state $s(t)$ is observed at time $t$, its temporal representation is updated with the following scheme:

$$\begin{aligned} \mu &\leftarrow \frac{1}{d+1}(d\mu + s(t)), \\ \gamma_k &\leftarrow \frac{1}{d+1}(d\gamma_k + (s(t) - \mu)e^{-jtw_k}), \quad \forall \omega_k \in \Omega, \\ d &\leftarrow d + 1, \end{aligned} \tag{4.10}$$

where $d$ represents the number of observations and $\mu$ the mean. The proposed update step is analogous to incremental averaging. The absolute values of $|\gamma_k|$ correspond to the average influence of a periodic process with frequency $\omega_k$ on the values of $s(t)$. The choice of set $\Omega$, which determines the periods of the potential cyclic processes, depends on the memory size that can be allocated for the model and the longest period that is going to be modelled. In the case of uniform sampling, the spectrum generated by Equation 4.10 and FFT are identical. However, while the set of modeled periodicities of the FFT-based method scales naturally with the duration of the data, the set of period $\Omega$ captured by the non-uniform scheme is fixed. This means that

the size of the representation is independent of the number of observations, which means that the memory requirements do not grow with time.

**Toy example**

To illustrate the process, let us take the example of a single cell in a random environment with $k = 8$ bins discretising every 45 degrees the full circumference, and with a temporal discretisation of 1 hour time intervals.

Figure 4.2a show the total people counts in each bin for the 48 time intervals composing the two days. Taking these counts, and normalising them within each interval, we obtain the distribution for each hour as shown in Figure 4.2b. The values of these normalised histograms are then the input given to the temporal spectral model. When building the model, the total number of detections in each bin is not used, and only the relative number of occurrences among all $k$ orientations are maintained.

### 4.1.4 Making predictions

As mentioned previously, the flow model is based on a spectral temporal representation. Applying the IDFT to recover the original function provides a function which is infinite in time, giving the ability to predict the probability of any state at any time in the past or future. This assumes that the human motion in each cell can be modelled by a combination of periodicities, which may be present due to the cyclical nature of human activities, such as the 24-hour circadian rhythm (Panda et al., 2002).

To predict the behaviour of human movement through a cell at a time $t$, first the set of values $\gamma_k$ is calculated for each cell and the orientations are sorted in descending order according to the absolute values $|\gamma_k|$. Then, the first $m$ elements $\gamma_j$ are extracted along with their corresponding frequencies $w_j$, magnitudes $\alpha_j = |\gamma_j|$ and phase shifts $\varphi_j = arg(\gamma_j)$. So, the probability for each discretised orientation $\theta$, ($\theta = i\frac{2\pi}{k}$ and $i \in \{0 \dots k-1\}$) for time $t$ is computed as:

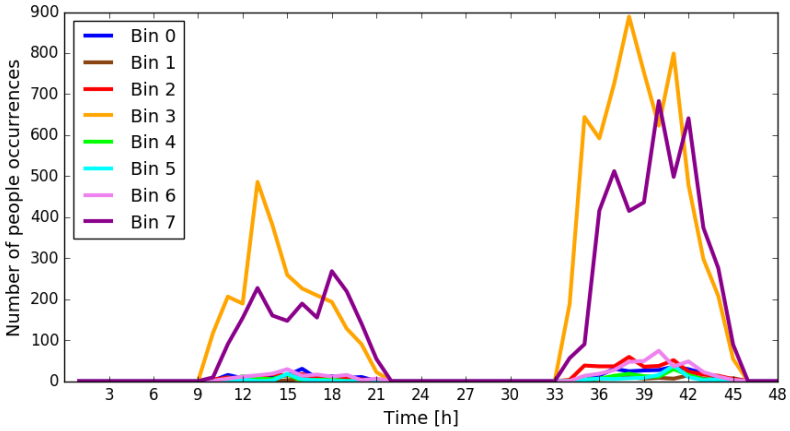


(a)

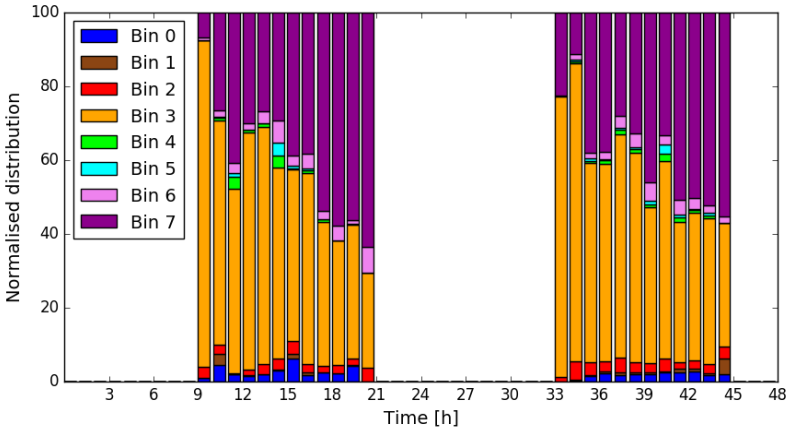


(b)

Figure 4.2: (a) Total counts per bin over two day using 1 hour interval. (b) Normalised distributions in each predefined interval.

$$p_\theta(t) = \alpha_0 + \sum_{j=1}^{m} \alpha_j \cos(\omega_j t + \varphi_j). \tag{4.11}$$

where $\alpha_0$ is the stationary probability (zero frequency).

The choice of $m$ determines how many periodic processes are considered for prediction. Setting $m$ too low means omitting other less prominent environment processes, while setting it too high might decrease the generalisation capabilities of the model. The choice of set $\Omega$, which determines the periods of the potential cyclic processes, depends on the memory size that can be allocated for the model and the potential longest period that needs to be modelled.

Each $p_\theta(t)$ function is independent from the other bins in the cell, hence for a pre-

dicted instant of time it may happen that the sum of all $k$ predicted probabilities can sum more than 1. To avoid this problem, a normalisation step is applied for each $t$ as:

$$p_{\theta\ norm}(t) = p_\theta(t) / \sum_{i=0}^{i=k-1} p_i(t), \tag{4.12}$$

### Toy example

Following the example introduced in Section 4.1.3, let us assume that a STeF-map model containing a single cell with $k = 8$ orientations has been updated with the data shown in Figure 4.2.

Figure 4.3 shows the frequency spectra obtained for bins 3 and 7, which are the ones containing more people detections, with the frequency distribution defined in Equation 4.13 after the two training days. Both bins present similar spectra distribution with two peaks around the frequencies of $\frac{7}{week} = \frac{1}{24h}$ and $\frac{14}{week} = \frac{1}{12h}$, however the phases values for those two frequencies, which are $\phi_{bin3}\{\frac{1}{24h}, \frac{1}{12h}\} = \{-2.85, 0.48\}$ and $\phi_{bin7}\{\frac{1}{24h}, \frac{1}{12h}\} = \{-1.18, -2.36\}$, indicate that both states present a different phase shift.

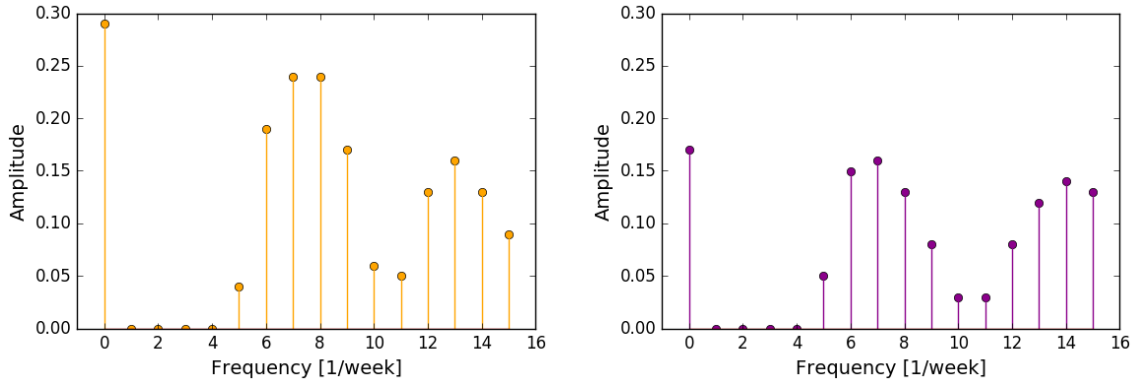


(a) $bin = 3$ (b) $bin = 7$

Figure 4.3: Frequency spectra for $bin = 3, 7$ in the cell example.

The results of the Inverse Fourier Transform applied to all bins from $m = 0$ (constant value) to $m = 7$ (taking the seven spectral components with higher magnitude) can be seen in Figure 4.4. As expected from the input orientation distributions given to

the STeF-map model, the bins 3 and 7 are the predominant orientations. However, both orientations do not completely overlap, instead they have an offset of around 3 hours according to the functions obtained with $m = 1$ and onward. The number of spectral components also affects the shape and amplitude of the function. For example, with $m = 1$ the waves obtained for each bin correspond to a pure sinusoidal wave. As more spectral components are added ($m = 2, 3, 4...$) the amplitude tends to increase due to the addition of the multiple harmonic components.

In order to standardise the outputs, the normalisation step defined in Equation 4.12 is applied, obtaining the outcome presented in Figure 4.5. The results show that after two days of training, the model is able to predict that during certain parts of the day, the probability of finding people moving in the direction defined by bin 3 is higher during the morning with respect to bin 7. But as the predictions are not static in time, the orientation defined by bin 7 becomes more predominant in the afternoon.

## 4.2 Quantitative Evaluation

To evaluate the Spatio-Temporal Flow Map (STeF-map) model presented, a set of experiments have been carried out using the dataset taken from the literature, plus the two datasets recorded by the author (described in Chapter 3). All of them provide people detections with information containing at least the person position, orientation and timestamp of the detection $(x, y, \alpha, t)$, which provides the minimum information required to build the STeF-map.

The experiments are aimed at analysing the generalisation and prediction capabilities of the model, evaluating the improvement of using the spectral-based representation over a static one. Following an approach used in the machine learning field, for the evaluation, the available amount of days in each dataset have been divided into three subsets, training, validation and testing (none of the days overlap with the ones from other subsets):

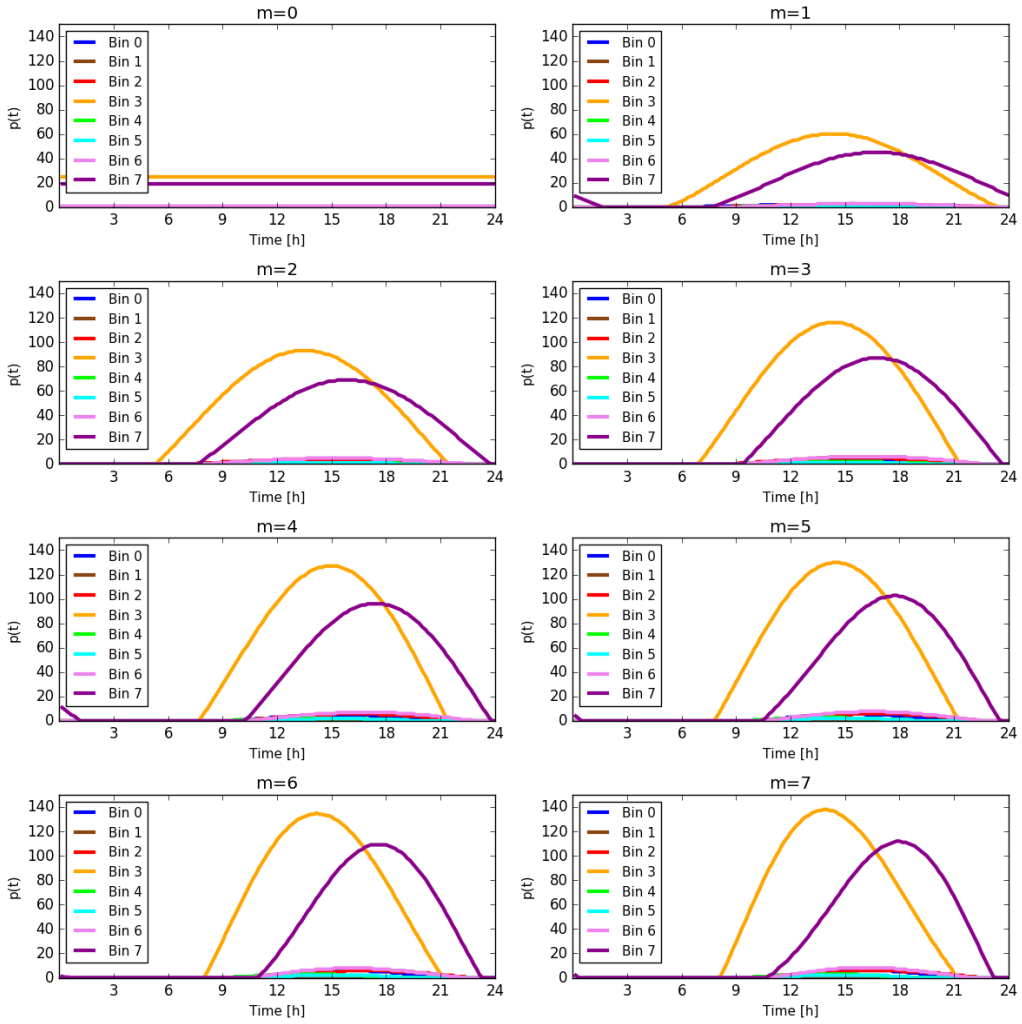


Figure 4.4: Output without normalisation for each of the $k = 8$ bins with different model orders ($m = 0, 1, 2, 3, 4, 5, 6, 7$).

- Training: the days in this subset are used to build the model, as described in Section 4.1.3.
- Validation: the validation days are used to find the model order ($m$) that fits best for each cell.
- Testing: these days are the ones used to compute the actual model prediction performance.

### 4.2.1 Model building parameters

In the experiments, the space is discretised into $1 \times 1$ meter cells for all environments, resulting in a total of $C = 1248$ , $C = 117$ and $C = 126$ active cells, respectively,

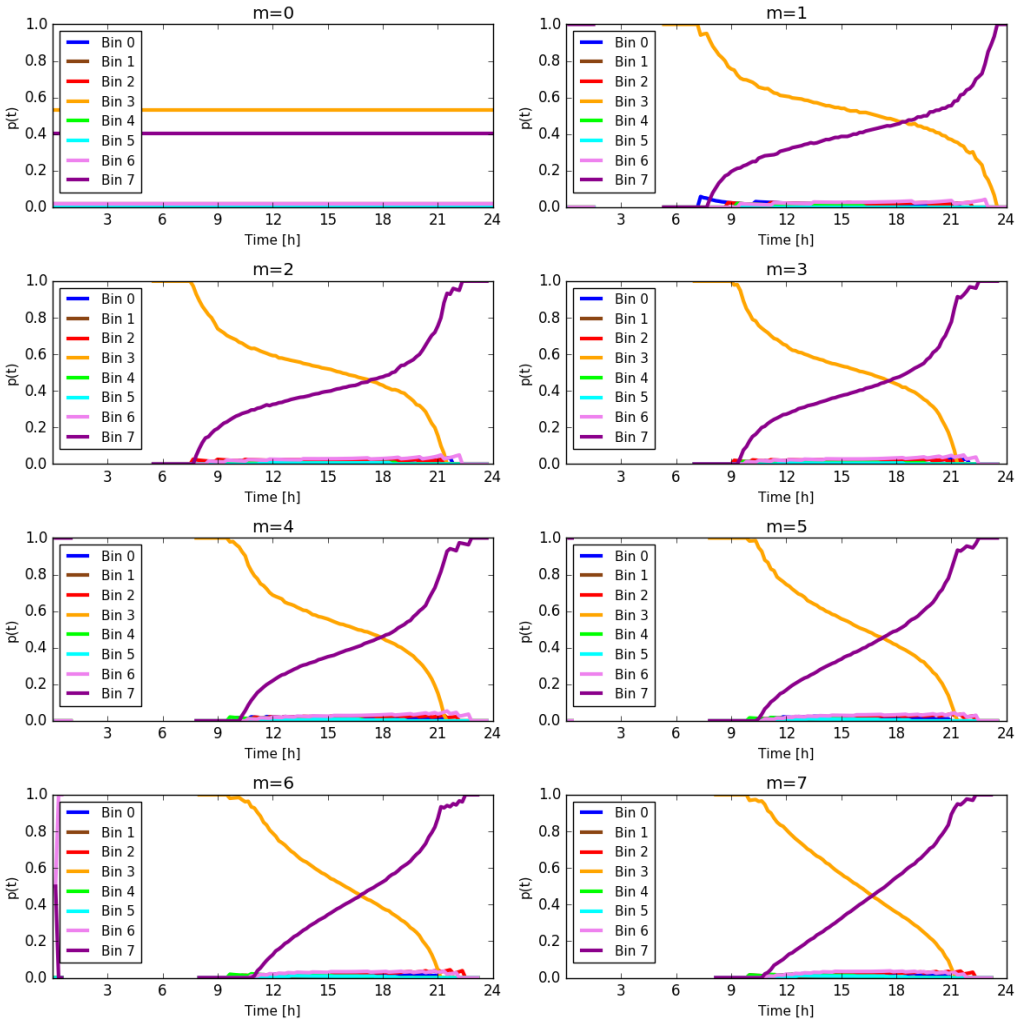


Figure 4.5: Normalised output for each of the $k = 8$ bins with different model orders ($m = 0, 1, 2, 3, 4, 5, 6, 7$).

where a cell is considered to be 'active' if it contains at least one detection during the training days.

The number of bins chosen to discretise the orientations is $k = 8$, distributed as shown in Figure 4.6, which divides the full circumference into eight bins, each covering 45 degrees. Regarding time, for all the environments the intervals for creating the histograms used as the input for the STeF-map model is set to 10 min. However, for each dataset a different number of training days was used depending on the availability for each environment. The division of the days in each subset for the three environments can be found in Table 4.1. For the Corridor and Office datasets

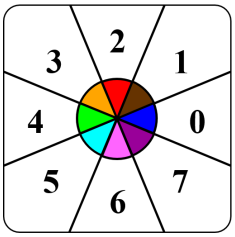


Figure 4.6: Bin discretisation.

the total number of available days were used, but for the ATC dataset only half of the total 92 available days were used.

| Dataset | Train | Validate | Test | Cell size | Cells (C) |
|---|---|---|---|---|---|
| ATC | 42 days | 2 days | 2 days | 1×1 m | 1248 |
| Corridor | 10 days | 2 days | 2 days | 1×1 m | 117 |
| Office | 18 days | 2 days | 2 days | 1×1 m | 126 |

Table 4.1: Summary of the spatial and temporal parameters used in each data set.

For the prediction, the spectral components $\omega_j$ are drawn from a set $\Omega$ of $\omega_k$ periodicities ranging from hours to 1 week with the following distribution:

$$\omega_k = \frac{7 \cdot 24 \cdot 3600}{1+s}, \quad s \in 0, 1, 2, 3, 4, ..., 15 \tag{4.13}$$

### 4.2.2 Evaluation metric

In order to compare the performance of the different models, a metric is needed to evaluate how good the predictions are when compared to the ground truth.

The output of the trained spectral models provides a function for each orientation in each cell. So, for every time $t$, we can obtain a normalised distribution describing how probable it is to find a person moving in each direction (Figure 4.5). However, obtaining the same orientation distribution with real data at a single time instance $t$ is not possible, because we cannot count sufficient detections to build a meaningful distribution. Instead, the proposed idea is to compare the distribution obtained with the predictions against the ground truth during a defined interval of time. Then, assuming both prediction and ground truth histograms are normalised, in order to compare the similarity between them, the Chi-squared ($\chi^2$) distance is used.

The $\chi^2$ histogram distance comes from the $\chi^2$ test-statistic (Cochran, 1952), where it is used to test the fit between a distribution and the observed frequencies. This is a common bin-to-bin distance for comparing histograms (Pele et al., 2010), which has been successfully applied in different domains such as texture and object categories classification (Cula et al., 2004; Zhang et al., 2007; Varma et al., 2008), near duplicate image identification (D. Xu et al., 2010), matching of local descriptors (Forssén et al., 2007) or shape classification (Belongie et al., 2002; Ling et al., 2007).

In this work, the $\chi^2$ distance indicates the level of similarity between the predicted and ground truth discrete human motion distributions. The higher the distance, the less accurate is the model prediction compared to the ground truth. The total distance of a whole map for a single interval can be defined as:

$$\chi^2_{map} = \sum_{c=1}^{C} \left( \sum_{b=1}^{k} \frac{(x_b - y_b)^2}{(x_b + y_b)} \right), \tag{4.14}$$

where $C$ is the number of active cells in the map, $k$ is the number of angular bins, $x_b$ is the value of bin $b$ in the predicted orientation histogram, and $y_b$ is the value of the same bin $b$ obtained from the ground truth data.

Since the $\chi^2$ distance is not a very intuitive measure as it has no units, in the results section the prediction accuracy is expressed as a percentage of how much better or worse the model prediction is compared to the distance obtained with the prediction with $m = 0$ . With $m = 0$, the prediction corresponds to the average value of all the past data and is kept as a constant value over time (no frequency components).

### 4.2.3 Results

In this section the results obtained for each of the three datasets is presented. For each one, two evaluation procedures have been tested. One where all the cells in the environment are predicted with a fixed number of $m$ spectral components, i.e. without taking into account the validation days, and another where the validation days are used to choose the best $m$ for each cell, values then used for the prediction in the testing days. For every $m$ combination chosen, the prediction accuracy is

computed for multiple time intervals: 10min, 30min, 1h, 2h, 3h, 4h and 6h, which divide the 24-hour period corresponding to one day into 144, 48, 24, 12, 8, 6 and 4 intervals respectively. From those intervals, only the ones containing at least one detection in the ground truth are considered for the final $\chi^2$ distance calculation.

Moreover, for the case of the 2 h time interval, the map of the environment is drawn with the best model order $m$ for each cell using the respective validation days, together with the temporal evolution of the prediction accuracy with respect to the model predicted with $m = 0$ along the training days.

### ATC dataset

The prediction results for this dataset after 42 days of training are summarised in Table 4.2, showing clear improvement over a static model (constant in time, namely $m = 0$) for all combinations. Looking at the temporal evolution in Figure 4.8, we see that this improvement is achieved from the very beginning of the training days, and it is kept slightly but consistently better as the day passes and the model is updated with more data. From the Table 4.2 it is clear that the more spectral components used for prediction, the better the improvement obtained, however the improvement step decreases with each component addition. It is also interesting to see that even when the $m$ value is fixed for all cells in the map, for most combinations the results obtained also improve the constant model prediction. This is a somehow a reasonable result if we look at Figure 4.7, which shows the model order $m$ obtaining the lowest $\chi^2$ distance for each cell for the two validation days. The fact that almost 84% of the cells in the map obtain better results when $m > 0$ explain why the results are better even when using a fixed value of $m$.

### Corridor dataset

In this second dataset, the results obtained tell that the improvement achieved by including the temporal dimension in the prediction is greater (Table 4.3). However, for this environment, adding more spectral components to the prediction does not mean an increase in prediction accuracy, but the optimal result is achieved with $m = 2$. For example, with the fixed $m = 5$, the system predicts worse results than

| Spectral Components | | Interval | | | | | | |
|---|---|---|---|---|---|---|---|---|
| | | 10' | 30' | 1h | 2h | 3h | 4h | 6h |
| fixed m | m = 0 | 0.0 | 0.0 | 0.0 | 0.0 | 0.0 | 0.0 | 0.0 |
| | m = 1 | -0.7 | -0.5 | -0.2 | 0.2 | 1.3 | 0.7 | 1.2 |
| | m = 2 | -0.6 | -0.2 | 0.5 | 1.3 | 2.4 | 2.6 | 3.0 |
| | m = 3 | -0.4 | 0.1 | 1.1 | 2.5 | 2.8 | 4.4 | 3.8 |
| | m = 4 | -0.1 | 0.6 | 1.6 | 3.1 | 3.9 | 5.3 | 4.7 |
| | m = 5 | 0.0 | 0.8 | 1.9 | 3.3 | 4.4 | 5.3 | 5.6 |
| variable m | m = 0/1 | 0.1 | 0.3 | 0.6 | 0.8 | 2.0 | 1.2 | 1.9 |
| | m = 0/1/2 | 0.4 | 0.8 | 1.3 | 1.9 | 3.1 | 2.8 | 3.5 |
| | m = 0/1/2/3 | 0.6 | 1.2 | 2.0 | 3.1 | 3.7 | 4.4 | 4.6 |
| | m = 0/1/2/3/4 | 0.9 | 1.6 | 2.6 | 3.6 | 4.5 | 5.1 | 5.4 |
| | m = 0/1/2/3/4/5 | 1.0 | 1.8 | 2.7 | 3.8 | 4.9 | 5.2 | 5.9 |

Table 4.2: STeF-Map prediction results (in % with respect the $\chi^2$ distance obtained with $m = 0$) for the ATC dataset.

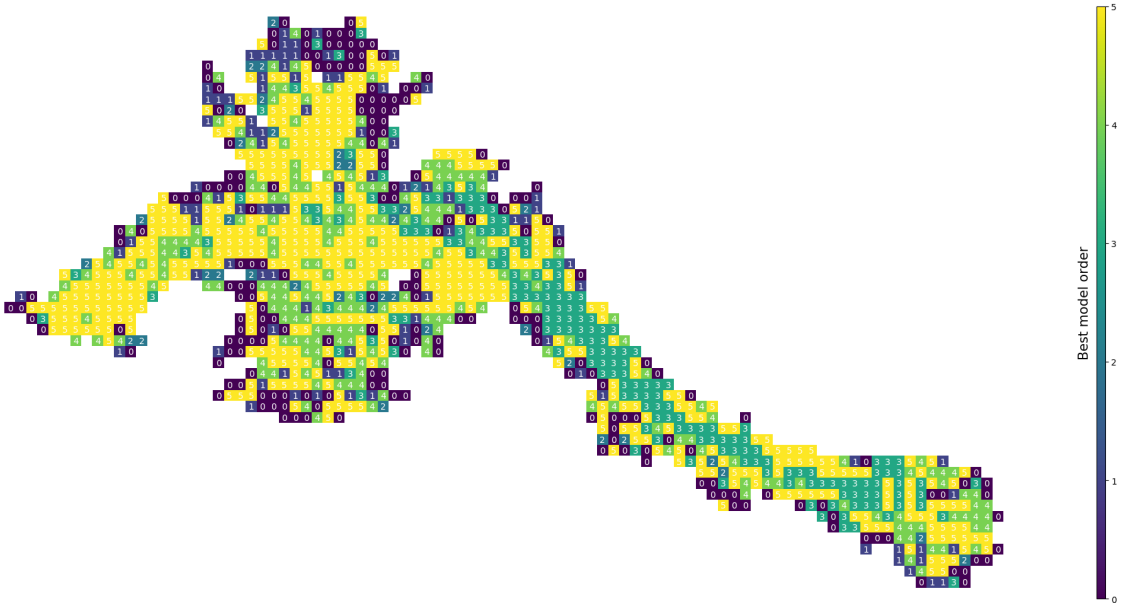


Figure 4.7: Best order ($m = 0/1/2/3/4/5$) estimated using the 2 validation days, after the 42 training days using 2 h intervals for the $\chi^2$ distance calculation.

with $m = 0$ when the intervals are short (10', 30' and 1h). Nonetheless, even with a fixed $m$ value, the overall result at end of the training days is positive due again to a majority of cells (53% in Figure 4.9) which have an optimal $m$ value greater than 0. I say "at the end of the training day" because looking at Figure 4.10, it can be noticed that during the first days of the training phase, the prediction accuracy is worse than for the static model. Probably the fact that this dataset contains fewer

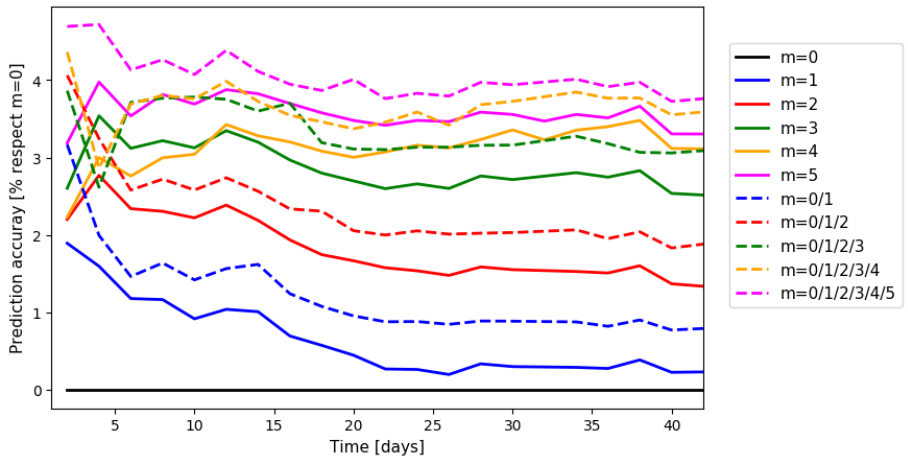


Figure 4.8: Temporal evolution of the prediction accuracy with respect the model predicted with $m = 0$ along the 42 training days.

| Spectral Components | | Interval | | | | | | |
|---|---|---|---|---|---|---|---|---|
| | | 10' | 30' | 1h | 2h | 3h | 4h | 6h |
| fixed m | m = 0 | 0.0 | 0.0 | 0.0 | 0.0 | 0.0 | 0.0 | 0.0 |
| | m = 1 | -5.7 | -3.6 | -1.0 | 06.9 | 8.0 | 13.2 | 17.2 |
| | m = 2 | 15.8 | 16.4 | 17.0 | 18.5 | 18.5 | 21.4 | 23.2 |
| | m = 3 | 10.8 | 11.8 | 12.1 | 15.3 | 10.8 | 19.5 | 19.7 |
| | m = 4 | 3.3 | 05.1 | 08.8 | 15.5 | 16.3 | 21.4 | 23.2 |
| | m = 5 | -6.7 | -5.3 | -2.8 | 6.6 | 9.8 | 18.3 | 20.5 |
| variable m | m = 0/1 | 5.6 | 5.6 | 7.2 | 9.9 | 10.3 | 14.8 | 16.7 |
| | m = 0/1/2 | 11.6 | 11.0 | 13.5 | 15.0 | 13.6 | 15.8 | 17.4 |
| | m = 0/1/2/3 | 11.3 | 10.5 | 12.6 | 13.8 | 14.0 | 15.7 | 16.5 |
| | m = 0/1/2/3/4 | 10.4 | 09.7 | 12.4 | 13.8 | 13.9 | 15.0 | 16.7 |
| | m = 0/1/2/3/4/5 | 10.0 | 09.3 | 11.9 | 13.1 | 13.6 | 15.5 | 16.0 |

Table 4.3: STeF-Map prediction results (in % with respect the $\chi^2$ distance obtained with $m = 0$) for the Corridor dataset

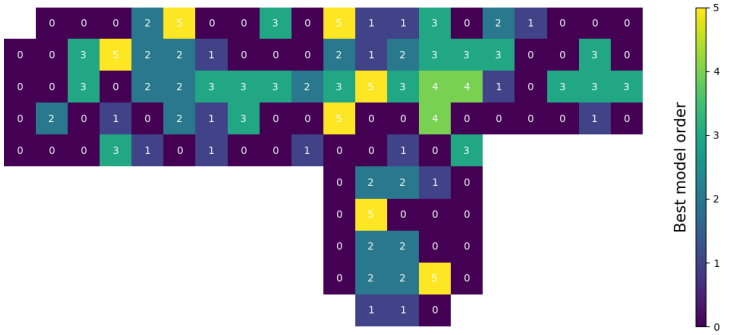


Figure 4.9: Best order ($m$) estimated using the 2 validation days, after the 10 training days using 2 h intervals for the $\chi^2$ distance calculation.

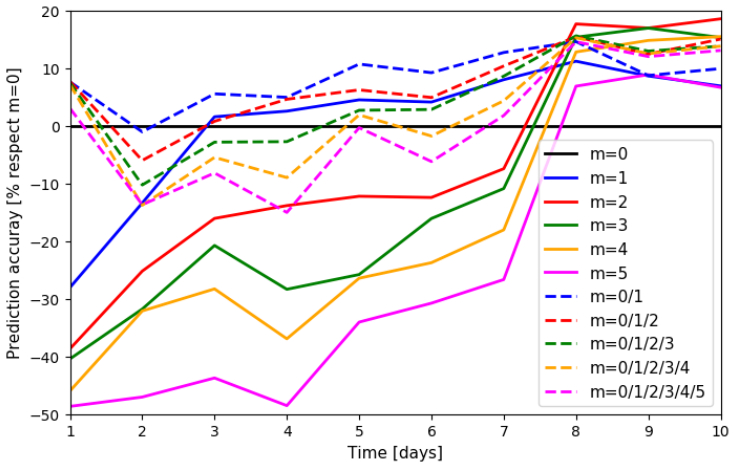


Figure 4.10: Temporal evolution of the prediction accuracy with respect the model predicted with $m = 0$ along the 10 training days.

people detections compared with the first dataset, and the days are more sparse, makes the learning of the frequency spectra components more challenging.

### Office dataset

In this third environment, a new case is presented in that only 42% of the cells (Figure 4.11), according to the validation days, are best suited to be represented with at least 1 spectral frequency component. This creates the result that when the value $m$ is fixed for all the cells (Table 4.4), the prediction results are worse when compared with $m = 0$, regardless of the time granularity. This is also confirmed by taking a look at the temporal evolution in Figure 4.12, where at any point in time the models with fixed $m$ show a better performance.

Nonetheless, when the value $m$ is chosen for each cell using the validation days to make the prediction, the results show a slight but consistently better performance than a model which does not take into account the temporal aspect. As in the previous Corridor dataset, there is no relation between adding more spectral components to an increase in prediction accuracy, obtaining in general the best results with just 1 or 2 components.

| Spectral Components | | Interval | | | | | | |
|---|---|---|---|---|---|---|---|---|
| | | 10' | 30' | 1h | 2h | 3h | 4h | 6h |
| fixed m | m = 0 | 0.0 | 0.0 | 0.0 | 0.0 | 0.0 | 0.0 | 0.0 |
| | m = 1 | -1.9 | -2.7 | -2.3 | -0.7 | -1.6 | -1.8 | -0.8 |
| | m = 2 | -2.3 | -2.8 | -3.3 | -2.7 | -2.9 | -1.3 | -5.6 |
| | m = 3 | -3.6 | -4.9 | -5.8 | -6.5 | -8.3 | -7.9 | -8.9 |
| | m = 4 | -3.0 | -4.2 | -4.8 | -5.4 | -6.9 | -6.7 | -9.4 |
| | m = 5 | -3.9 | -5.6 | -5.9 | -6.3 | -8.2 | -8.5 | -9.9 |
| variable m | m = 0/1 | 0.5 | 0.7 | 1.1 | 2.4 | 2.0 | 3.2 | 4.4 |
| | m = 0/1/2 | 0.2 | 0.8 | 0.8 | 1.0 | 1.8 | 3.5 | 4.6 |
| | m = 0/1/2/3 | 0.0 | 0.6 | 0.6 | 1.2 | 2.0 | 3.3 | 4.0 |
| | m = 0/1/2/3/4 | -0.1 | 0.7 | 0.8 | 1.4 | 2.8 | 3.1 | 3.7 |
| | m = 0/1/2/3/4/5 | 0.1 | 0.5 | 0.7 | 1.1 | 2.6 | 2.8 | 3.2 |

Table 4.4: STeF-Map prediction results (in % with respect the $\chi^2$ distance obtained with $m = 0$ for the Office dataset.

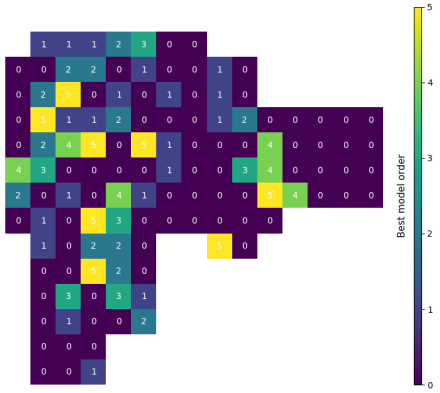


Figure 4.11: Best order ($m$) estimated using the 2 validation days, after the 18 training days using 2 h intervals for the $\chi^2$ distance calculation.

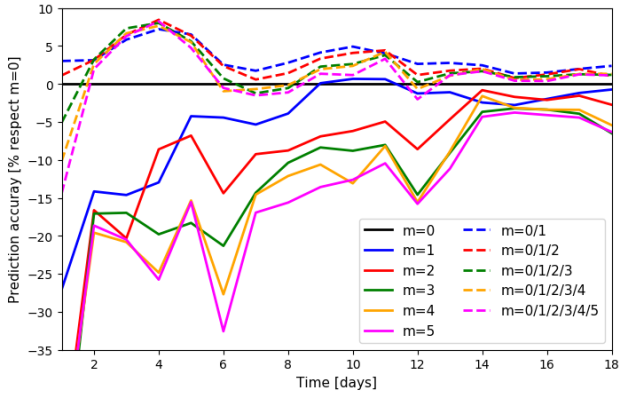


Figure 4.12: Temporal evolution of the prediction accuracy with respect the model predicted with $m = 0$ along the 18 training days.

**Summary**

As a general overview, the experiments show that although not all the dynamics in the cells are periodic, taking into account the rhythmic patterns enables us to calculate more accurate predictions of people movement compared to models that neglect the temporal domain. In all cases, using longer time intervals for the results increases the relative improvement percentage in exchange for a coarser temporal grid, however adding more frequency components does not always lead to better predictions results, as observed with the Corridor and Office datasets.

Moreover, the results show that fixing an $m$ value for all the cells in the map is not always a good strategy, as it depends on the characteristics of the environment, namely on the amount of cells that perform better with just a static model over time. Checking the best order map for each dataset (especially noticeable in the first two environments), the cells which are best represented with $m = 0$ tend to be at the edges of the reachable map. Probably the fact that the human activity on those areas is lower than in the middle areas makes it more difficult for the model to learn a generalisation, as the input data is much more sparse and less representative.

## 4.3 Qualitative evaluation

For a better understanding of the approach, the results obtained and the model capabilities, a qualitative evaluation of the STeF-map has been also performed. In the attempt of doing so, a set of maps has been drawn for both the ground truth and model predictions, explicitly showing the main flow per cell at different time intervals.

For the ground truth, the orientation chosen in each cell corresponds to the one with the highest number of occurrences over a time interval specified ($\Delta t$). While, for the model prediction, the cumulative probability values are computed in the same time interval ($\Delta t$) for all the orientations and one with the largest number is picked:

$$cell_o = \arg\max(\int_{\Delta t} p_\theta(t)), \qquad \theta \in i\frac{2\pi}{k}, \;\; i \in \{0, 1, \ldots, k-1\}. \tag{4.15}$$

In the case where all orientations present zero occurrences for the ground truth, or zero probability on the prediction side, the cell will be presented as empty. The results obtained for all three datasets are presented in the following subsections. In all three cases, the day selected for representation purposes was the first day of the testing subset.

### ATC dataset

The model chosen for presentation in Figure 4.13 is of order 5, meaning that we are taking the 5 most prominent spectral components. The interval time selected is 4 hours, so the ground truth and predictions are calculated from 09:00 to 13:00, from 13:00 to 17:00, and from 17:00 to 21:00. Looking at the ground truth (Figure 4.13(a)), one quickly notices both the central square area and the "West" corridor present a noticeable change in the flow during the day. In the former, the flow of people changes from the "West" direction (green) in the morning to the "East" direction (dark blue) in the afternoon, while in the latter, the changes occurs from "North-West" (orange) to "South-East" (purple). Checking the same intervals for the orientations predicted (Figure 4.13(b)), in both cases the model is able to capture and learn the periodicities occurring, being able to predict those changes with a high degree of fidelity for future states. It can be also noticed that the model is able to capture that the people tend to walk on the left side when traversing corridors, as happens in the "East" one (light blue and brown arrows) and the "West" one (purple and orange arrows).

### Corridor dataset

For the Corridor dataset, it was decided to plot the results taking only two periodicities, as this produced the best results in the quantitative, picking intervals of 2 hours. The results shown in Figure 4.14 correspond to the intervals from 08:00 to 10:00, from 12:00 to 14:00 and from 16:00 to 18:00. The biggest change in flow occurring in the scenario is in the central area, alternating from "West" to "East" as the day progresses. And, although the change is not as pronounced as in the previous dataset, there is definitely a certain number of cells whose associated human

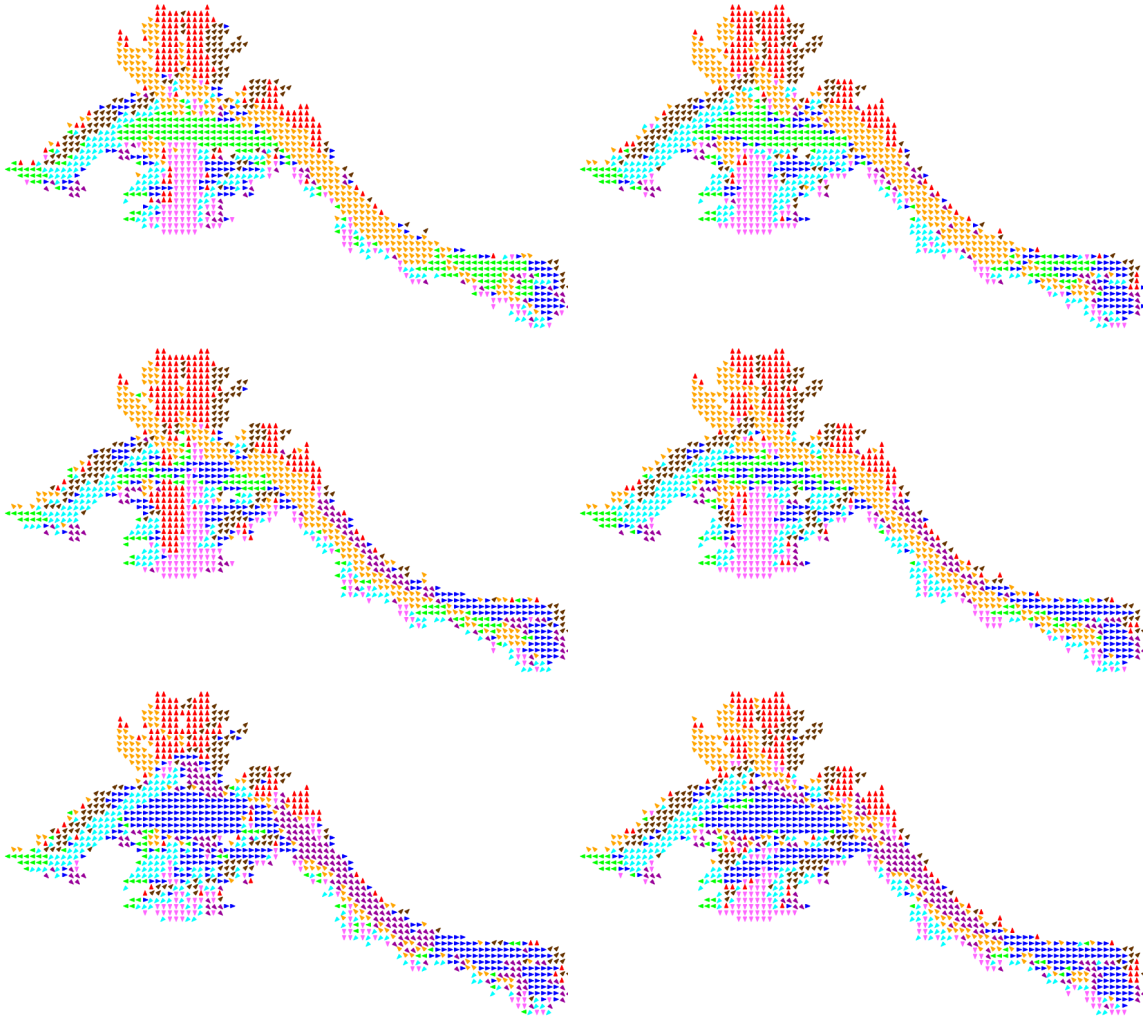

(a) Ground truth (b) Model prediction

Figure 4.13: Ground truth vs model prediction for 3 different 4 hour intervals in the ATC dataset. From top to bottom: 9:00–13:00, 13:00–17:00 and 17:00–21:00.

behaviour is changing over time. It can be noticed also that, although the ground truth presents empty cells in many cases (see Figure 4.14(a) 8:00-10:00), the model is able to make a generalisation of the past observations and provide a meaningful prediction.

### Office dataset

In this third scenario, the results are quite similar to the ones obtained in the previous one, in the sense that only a few cells placed in the center of the map change their predominant orientation over the day. These make reference to people entering the

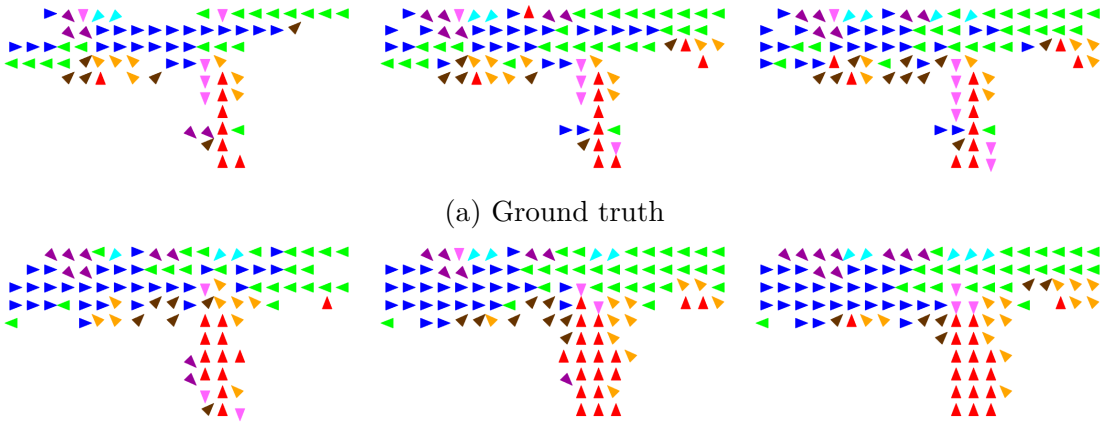

(a) Ground truth

(b) Model prediction

Figure 4.14: Ground truth vs model prediction for 3 different 2 hour intervals in the Corridor dataset. From left to right: 8:00–10:00, 12:00–14:00 and 16:00–18:00.

office during morning hours (arrows in blue pointing to the "West" direction) and leaving from work in the afternoon (arrows in green pointing to the "East" direction).

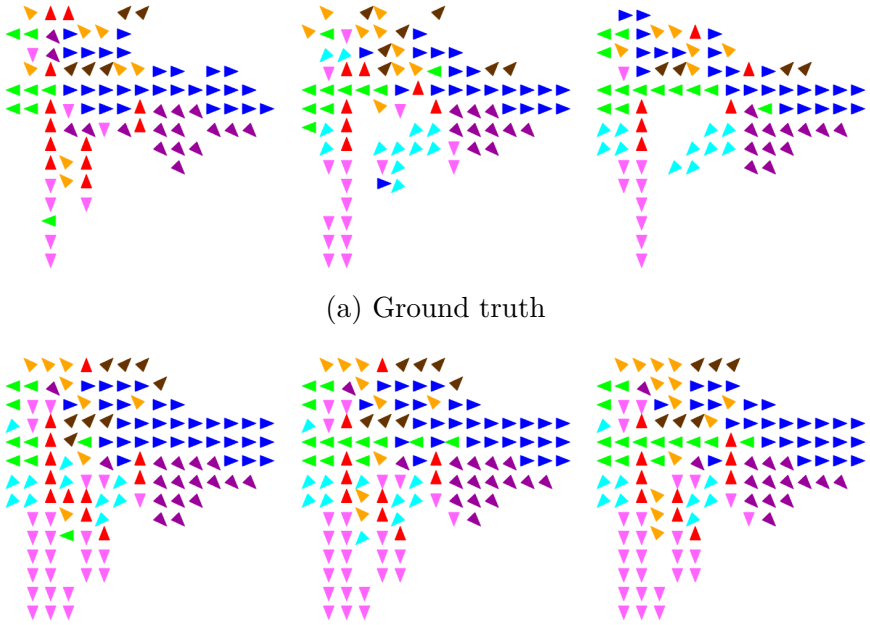

(a) Ground truth

(b) Model prediction

Figure 4.15: Ground truth vs model prediction for 3 different 2 hour intervals in the Office dataset. From left to right: 8:00–10:00, 12:00–14:00 and 16:00–18:00

## 4.4 Summary

In this chapter, the Spatio-Temporal Flow map (STeF-map) has been described and a set of experiments to exemplify the contribution of this new approach in the human motion modelling field have been carried out. The model assumes long-term temporal human motion patterns to learn a probabilistic grid-based map of people motion. In contrast to most of the literature reviewed, the probabilities in each cell are treated as a function in time, which is modelled by a combination of harmonic components that allow a generalisation of the human behaviour at each discretised point in the map. This representation allows a very compact model that does not increase in size over time and it is very computationally efficient. This makes it is suitable and easier to scale modelling much larger environments when compared with for example Gaussian Processes, which are much slower to run. Another advantage of using the spectral analysis for the model is that the temporal patterns/periodicities can be found and adjusted on the fly. Moreover, the model is capable of being updated with sparse data in space and time, allowing it to be used in mobile robot systems where regular data gathering is not possible.

In the work carried out during this thesis, the STeF-map model has been applied to model mainly spatio-temporal pedestrian motion. However, the representation is very flexible and, without any major changes, could be applied in many other fields. The only data input requirement is a timestamp together with a position and a orientation, which could come from any moving entity (vehicles, other robots, animals, wind, etc.).

### 4.4.1 Limitations

STeF-map has numerous advantages summarised in the previous section. However, as with any other method, it suffers from certain limitations. First, the model introduces a strong assumption that the human activities present periodic patterns over time that can be learned, which may not always be the case in all environments. This assumption can be countered by the fact that each cell can contain the best fit

regarding the frequency components, however the cyclicality is still an assumption that is not always present.

In order to achieve a sparse temporal update of the frequency spectra, it is necessary to define beforehand a set of fixed "available" periodicities to be used. As those periodicities are defined before starting to gather any information and are never changed again later, it may happen that the periodicities chosen do not reflect the temporal patterns present in the environment which may lead to a decrease in prediction accuracy.

Similar to the temporal issue aforementioned, the proposed representation in space is discrete and parametric, introducing a bias on how the flow looks. All the measures gathered within the boundaries of the spatial cell are accumulated in the center of the cell, so depending on the cell size we can lose some local patterns in pursuit of greater generalisation. The orientations are also discretised into only 8 possible orientations, meaning that motion patterns whose orientation differs by less than $\pi/4$ are merged. Moreover, the effect of the parameterisation is increased by the fact that it is not considered any spatial relation between the adjacent cells, as all of them contain independent models. So for example, seeing a "North" flow at the "South" end of a corridor at time $t$, could set a strong prior that there will be a "North" flow at the "North" end at $t + 1$ which right now is not exploited.

Finally, as STeF-map is presented here, the people density is lost as the detections counted per orientation are normalised at the end of the time interval. This intensity information could be useful in the prediction stage, as it could be exploited together with prediction of the main direction of flow as an extra input for the robot's path planning and navigation algorithms (Tipaldi et al., 2011).

# Chapter 5

# Comparison of human motion models

In the previous chapter, the STeF-map representation was introduced. The time-dependent representation was evaluated and compared against a non-time-dependent version, which provides a constant, averaged model of the previously observed data. In this chapter, the experimental evaluation is extended with a comparison to other state-of-the-art methods in the literature for human motion modelling. The comparison is done in a two-fold way. The first part is aimed at evaluating the prediction quality of the different models, and the second part is aimed at performing a social cost-based evaluation, to indicate how useful these models would potentially be for robots moving in human-populated environments.

This chapter is divided into three main sections. In Section 5.1 the models included in the comparison are explained, together with a qualitative evaluation of their representation characteristics, Section 5.2 addresses the human motion prediction evaluation, and Section 5.3 presents the social cost comparison.

## 5.1 Evaluated approaches

In this section the models are described and a table with a qualitative evaluation defining their main characteristics is presented. The models compared against the STeF-map representation are:

- Warped Hypertime (WHyTe) (Krajnik et al., 2019),
- Directional Grid Maps (DGM) (Senanayake et al., 2018),
- Circular Linear Flow Field (CLiFF-map) (Kucner et al., 2017), and a

- Long Short Term Memory (LSTM) network (Hochreiter et al., 1997).

All of the method's original authors (Tomas Krajnik, Tomas Vintr, Ransalu Senanayake and Tomasz Kucner) were involved in the study, with the exception of the LSTM, which was implemented by George Broughton, and agreed on the protocols and metrics.

### 5.1.1 Warped Hypertime (WHyTe)

The general idea of WHyTe (Krajnik et al., 2019) is the projection of linear time $t$ onto a set of circles, where every circle is derived from a periodicity found in the data to model. Assuming, for example, that the model is given a set of $l$ measurements of a given phenomenon, containing tuples $(a_i, \mathbf{x}_i, t_i)$, where $i \in 1, ..., l$, the vector $\mathbf{x}_i$ describes the location of the measurement (e.g. position of a detected person or obstacle), $t_i$ corresponds to the time of the measurement and $a_i$ represents the measurement value, (e.g. number of detected persons or likelihood of an obstacle in the vicinity of $(\mathbf{x}_i, t_i)$,respectively). This method aims to find a $p(a|\mathbf{x}, t)$, which would represent the conditional probability density function of the variable $a$ given the position $\mathbf{x}$ and time $t$. To do so, the proposed approach is composed of five stages:

- initialisation;
- spatio-temporal clustering;
- model error estimation;
- identification of periodicities;
- hypertime space extension.

To *initialise* the algorithm, all measurements $(a_i, x_i)$ are first stored in ${}^h x_i$, where $h$ corresponds to the number of known periodicities. Since during initialisation, the number of periodicities is unknown, $h$ is set to 0.

In the *spatio-temporal clustering* step, the vectors $({}^h x_i)$ are clustered, obtaining a Gaussian mixture model using the Expectation Maximisation algorithm, which rep-

resent the spatio-temporal distribution of the given phenomenon ($p(a, x, t)$) and allows to calculate conditional probability function $p_h(a|x, t)$ as

$$p(a, \mathbf{x}, t) = \beta \sum_{j=1}^{n} w_j u_j(a, \mathbf{x}, {}^h\mathbf{t}), \tag{5.1}$$

where $u_j(a, \mathbf{x}, {}^h\mathbf{t})$ is a multivariate Gaussian function of the $j^{th}$ cluster, $w_j$ is the cluster weight, ${}^h\mathbf{t} = (\cos(2\pi\frac{t}{T_1}), \sin(2\pi\frac{t}{T_1}), ..., \cos(2\pi\frac{t}{T_h}), \sin(2\pi\frac{t}{T_h}))$ is the projection of time in the hypertime space and $\beta$ is a scaling constant.

In the *model error estimation*, the mean $\mu_i$ of $p_h(a|x, t)$ is calculated for all training samples. the error time series ${}^h\epsilon(t_i)$ as ${}^h\epsilon(t_i) = \mu_i - a_i$ and its mean squared value $E_h$ is calculated as

$$E_h = \sum_{i=1}^{l} {}^h\epsilon^2(t_i) = \sum_{i=1}^{l} (\mu_i - a_i)^2. \tag{5.2}$$

Then, during the *identification of periodicities*, the Frequency Map Enhancement (FreMEn-Krajník et al., 2017) method, which, unlike traditional Discrete or Fast Fourier transforms, is suitable for finding periodicities in non-uniform and sparse data, is used to perform spectral analysis of ${}^h\epsilon(t_i)$. The most prominent spectral component is calculated and its period $T_{h+1}$ is stored as:

$$T_{h+1} = \arg\max_{T_k} \sum_{i=1}^{l} |({}^h\epsilon(t_i) - {}^h\hat{\epsilon}) e^{-j2\pi t_i/T_k}|, \tag{5.3}$$

where ${}^h\hat{\epsilon}$ is the average error ${}^h\epsilon(t_i)$.

After that, the *hypertime space extension* step is performed, which extends each vector ${}^h\mathbf{x}_i$ by 2 dimensions representing a given periodicity of the temporal domain, i.e.

$${}^{h+1}\mathbf{x}_i \leftarrow ({}^h\mathbf{x}_i, \cos(2\pi\frac{t_i}{T_{h+1}}), \sin(2\pi\frac{t_i}{T_{h+1}})). \tag{5.4}$$

Then, $h$ is incremented by one and the steps of *spatio-temporal clustering* and *model error estimation* are repeated on the now extended vector ${}^h\mathbf{x}_i$, obtaining a new error $E_h$. This new model error is compared with the error obtained in the previous iteration $E_{h-1}$ and if $E_h < E_{h-1}$, the algorithm proceeds with the *identification of periodicities* and *hypertime space extension*, extending the vector ${}^h\mathbf{x}_i$ with another two dimensions representing another potential periodicity of the modeled phenomenon.

In the opposite case, i.e. $E_h \geq E_{h-1}$, the model $p_{h-1}(a, \mathbf{x}, t)$ from the previous iteration is returned as $p(a, \mathbf{x}, t)$ and the method is terminated.

The resulting model allows to estimate the likelihood of each value $a$ of a given phenomenon at location $x$ and time $t$. An illustrative example of the method, which estimates $p(a|t)$ through projection into $p(a|\cos(2\pi t/T), \sin(2\pi t/T))$ is given in Figure 5.1. For the sake of simplicity, this example uses only one periodicity $T$ and the spatial domain is neglected, i.e. $x \in \mathbb{R}^0$.

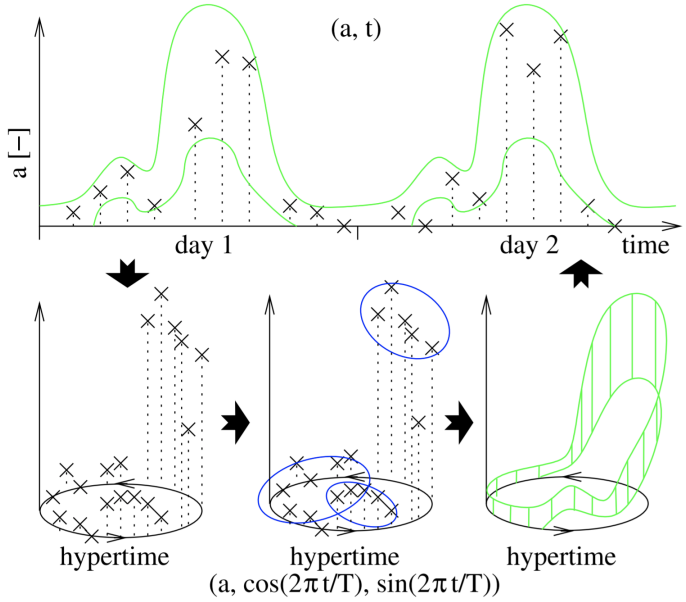


Figure 5.1: Example of the warped hypertime projection. The data points $(a, t)$ observed (top, black) are first processed by a frequency analysis to determine a dominant periodicity $T$. Then, the time $t$ is projected onto a 2D space (hypertime) and the vectors $(a, t)$ become $(a, \cos(2\pi t/T), \sin(2\pi t/T))$ (bottom left). The projected data are then clustered (bottom center) to estimate the distribution of $a$ over the hypertime space (bottom right). Projection of the distribution back to the unidimensional time domain allows to calculate the probabilistic distribution of $a$ for any past or future time.

### Human motion modelling

In this case the aim of the method is to estimate the Bernoulli distribution of spatio-direction-temporal people occurrences at time $t_i$, position $x_i, y_i$ with the speed $v_i$ and angle $\theta_i$. Assuming a pedestrian tracking system providing the vectors

$(x_i, y_i, v_i, \theta_i, t_i)$, these can be transformed to $(x_i, y_i, v_i \cos\theta, v_i \sin\theta)$ to avoid the angle ambiguities and are denoted $(\mathbf{x}_i, t_i)$.

So let us have a set of detections $D(\mathbf{x}_i, t_i), i = 1, ..., l$ of occurrences and non-ocurrences, where $D(\mathbf{x}_i, t_i) = 1$ for the detected and $D(\mathbf{x}_i, t_i) = 0$ for non-detected occurrences of the studied phenomenon (the non-occurrences are added artificially as explained in Section 5.2.1). To model the Bernoulli distribution of $D(\mathbf{x}_i, t_i)$, the dataset is split into occurrences and non-occurrences (mutually exclusive) and the WHyTe model is built for both subsets. These models are optimised following the iterative scheme presented in the previous subsection using the RMSE between the model predictions $M(\mathbf{x}_i, , t_i)$ and the test subset values $D(\mathbf{x}_i, t_i)$ as the error to minimise:

$$RMSE = \sqrt{\frac{1}{l}\sum_{i=1}^{l}(M(\mathbf{x}_i, t_i) - D(\mathbf{x}_i, t_i))^2}, \tag{5.5}$$

The probability of the occurrence of $(\mathbf{x}_i, t_i)$ is given by the following ratio based on its hypertime projection ${}^h\mathbf{x}_i$:

$$M(\mathbf{x}_i, t) = \frac{M_1({}^h\mathbf{x}_i)}{M_1({}^h\mathbf{x}_i) + M_0({}^h\mathbf{x}_i)}, \tag{5.6}$$

where the overall probability $M_{\{0,1\}}({}^h\mathbf{x}_i)$ of generating an occurrence of ${}^h\mathbf{x}$ by a mix of $n$ Gaussian distributions $GMM_{\{0,1\}}$ characterised by the cluster weights $w_{\{0,1\}j}$, cluster centers $\mu_{\{0,1\}j}$ and covariances $\Sigma_{\{0,1\}j}$ is computed as:

$$M_{\{0,1\}}({}^h\mathbf{x}_i) = \sum_{j=1}^{n} w_j P\left[Q \geq (\mathbf{x}_i - \mu_{\{0,1\}j})^T \Sigma^{-1}_{\{0,1\}j}(\mathbf{x}_i - \mu_{\{0,1\}j})\right]. \tag{5.7}$$

$P\left[Q \geq (\mathbf{x}_i - \mu_j)^T \Sigma_j^{-1}({}^h\mathbf{x_i} - \mu_j)\right]$ is the probability of a data point belonging to the $j^{th}$ multivariate normal distribution defined by $\mu_j$ and $\Sigma_j$, and $(\mathbf{x}_i - \mu_j)^T \Sigma_j^{-1}(\mathbf{x_i} - \mu_j)$ is the generalised squared interpoint distance (Gnanadesikan et al., 1972).

In the experimental part of this chapter, the number of clusters $n$ found is 3 and the number of hypertime circles $h$ is 2 in the first comparison and 3 in the second one, corresponding to periodicities of 12 and 24 hours, and 6, 12 and 24 hours, respectively.

### 5.1.2 Directional grid maps (DGM)

Directional grid maps or DGM (Senanayake et al., 2018) are formally defined as a multi-dimensional field that maintains probability measures given by a probability density function of the directional uncertainty of the cells in a spatial lattice. The inputs to the model are the motion direction of people moving at different locations of the environment, and the outputs are a set of von Mises direction distributions indicating the most probable directions of pedestrian motion in various locations of the environment. An example of the output can be seen in Figure 5.2.

In order to build the DGM, firstly, the environment is divided into a fixed-sized grid. Then, assuming that each location has $M$ multi-modal movements, each cell can be represented by a probability density function with $M$ von Mises distributions (Mises, 1981) as:

$$\mathcal{VMM}(\theta; \alpha, \mu, \kappa) = \sum_{m=0}^{M} \alpha_m \mathcal{VM}(\theta; \mu_m, \kappa_m), \tag{5.8}$$

where the von Mises distribution is given by

$$\mathcal{VM}(\theta; \mu, \kappa) = \frac{1}{2\pi J_0(\kappa)} \exp(\kappa \cos(\theta - \mu)). \tag{5.9}$$

In order to obtain the optimal parameter set $\{(\alpha_m, \mu_m, \kappa_m)\}_{m=1}^{M}$, the EM algorithm (Dhillon et al., 2003) is used. The estimated number of modalities/von Mises components $M$ present in each cell is determined by the number of density-wide clusters using the DBSCAN algorithm (Ester et al., 1996).

Since the directional grid maps are not designed to deal with the temporal domain, in the experiment, the time is also discretised every 15 minutes in addition to the 2 m $\times$ 2 m spatial discretisation, and applying a predefined 24h temporal correlation. For the comparison, as a proxy, the estimation of the people density is done by considering the cells where the initial set of mixture parameters changes with time. Therefore, the proxy count probabilities are always either 0 or 1, and not the exact people density.

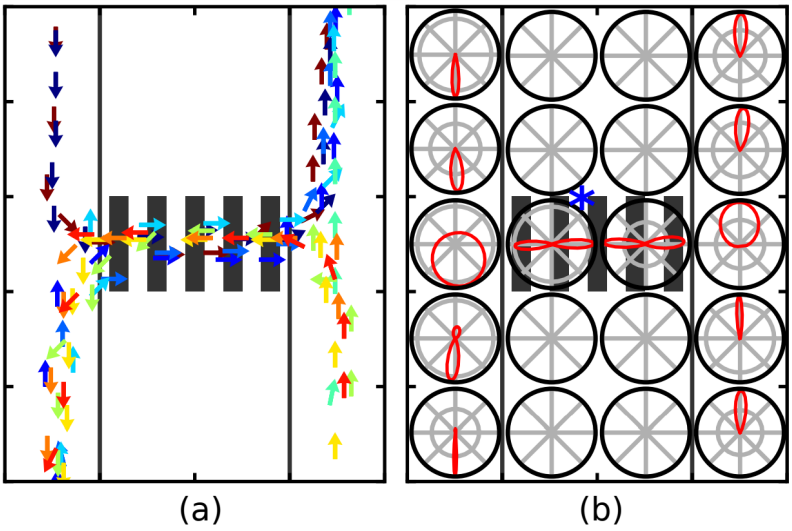


Figure 5.2: (a) Human detections in a crosswalk scenario. (b) Directional grid map modeled using the mixture of von Mises distributions. Taken from Senanayake et al., 2018

.

### 5.1.3 Circular Linear Flow Field (CLiFF-Map)

The Circular Linear Flow Field map or CLiFF-map (Kucner et al., 2017) is a representation for encoding patterns of movement as a field of Gaussian mixtures. The input of the model is a velocity vector $\boldsymbol{V}$ combining the orientation ($\theta \in [0, 2\pi)$) and speed ($\rho \in \mathbb{R}^+$) for every person detection. To build the probabilistic model of the velocities, the space is first divided into a fixed-sized grid. Then, in order to model and preserve the multi-modality of the pedestrian motion, a 'semi-wrapped' Gaussian mixture model (SWGMM) (Roy et al., 2016) is employed. A *SWGMM* is a probability density function represented as a weighted sum of $M$ semi-wrapped normal distributions (SWND):

$$p(\boldsymbol{V}|\boldsymbol{\xi}) = \sum_{m=1}^{M} \pi_m \mathcal{N}^{\mathcal{SW}}_{\boldsymbol{\mu}_m, \boldsymbol{\Sigma}_m}(\boldsymbol{V}), \tag{5.10}$$

where $\mathcal{N}^{\mathcal{SW}}_{\boldsymbol{\mu},\boldsymbol{\Sigma}}(\boldsymbol{V})$ is the SWND, which is in fact distributed on a cylinder, where one of the dimensions is wrapped around the circumference and the other along its height.

$$\mathcal{N}^{\mathcal{SW}}_{\boldsymbol{\mu},\boldsymbol{\Sigma}}(\boldsymbol{V}) = \sum_{k \in \mathbb{Z}} \mathcal{N}_{\boldsymbol{\mu},\boldsymbol{\Sigma}} \left( \begin{bmatrix} \theta \\ \rho \end{bmatrix} + 2\pi \begin{bmatrix} k \\ 0 \end{bmatrix} \right). \tag{5.11}$$

$\boldsymbol{\xi}$ denotes a finite set of components $\xi_m$ defined by their means $\mu_m$ covariances $\Sigma_m$ and mixing factor $\pi_m$. To estimate the parameters of each SWGMM ($\boldsymbol{\xi}$) a two-step approach is used. First, the number of clusters and their positions are estimated using the Mean Shift algorithm (Cheng, 1995). These clusters are then used as the initial conditions for the Expectation Maximisation algorithm (Dhillon et al., 2003).

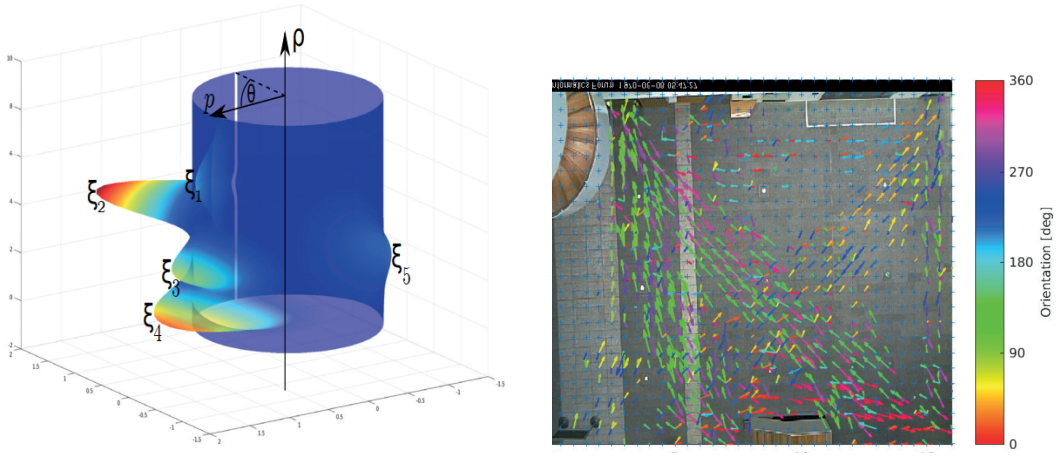


(a) (b)

Figure 5.3: (a) Example of SWGMM wrapped on a unit cylinder with five modes ($\xi_m$). The position along $\rho$ axis represents the velocity, the orientation is denoted as $\theta$ and the distance from the surface of the cylinder corresponds to the probability $p$. (b) Example of CLiFF-map for the Edinburgh pedestrian dataset(Majecka, 2009), with a grid of 0.5m.

### 5.1.4 LSTM

In contrast to the aforementioned analytic methods, for comparison purposes, a long short term memory (LSTM) network (Hochreiter et al., 1997) was also implemented. An LSTM network is a kind of recurrent neural network used in the field of deep learning capable of learning long-term dependencies, which unlike standard feedforward neural networks has feedback connections. LSTM networks are well-suited to classifying, processing and making predictions based on time series data.

An LSTM network has LSTM units in place of the standard neural network layers. A common LSTM unit is composed of a cell (the memory part of the LSTM unit) and three regulators, usually called gates, of the flow of information inside the LSTM

unit: an input gate $i$, and output gate $o$ and a forget gate $f$. Figure 5.4 shows a graphical representation of an LSTM cell.

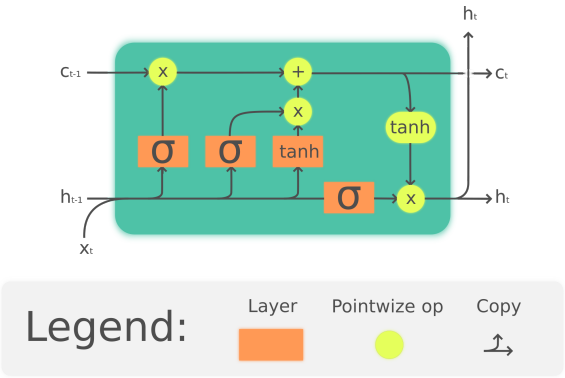


Figure 5.4: LSTM cell diagram (Chevalier, 2018).

The cell is responsible for keeping track of the dependencies between the elements in the input sequence. The input gate controls the extent to which new values flows into the cell, the forget gate controls the extends to which a values remains in the cell, and the output fate control the extent to which the value in the cell is used to compute the output activation of the LSTM unit. The compact forms of the equations for the forward pass of an LSTM unit are ( Hochreiter et al., 1997; Gers et al., 1999):

$$\begin{aligned} f_t &= \sigma_g(W_f x_t + U_f h_{t-1} + b_f) \\ i_t &= \sigma_g(W_i x_t + U_i h_{t-1} + b_i) \\ o_t &= \sigma_g(W_o x_t + U_o h_{t-1} + b_o) \\ \tilde{c_t} &= \sigma_c(W_c x_t + U_c h_{t-1} + b_c) \\ c_t &= f_t \circ c_{t-1} + i_t \circ \tilde{c_t} \\ h_t &= o_t \circ \sigma_h(c_t) \end{aligned} \tag{5.12}$$

where the initial values $c_o = 0$ and $h_o = 0$ and the operator $\circ$ denotes the Hadamard product (element-wise product). The subscript $t$ indexes the time step. $x_t \in \mathbb{R}^d$ is the input to the LSTM unit, $f_t \in \mathbb{R}^h$ is the forget gate's activation vector, $i_t \in \mathbb{R}^h$ is the input/update gate's activation vector, $o_t \in \mathbb{R}^h$ is the output gate's activation vector, $h_t \in \mathbb{R}^h$ is the hidden state vector also known as output vector of the LSTM unit, $\tilde{c_t} \in \mathbb{R}^h$ is the cell input activation vector, $c_t \in \mathbb{R}^h$ is the cell state vector, and $W \in \mathbb{R}^{h \times d}$, $U \in \mathbb{R}^{h \times h}$ and $b \in \mathbb{R}^h$ are the weight matrices and bias vector parameters

which need to be learned during training, where the superscripts $d$ and $h$ refer to the number of input features and number of hidden units, respectively. $\sigma_g$ is the sigmoid function, $\sigma_c$ is the hyperbolic tangent function, and $\sigma_h$ is the hyperbolic tangent function, or the peephole LSTM papers Gers et al., 2001; Gers et al., 2002 suggest, $\sigma_h(x) = x$.

The LSTM network was trained on $n = 5$ consecutive human observations $O$ to predict the presence or absence of a person walking in a certain location with a certain orientation in future time steps. Where $O = \{o_t, ..., o_{t+n}\}$ and each observation $o_t$ is defined by 5 features: $o_t = \{time_t, x_t, y_t, \theta_t, presence_t\}$.

The proposed network architecture is a sequential model consisting of a linear stack with a combination of 3 different types of layers (LSTM layer, dropout layer and densely-connected Neural Network layer), following the structure shown in Figure 5.5. The network was built using Keras Python API (*Keras* 2020) running on top of the machine learning platform TensorFLow (*TensorFlow* 2020). Each stacked LSTM

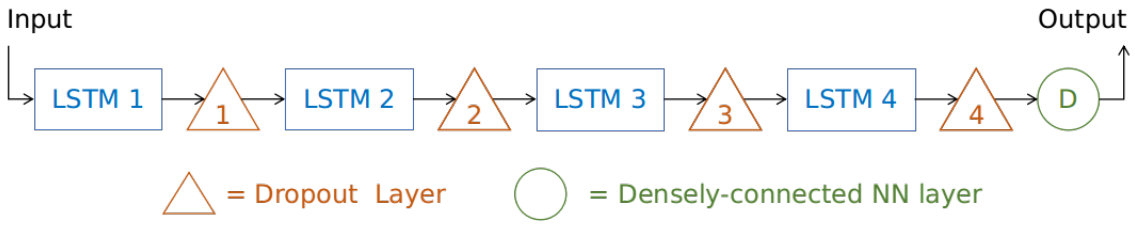


Figure 5.5: LSTM network structure used

.

layer has a size of 50 units. The dropout layers randomly set inputs units to 0 with a frequency of $rate = 0.2$ at each step during the training time, which helps prevent overfitting (inputs not set to 0 are scaled up by $1/(1 - rate)$ such that the sum over all inputs is unchanged). The densely-connected Neural Network layer at the end contains just 1 output unit, reducing the dimensionality to the required output. This layer can be defined with the equation: $y_t = W \cdot h_t$ where $W$ is the weights matrix. The output shape and number of trainable parameters per layer are presented in Table 5.1.

The Adam optimiser is used for training (Kingma et al., 2014). This is a stochastic gradient descent method based on adaptive estimation of first-order and second-order

| Layer | Ouput Shape | # Trainable parameters |
|---|---|---|
| LSTM 1 | (5,50) | 11200 |
| Dropout 1 | (5,50) | 0 |
| LSTM 2 | (5,50) | 20200 |
| Dropout 2 | (5,50) | 0 |
| LSTM 3 | (5,50) | 20200 |
| Dropout 3 | (5,50) | 0 |
| LSTM 4 | (50) | 20200 |
| Dropout 4 | (50) | 0 |
| Dense | (1) | 51 |

Table 5.1: Sequential layered model summary.

moments. The Adam algorithm pseudo-code can be seen in Algorithm 1. The learning rate ($\alpha$) was set to 0.001, the exponential decay rate for the 1st and 2nd moment estimates ($\beta_1, \beta_2$) were set to 0.9 and 0.999, respectively, and the epsilon constant to 1e-7. For this model, the training data subset used in the models comparison was divided in two inner subsets. One of them containing 80% of that data which was the training data and the rest was used for validation, but after each epoch the data split was shuffled to ensure a good generalisation (keeping always the 80/20 ratio). The loss function used during the optimisation process was the mean squared error between the model prediction and the real observations. The learning of the LSTM model was done using four NVIDIA Tesla V100 SXM2 32GB.

### 5.1.5 Qualitative comparison

Table 5.2 summarises the different properties for each method, providing an overview of the temporal capabilities and the type of representation (continuous or discrete) for time, space, intensity, direction and speed of the human motion model.

Regarding temporal predictions, only CLiFF-map does not offer any capabilities. LSTM is focused on short-term motion predictions, while STeF-map, WHyTe and DGM offer long-term predictions. However, DGM fixes a 24h period from the beginning, while STeF-map and WHyTe can adapt to the most appropriate temporal patterns. Also the time representation in DGM relies on a pre-defined discretisation, which differs from the rest of the methodologies. For STeF-map, note that although

**Require:** $\alpha$: Stepsize
**Require:** $\beta_1, \beta_2 \in [0, 1)$: Exponential decay rates for the moment estimates
**Require:** $f(\theta)$: Stochastic objective function with parameters $\theta$
**Require:** $\theta_0$: Initial parameter vector

**begin**
  $m_0 \leftarrow 0$ (Initialise 1st moment vector);
  $v_0 \leftarrow 0$ (Initialise 2nd moment vector);
  $t \leftarrow 0$ (Initialise timestep);
  **while** $\theta_t$ *not converged* **do**
    $t \leftarrow t + 1$;
    $g_t \leftarrow \nabla_\theta f_t(\theta_{t-1}$ (Get gradients w.r.t. stochastic objective at timestep $t$);
    $m_t \leftarrow \beta_1 \cdot m_{t-1} + (1 - \beta_1) \cdot g_t$ (Update biased first moment estimate);
    $v_t \leftarrow \beta_2 \cdot v_{t-1} + (1 - \beta_2) \cdot g_t^2$ (Update biased second raw moment estimate);
    $\hat{m}_t \leftarrow m_t / (1 - \beta_1^t)$ (Compute bias-corrected first moment estimate);
    $\hat{v}_t \leftarrow v_t / (1 - \beta_2^t)$ (Compute bias-corrected second raw moment estimate);
    $\theta_t \leftarrow \theta_{t-1} - \alpha \cdot \hat{m}_t / (\sqrt{\hat{v}_t} + \epsilon)$ (Update parameters)
  **end**
**end**
**return** : $\theta_t$ (Resulting parameters)

**Algorithm 1:** Adam optimiser pseudo-code. $g_t^2$ indicates the element-wise square $g_t \odot g_t$. All operations on vectors are element-wise. The terms $b_1^t$ and $b_2^t$ are used to denote $\beta_1$ and $\beta_2$ to the power $t$.

the inputs for the temporal models are indeed discrete (see Section 4.1.3), the output of the model prediction is continuous and infinite in time as it is a composition of harmonic functions.

Taking a look at the representation column, STeF-map is the only one that does not strictly model the intensity. As explained in the previous chapter, before the people data counts are fed into the system, a normalisation step is applied (Section 4.1.3). The other methods do not need this step, allowing them to keep the information regarding the intensity of the people presence. Also STeF-map together with DGM do not encode the speed in the model, due to their focus on modelling the direction of motion. However, speed is an important element in the CLiFF-map representation, as one of the original application of this method was to model velocity wind maps. Another difference between STeF-map and the other methodologies is that in the former, the direction is discretised into a finite number of bins. This is not the

| Method | | Time | | Representation | | | | |
|---|---|---|---|---|---|---|---|---|
| **Name** | **References** | **long-term** | **short-term** | **time** | **space** | **intensity** | **direction** | **speed** |
| STeF-map | Molina et al., 2018 | ✓ | × | C | D | × | D | × |
| WHyTe | Vintr et al., 2018 | ✓ | × | C | C | C | C | C |
| DGM | Senanayake et al., 2018 | ✓ | × | D | D | C | C | × |
| CLiFF-map | Kucner et al., 2017 | × | × | × | D | C | C | C |
| LSTM | Hochreiter et al., 1997 | × | ✓ | C | C | C | C | C |

Note 1: In the 'Representation' columns, C stands for the continuous, and D for the discrete representation of variables provided by the method.

Table 5.2: Qualitative Comparison Of Methods

case for the rest as they used continuous functions such as von-Mises or Gaussian distributions.

WHyTe together with the LSTM have the advantage that every domain is based on a continuous representation. This avoids the dependency on a spatio-temporal grid parameterisation when defining the model. Moreover, apart from human motion prediction, these two methodologies have already been used and tested in a wider set of applications. For example, WHyTe has been applied to prediction of binary states such as a door being open or closed, topological robot localisation, robot velocity prediction or human presence (Krajnik et al., 2019). LSTMs have also been shown to be useful in other time series prediction tasks such as speech recognition (Graves et al., 2013), people activity recognition (Ordóñez et al., 2016) or short-term traffic forecasting (Zhao et al., 2017).

## 5.2 Human motion prediction

In this section, the comparison focuses on the ability of the different methodologies described to make accurate predictions of spatio-temporal people motion, assuming they are given some data from the past. At the same time, this approach implicitly evaluates the learning and generalisation capabilities to model the human motion patterns found in the environment. From a mobile robot application point of view,

increasing the accuracy of predictions means that the robot knows with higher fidelity how people are likely to move, not only in parts of the environment which are beyond its sensory range, but also at given points in time in the future. This information could then be incorporated or exploited by the robotic system to optimise, for example, the path planning and navigation strategies.

### 5.2.1 Dataset

The evaluation is done using the Corridor dataset described in Chapter 3, which is also used in Chapter 4 for the analysis of the STeF-map model. Following a similar approach as in the experimental section of Chapter 4 and the work by Oliveira et al., 2018, from the dataset are taken the first 9 days, which are split into training and testing subsets, consisting of 7 and 2 days, respectively. The data in the testing subset is never seen by any of the models before the computation of the evaluation metrics. Similar to O'Callaghan et al., 2012, apart from the people occurrences given by the dataset, 70000 "no detections" are artificially added containing vectors of position, orientation, and speed where no human is detected, as in the nights. As some of the methods in the comparison do not model the speed, this value is set to $v = 1.0m/s$ for every measurement.

### 5.2.2 Evaluation Criteria

In order to measure the quality of the predictions, two different criteria are used. The first one is the level of similarity between human motion distributions, occurring at certain times and positions from the 2 test days and the ones predicted by the models. The similarity measure is computed using the Chi-squared distance ($\chi^2$) explained in Section 4.2.2. This distance indicates the level of similarity between two discrete distributions or histograms, so the higher the distance, the less accurate is the model prediction with the gound truth test data. This criterion requires a discrete number of bins dividing the full circumference, hence for the models which have a continuous representation of the orientation, this was discretised into 8 bins taking the angles 0, 45, 90, 135, 180, 225, 270 and 315 for each one (as seen in Figure 4.6).

The second criterion used to measure the human motion prediction quality of the compared models is the root mean square error (RMSE) (Hyndman et al., 2006) between the pedestrian detections in test subset $D(x_i, y_i, v_i, \phi_i, t_i)$ and model predictions $M(x_i, y_i, v_i, \phi_i, t_i)$, which is widely used in time series forecasting (Hyndman et al., 2018):

$$RMSE = \sqrt{\frac{1}{n}\sum_{i=1}^{n}(M - D)^2}, \tag{5.13}$$

where $n$ is the number of human detections in the test subset.

### 5.2.3 Evaluation Results

The results of the evaluation are summarised in Table 5.3. The STeF-map predictions used to calculate both the $\chi^2$ distance and the RMSE metrics are computed using always 4 spectral components in all the cells. For the $\chi^2$ distance the performance was computed for multiple time intervals: 10min, 30min, 1h, 2h, 3h, 4h and 6h, which divide the two testing days into 288, 96, 48, 24, 16, 12 and 8 intervals respectively. The time intervals that contain no detections in the ground truth are assigned equal probabilities for every orientation.

The values obtained show that STeF-map achieves the lowest score for the $\chi^2$ distances and the second lowest for RMSE. The reason behind the increase of performance in the $\chi^2$ distance between the STeF-map representation and the rest could be that this model associates each orientation for every location with an independent temporal model. By contrast, the other methodologies model a continuous function in each location or cell which may not capture as well the relative intensities between orientations. The $\chi^2$ distance tends to decrease as the length of the time interval increases because the distances shown are the sum of of all interval distances, without applying any normalisation based on the number of intervals.

Checking the RMSE values, we see that WHyTe obtains the lowest score of the 5 approaches. This metric focuses more on how likely the model is able to predict that a person is going to be in a certain place walking in a certain orientation, rather than the probability distribution over all orientations for that location. Considering that the STeF-map representation was not built with modelling of people presence

intensity in mind, achieving the second best score is a really interesting outcome. The LSTM is tailored for short-term predictions (compared to the prediction horizons of STeF-map and WHyTe), so its predictions quickly converge to the mean probability of people directions across the entire training dataset (both spatially and temporally).

| **Model** | $\chi^2$ **10'** | **30'** | **1h** | **2h** | **3h** | **4h** | **6h** | **RMSE** |
|---|---|---|---|---|---|---|---|---|
| STeF-map | **5.38k** | **1.73k** | **1.11k** | **2.65k** | **0.43k** | **0.89k** | **0.54k** | 0.46 |
| WHyTe | 7.08k | 3.85k | 2.77k | 3.90k | 1.12k | 1.61k | 1.01k | **0.40** |
| DGM | 7.33k | 4.01k | 2.89k | 3.98k | 1.17k | 1.66k | 1.00k | 0.75 |
| CLiFF-map | 7.11k | 2.77k | 1.89k | 3.29k | 0.72k | 1.20k | 0.74k | 0.50 |
| LSTM | 7.67k | 4.09k | 2.92k | 4.00k | 1.18k | 1.67k | 1.05k | 0.48 |

Table 5.3: Prediction performance of the evaluated models with both criteria.

When comparing models that are aimed to be used by mobile platforms for real applications, one also has to take into account the implementation constraints. Hence Table 5.4 presents a summary of the memory and training time requirements for each method. CLiFF-map was developed and trained using MatLab, while the rest of the methods are all Python-based. Regarding memory consumption, all the methodologies are suitable for running in on-board computers and could handle an increase in map size. However, taking a look at the training time required, only STeF-map, WHyTe and DGM are suitable for a regular continuous update of the human motion model (e.g. every hour or every half a day), since CLiFF-map and LSTM present times which are at least 4 orders of magnitude larger.

| **Model** | **Memory [kB]** | **Train time [s]** |
|---|---|---|
| STeF-map | 140 | **20** |
| WHyTe | **2** | 60 |
| DGM | 20 | 72 |
| CLiFF-map | 6k | $10^4$ |
| LSTM | 900 | $10^6$ |

Table 5.4: Memory requirements and training time needed by the evaluated models.

## 5.3 Social cost evaluation

One of the main focuses of this thesis is to develop a representation able to map the human motion patterns. Until now, it has been described and compared with other approaches from the perspective of prediction performance. However, as mentioned previously, the main purpose of the representations developed in this thesis is to provide information for other parts of a robotic system, such as the path planning and, consequently, the navigation. Hence, in this subsection, the evaluation methods proposed focus more on the application side. More specifically, the evaluation aims to quantify the impact of the predictions by the different models on the robot's navigational ability from a social compliance point of view.

### 5.3.1 Methods compared

Apart from the state-of-the-art methods STeF-map, WHyTe and CLiFF-map described in Chapter 4, Section 5.1.1 and Section 5.1.3, respectively, for comparison purposes three historical average-based models and one time series forecasting model are added. The average-based models are:

- mean: which predicts the mean of its past measurements for each spatial segment,
- histogram daily: which describes the average of the days, and
- histogram weekly: which averages the weeks.

Both histogram daily and weekly split their period into one-hour-long segments and compute the average values for time and space in each segment. Regarding the time series forecasting, the tool Prophet (Taylor et al., 2018) is used, being trained with measurements also condensed into one-hour-long time steps.

### 5.3.2 Dataset

The evaluation is performed with a dataset collected in the Building M at the University of Technology of Belfort-Montbeliard (UTBM). The recording set-up followed

mimics the approach explained in Section 3.2.1, but in this case with a static Velodyne HDL-32 placed at 1.2 meters height. The recordings provide around 300 000 human detections per day with a coverage of $150m^2$ (see Figure 5.6 top). From the three full months provided by the dataset, in the experiments carried out here 11 days are used for training the models and 1 day for testing.

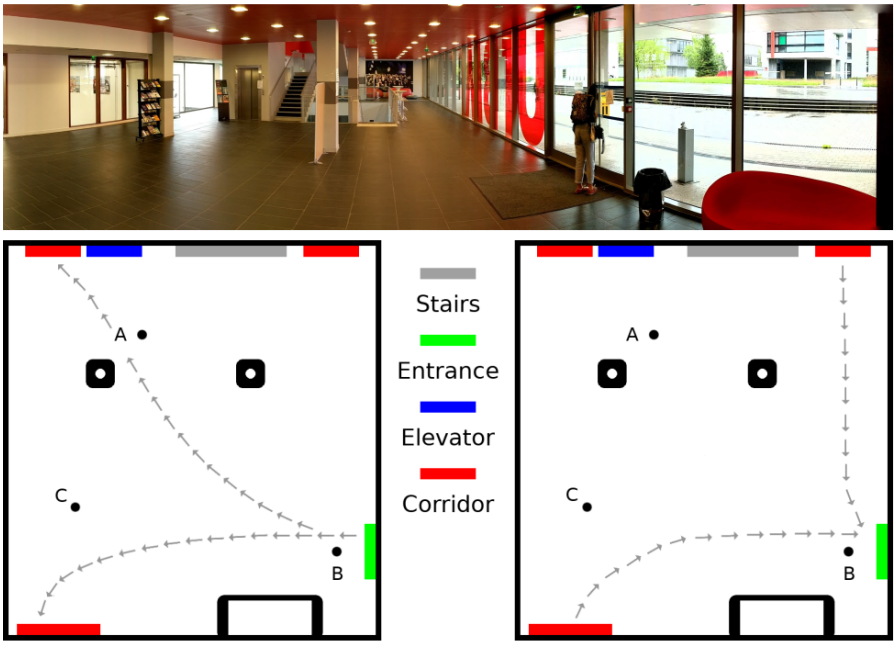


Figure 5.6: Top: photo of the entrance hall of the building M at the University of Technology of Belford-Montbeliard, where the dataset was recorded. Bottom: visualisation of the environment with the starting and goal points (A, B, C) and the most prominent pedestrian flows during morning (left) and evening (right). Taken from Vintr et al., 2020.

### 5.3.3 Methodology

The evaluation is based on the traditional navigation paradigm used in mobile robotics, where the robot path is calculated by minimising some criterion, which is usually referred to as a cost. To this end, let us assume there is an scenario with three locations (A,B and C) as shown in Figure 5.6 bottom. From these locations, there is a starting point (A) and two-goal positions (B,C), of which the robot has to decide the order to visit, i.e. (A, B, C, A) or (A, C, B, A). The order and the navigation path are decided by the Dijkstra's algorithm based on a social cost map,

where the costs are predicted by the pedestrian flow models using the Extended Upstream Criterion proposed by Palmieri et al., 2017:

$$cost(\theta) = \sum_{i=0}^{7} p(i)(1 - \cos(\theta - (i\frac{\pi}{4}))), \tag{5.14}$$

where $p(i)$ denotes the human motion predictions given by the different models at angles $i\frac{\pi}{4}$ [rad]. These costs, which can be interpreted as the likelihood of forcing a human to alter their path to avoid the robot, are calculated for every cell in each one of the eight main cell transition directions, i.e. $\theta = j\frac{\pi}{4}, j \in 0, 1, ...7$. So the idea is that the better a model can predict the human behaviour, and as a consequence the associated social cost map, the more compliantly the robot should move in the scenario with respect to the humans. Those model whose predictions are time dependant means that the associated costs are also time dependant.

### 5.3.4 Evaluation Criteria

The criterion proposed to measure the robot compliance is the service social cost (SSC), which is defined as the sum of the robot-human encounters $e_k$ during the planned patrolling actions $p$ (i.e. visiting the locations in sequence A, B, C, A or A, C, B, A) based on the specified servicing ratio $r$ (the ratio defines the percentage of patrolling tasks the robot has to perform in a day with respect to the total number that can be allocated).

$$SSC(r) = \sum_{k=1}^{p \cdot r} e_k \tag{5.15}$$

Assuming a model that can predict the social cost $c_i, i = 1, 2, .., p$ (using the Extended Upstream Criterion) for every planned path through the environment starting at time $t_i$, the plans are reordered in ascending order by $c_i$ and re-indexed such that $k = 1, 2, .., p$ and $c_k \leq c_{k+1}$ for all $k$. When $r = 1$, the robot has no choice in choosing the best patrolling times, hence the score obtained at $r = 1$ reflects the similarity between the model and the spatial dynamics of the environment. An encounter $e$ is triggered when a person enters the robot's social influence area, which in this case is defined as a circumference of 1 m radius. Also, the people and robots are considered as "blind" all the time, so there are no reactive behaviours by any of the two entities.

### 5.3.5 Results

The results obtained correspond to the SSC values obtained with 1 testing day in the UTBM dataset. Figure 5.7 summarises the values for all the compared human flow models for a servicing ratio going from 0 to 100%. The STeF-map predictions used to calculate the social cost are computed using always 4 spectral components in all the cells.

The plot indicates that the SSC achieved by the models which neglect the temporal variation of the flows such as the CLiFF-map or the mean scale more or less linearly with the servicing ratio. However, the time-aware representations like STeF-map and WHyTe can identify the times when it is less appropriate to navigate (because more encounters are expected and hence a higher social cost $c_i$) and choose not to do it. Thus, they can maintain a low SSC even when the servicing ratio increases. Nonetheless, even with a servicing ratio of 100% without any opportunity to reschedule the patrolling actions, STeF-map manages to minimise the human encounters at the lowest value when compared to the rest.

## 5.4 Summary

In this chapter, the STeF-map approach, which is one of the main contribution of this thesis, has been compared with other state-of-the-art human motion representation using two different approaches. The first one is aimed at measuring the quality of the predicted human motion likelihood in the environment at several location and times. The second evaluation focuses on analysing whether the differences in the prediction results translate also into differences when they are exploited by the robot navigation stack.

The results obtained in both parts conclude that the STeF-map is suitable for obtaining accurate spatio-temporal predictions of human flow, assuming that there are some rhythmic trends in the people's activities. It outperforms the rest of the strategies in the $\chi^2$ prediction accuracy metric, which translates also into a reduction of human-robot encounters measured by the SSC. This means that, in the long-term,

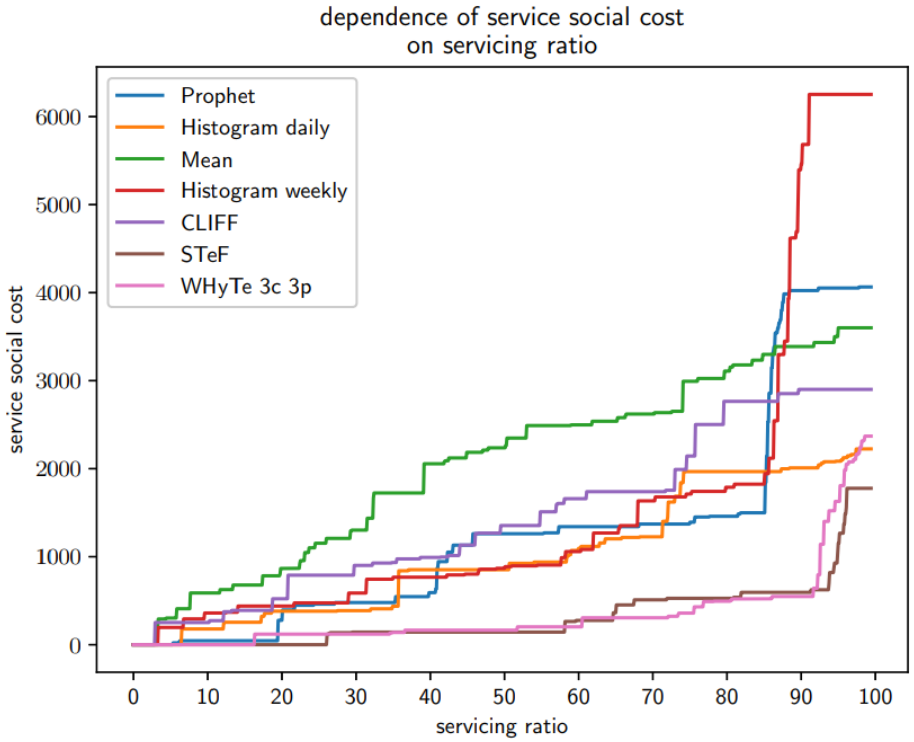


Figure 5.7: Dependence of the number of encounters (social cost) on the frequency of the traversals (servicing ratio) achieved by the pedestrian flow models. Taken from Vintr et al., 2020.

the number of people that could potentially be annoyed by the tasks performed by the mobile robot is reduced.

### 5.4.1 Limitations

In both evaluations, the predictions made for the comparisons are based on modelling pre-recorded data collected with a static sensor, which covers the whole environment. This is not a very realistic set-up, because usually the collected human data is recorded by the same mobile platform that needs to exploit this same data. The consequences of having this more realistic set-up include that human detections are only available from the locations where the robot was in the past, and also that those human motion detections could potentially be influenced by the robot itself.

Talking more specifically about the social cost evaluation, the comparison is based on encounters. Although encounters are an intuitive evaluation criterion, assessing the social compliance in a human-robot interaction experiment with just interactions

could not be enough, as right now, it is just a binary measure using a fixed radius. Other criteria could include the robot speed, direction of motion with respect to the surrounding people, and average distance to the closest person. Furthermore, the encounters are triggered by two passive entities moving: the simulated robot and a person following pre-recorded trajectories. Usually people and robots tend to be aware of their surroundings when moving, becoming active rather than passive entities, so the results obtained could change if active avoidance manoeuvres are included in the simulation.

Finally, the methodology applied for the patrolling assumes that when the servicing ratio is lower than 100%, the patrols can be rescheduled at any time with complete freedom. A mobile robot is usually more temporally constrained, meaning that the rescheduling is sometimes dependant on other tasks that the robot has to accomplish.

# Chapter 6

# Spatio-temporal exploration of human motion patterns

While the introduction of spatio-temporal models like STeF-map enables the robot to learn about environmental changes, exploration strategies to efficiently and intelligently build and maintain these models are also required.

The STeF-map results obtained in Chapters 4 and 5 were obtained by assuming full observability in space and time. In other words, all the people detections captured by the sensors, which covered the entire operational area under consideration, were used to calculate the inputs to the STeF-map model. However, realistically speaking, the situation where a robot is able to observe the whole environment at all times without any occlusions is very rare.

Usually a mobile robot is only able to observe a certain portion or region of the operational area at a given time, due to the limited field of view of its sensors and occlusions by other objects. Since the robot cannot be in two places at once, this means that while the robots is gathering information at one location, activities happening at other locations will remain unseen. Furthermore, a robot cannot usually employ 100% of its time for exploration activities. This time is limited by the fact that a robot usually has to complete other tasks, as per its overriding mission requirements, or has to take time out to recharge its batteries. So the robot can only devote a certain amount of time during the day for data gathering purposes.

Taking into account the aforementioned spatio-temporal constraints, a mobile robot should be provided with a exploration strategy with the primary aim of building and maintaining an up-to-date model of the environment. Without such a strategy, parts of the environment might remain unvisited for long periods, meaning that the

robot's knowledge of human activity patterns there would become out of date, or the robot might even remain completely ignorant of human activities that it has never had the opportunity to observe. Even if the time available for exploration is very limited, a good exploration policy should be able to suggest the most informative regions and times for data gathering, allowing the robot to prioritise these actions and make the most of the available opportunities to update and keep its map of the expected human activities up to date.

As discussed in Section 2.2, the majority of exploration strategies are not able to handle a changing environment, avoiding the need to actively decide how to build and maintain a environmental model that also changes over time (like the STeF-map). So, in this chapter, a new methodology for mobile robot exploration is introduced to maximise the knowledge of human activity patterns, by deciding where and when to collect observations. This is done through the introduction of an exploration policy driven by the entropy levels of the cells in a STeF-map computed from previous observations. Furthermore, a study is presented comparing multiple spatio-temporal exploration policies, evaluating their performance in building and refining a time-dependent probabilistic map (STeF-map).

As the name implies, each spatio-temporal exploration strategy is composed of both a spatial policy and a temporal policy, which define respectively the set of rules the robot must follows to decide the location and time to collect data. In the experiments the spatial and temporal policies are treated independently, so the impact of all the possible combinations can be seen. For each domain, the entropy-based policy is tested, plus two more uninformed policies (Random and Round-Robin).

The work presented in this chapter extends the methodology first presented in Molina et al., 2019. In Molina et al., 2019, a fixed 24-hour period for human activities was assumed, which is not always the case. In the current work, this assumption is relaxed and instead spectral analysis is performed in the time domain for each modelled cell in the environment model. Moreover, in the experiments carried out, a clustering algorithm is used to segment the environment into regions, the number of periodicities for each cell are learnt independently, and the fidelity of the simulation

is increased by modelling robot navigation in the environment. Moreover a new long-term pedestrian dataset is added, and further analysis and discussion of the results is presented.

## 6.1 Problem definition

This chapter addresses the problem of creating a spatio-temporal pedestrian flow model as accurately as possible from sparse observations of non-trivial environments, taking into account the limited sensory capabilities and time constraints of a mobile robot.

Assuming an indoor environment with a known spatial layout, which is divided into a set of $C$ square cells forming a grid, the main aim of the robot is to learn a spatio-temporal model of each cell that best represents the human motion patterns, i.e. minimising the error between the internal model and the true human motion distributions over time.

In order to simulate a robot's limited visibility, let us define a region $R_r$ as a subset of $c_r$ number of cells that can be observed simultaneously, such that by visiting $c_r$ during an interval of time $[t, t + \Delta t)$, the observations of the human motion distributions of only the $c_r$ cells that belong to $R_r$ are obtained. The other $C - c_r$ cells in the environment during that time interval remain unseen. The observations are performed over a predefined interval of time because, as opposed to other environmental variables such as the state of an occupancy cell (*free* or *occupied*), a human motion distribution can not be obtained in a single instant of time, since the robot cannot count enough detections to built a meaningful distribution. In the experiments carried out in this chapter, each subset corresponding to each $R_r$ is non-overlapping to the others so that $C = \sum_{r=1}^{\rho} c_r$, $\rho$ is the total number of regions $R$ into which the environment has been divided.

Although some improvement in the model accuracy can be achieved by visiting the regions as often as possible, the number of observations is typically limited and the robot can spend only a fraction of the total time on actual exploration. In the

experiments this fraction is referred as the exploration ratio $e$, e.g. if $e = 0.25$ this means that the robot can spend only 25% of its operational time on gathering information from the regions. The rest of time, the robot maintains a stationary position is "blind", i.e. no sensory information is obtained.

Therefore, given an exploration ratio $e$ and a set of $\tau$ non-overlapping time intervals $[t_j, t_j + \Delta t)$, it is the exploration strategy's job to define which regions to observe and in which time interval, complying with the $e$ ratio defined, to improve the accuracy of the spatio-temporal human motion model as much as possible.

## 6.2 Exploration

In this work, the physical uncertainty, also called the irreducible or aleatory uncertainty, is proposed as a means to guide the robot's exploration activities. This uncertainty refers to the inherent variation in the physical system to be modeled, being an intrinsic property of the system or variable (a human motion distribution in this case). In order to measure this uncertainty, one of the alternative options is to use the variance. However, the variance as a measure of uncertainty works well when the variable to measure presents a unimodal distribution. This is not the case for the motion distribution obtained to created the STeF-map, since spikes for more than one main direction can appear in a cell distribution. Hence, the entropy as a measure to define the different uncertainties of the multiple distributions is a better option, as with multimodal outcome distributions, variance may incorrectly characterise changes in uncertainty (Smaldino, 2013).

In the following subsections the definition of a cell's inherent entropy is explained, together with a description of the entropy-based heuristic policies for deciding when to explore and where to do it.

### 6.2.1 Information entropy

The concept of entropy in information theory was first introduced by Claude Shannon in a classic paper (Shannon, 1948). Entropy is a quantity in information theory

associated with any random variable, which can be interpreted as the level of uncertainty inherent in the variable's possible outcomes.

Considering a discrete random variable $X$ whose possible outcomes values are $\{x_1, x_2, ..., x_n\}$ with a probability mass function $P(X)$, the entropy $H$ associated to $X$ is defined as:

$$H[P(X)] = -\sum_{i=1}^{n} P(x_i) \cdot \log_b P(x_i), \tag{6.1}$$

where $b$ is the base of the logarithm used. Common values of $b$ are 2, $e$ and 10, which define the units of the entropy as bits, nats or bans respectively.

**Toy example.** Consider a variable with just two possible outcomes such as coin tossing, where the outputs $\{head, tails\}$ have associated probabilities that are $\{p, 1-p\}$.

In this scenario the entropy of the variable is

$$H[(P(X) = \{p, 1-p\}] = -(p \cdot \log_2(p) + (1-p) \cdot \log_2(1-p)) \; [bits], \tag{6.2}$$

plotted in Figure 6.1 as a function of $p$.

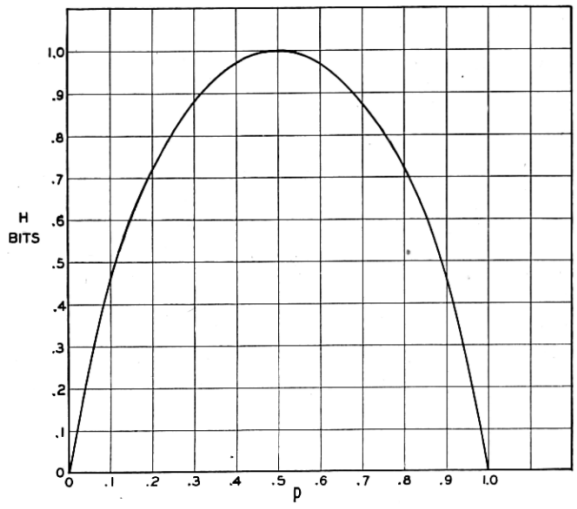


Figure 6.1: Entropy in the case of two possibilities with probabilities $p$ and $(1-p)$. Taken from Shannon, 1948.

If the coin tossing was completely fair with $p = 0.5$, then the uncertainty would be maximum ($H = 1$). The opposite situation arises when either heads or tails have a maximum bias, i.e. the outcome is always heads or always tails. In this case,

the level of uncertainty or surprise would be 0, as we know exactly the outcome in following coin tosses.

### 6.2.2 Defining entropy of a cell

As explained in Section 4.1.3 on model building, STeF-map is based on counting occurrences of people moving in multiple directions.

Taking, for example, a single randomly chosen cell $c$ with $N$ total people occurrences, its probability human motion orientation distribution is defined as $P(X) = \{x_1 = n_1/N, x_2 = n_2/N, ...., x_k = n_k/N\}$, where the count vector $n = \{n_1, n_2, ..., n_k\}$ accumulates the observed occurrences of each orientation bin $k$. Following the definition in the previous section, the entropy associated with a given cell is:

$$H_{cell}[P(X)] = -\sum_{i=1}^{k} P(\frac{n_i}{N}) \cdot \log_2(P(\frac{n_i}{N})). \tag{6.3}$$

Equation 6.3 yields the correct answer as $N/k$ tends to infinity, but in many practical cases, statistical fluctuations of small samples induce both statistical and systematic deviations of entropy estimates (Schürmann, 2004). To mitigate this issue, the first-order Miller and Madow correction (Miller et al., 1963) is applied,

$$H_{cell}[P(X)] = -\sum_{i=1}^{k} P(\frac{n_i}{N}) \cdot \log_2(P(\frac{n_i}{N})) + \frac{k-1}{2N} \cdot \log_2(e). \tag{6.4}$$

Although this estimate still retains some bias when $N << k$ or $N \sim k$ (Paninski, 2003), this is not the case for this application as the amount of people detections tends to be greater than the number of bins. This correction adds more entropy to the cells with fewer detections, expressing the fact that having fewer data to define the motion models indicates that the distribution obtained can be less trusted.

### 6.2.3 Entropy-based exploration

It is reasonable to think that cells in diverse parts of the environment could present different motion patterns at different times, so the Shannon entropy of a cell is used to characterise those patterns. Lower entropy values indicate that people tend to follow

well-defined motions, while the higher the entropy becomes, the more randomly people move across the boundaries of that cell.

In the experiments carried out, the exploration activities are not aimed at reducing the entropy levels in the environment, as the entropy is describing the inherent uncertainties. So, the entropy is not used as reducible epistemological uncertainty (as, for example, in the work by Santos et al., 2017 or in Marchant et al., 2012 where the covariance is used as a measure of reducible uncertainty), but as a way to bias the exploration towards areas/intervals that are more suitable or more worth visiting from a pattern-based spatio-temporal modelling perspective. Lower entropy levels means better-defined motions, and hence more predictable patterns. On the other hand, it is assumed that high entropy levels describe a situation where no matter how many times the robot gathers new data, the human motion patterns will likely be unpredictable, or at least more difficult to predict than lower entropy values with sparse data, because the persons' behaviour is closer to being random. There are approaches like Dempster–Shafer theory (Dempster, 2008; Shafer, 1976), that allow to unify multiple sources of uncertainties, like the inherent uncertainty and the epistemological uncertainty, which can appear due to the small number of data samples. However, this work considers that the uncertainty computed from the measurements only comes from the intrinsic "physical" characteristic that defines the motions (besides the Miller and Madow entropy bias correction). This approach also enables one of the key advantages of the STeF-map representation, i.e. that we do not need to store all past observations to update the model and make predictions for new data observations.

Therefore, in the following sections explaining the entropy-based policies for deciding when and where to perform new observations, the probabilities that define the likelihood of exploring given regions and time intervals are based on a heuristic which says that these probabilities are inversely proportional to the entropy values. This tells us that, for example, after gathering some data in a region during a certain time interval, if the resulting entropy is low, we want that region to have higher chances of being explored at future times. This is because, as already mentioned, the aim of this exploration is to build a model which is not constant in time, but

needs measurements at different points in time to properly describe the temporal motion patterns.

### 6.2.4 Defining when to explore

This subsection explains how, given a set of observable $\tau$ intervals occurring in the future, the entropy-based temporal policy decides which ones to explore complying with the exploration ratio $e$. The underlying idea is to use the map entropy from previous data gatherings to compute the entropy for the future $\tau$ time intervals, defining the chances of each interval to be chosen for exploration purposes. The steps proposed to do so are given as follows:

**I)** After each interval of time in which a data gathering action has been performed, the map entropy is calculated as the sum of all cell entropies:

$$H_{map}([t, t+\Delta t)) = \sum_{i=1}^{C} H_{cell_i}[P(X|[t, t+\Delta t))], \tag{6.5}$$

where $H_{cell}[P(X|[t, t+\Delta t))]$ is given by Equation 6.4 but the human motion counts are obtained just during a specific interval of time. For example, Figure 6.2 shows the entropy values $H_{cell}[P(X|[t, t+\Delta t))]$ calculated using 1 hour of non-overlapping time intervals of a randomly picked cell.

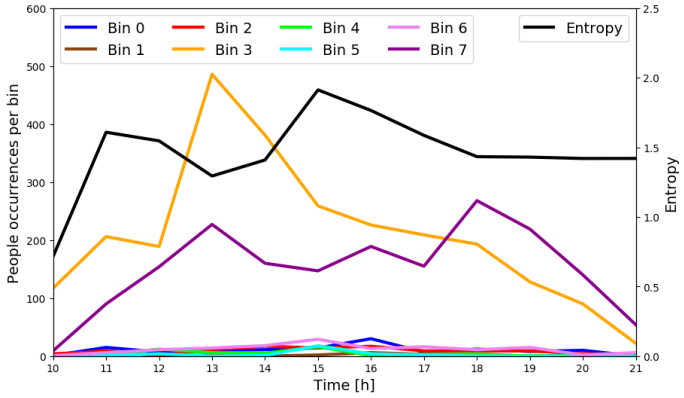


Figure 6.2: Entropy calculated over 1 day using the distributions obtained in a cell in 1 hour time intervals.

**II)** Treating $H_{map}$ as a signal over time, the next step is to compute the most prominent time correlation in the entropy values. To do so, a spectral analysis is

performed. Since the map entropy input values are not equally sampled in time due to the time constraints (when $e < 1$), the Non-Uniform Discrete Fourier Transform (NUDFT) is used for such analysis. Notice that the amount of input values used to calculate the NUDFT are determined by the exploration ration defined. The higher the value $e$, the more inputs available to compute the spectra. This frequency decomposition tells us which is the most prominent time correlation over the data by checking the periodicity $T$ with the biggest amplitude (discarding frequency 0). This can be then used to compute the averaged entropy of an interval following the correlation obtained as:

$$H_{int_j}([t_j, t_j + \Delta t)) = \frac{\sum_{z=1}^{(t_j - t_{start})/T} H_{map}([t_j - z \cdot T, t_j + \Delta t - z \cdot T))}{(t_j - t_{start})/T}, \quad j \in 1, 2, ..., \tau, \tag{6.6}$$

where $t_{start}$ is the time when the exploration activities started.

For example, Figure 6.3 shows the spectra of the three environments used in the experiments after gathering data for some time. Taking the example of the office dataset, the most prominent time dependency is 24 hours ($frequency = 7\ [1/week]$). Knowing this value, for instance the entropy measures for a 24-hour period corresponding to a day divided in 10 minutes intervals are computed by averaging the entropy values of the same 10-minute interval across multiple days (e.g. from 10:10 to 10:20 from day 1, 2, 3, ...). Note also the peak with a frequency of 1 week ($frequency = 1\ [1/week]$), which appears due to the different people behaviour between weekdays and weekends.

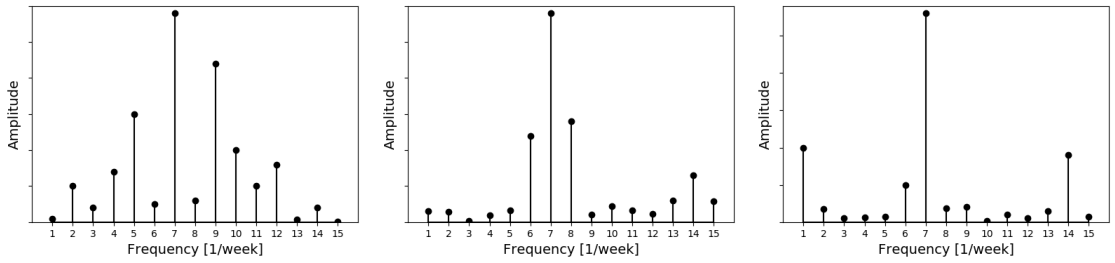


(a) ATC (b) Corridor (c) Office

Figure 6.3: Frequency spectra of the three environments map entropy values.

**III)** The probabilities that define the chances of each time interval to be chosen for data gathering are calculated as

$$P(int_j) = 1/\frac{H_{int_j}([t_j, t_j + \Delta t))}{\sum_{z=1}^{\tau} H_{int_z}([t_z, t_z + \Delta t))}, \quad j \in 1, 2, ..., \tau, \tag{6.7}$$

so that an array $I = P(int_j), \quad j \in 1, 2, ..., \tau$ containing the probabilities of all the intervals can be obtained. Finally, using $I$, the temporal entropy-based scheduling is determined by Algorithm 2.

---

**input :** $I, e, \tau$
**output:** $Q$ (array of 1s and 0s defining the intervals to explore)

```
begin
    Initialise Q to all 0s
    NumberOfIntervalsToExplore ← τ · e
    while sum(Q) ≠ NumberOfIntervalsToExplore do
        int_chosen ← Choose an interval(I) // the chances of an interval
            being picked are proportional to its probability
        if Q[int_chosen] == 0 then
            Q[int_chosen] = 1
        end
    end
end
```

**Algorithm 2:** Choose intervals to explore

### 6.2.5 Defining where to explore

In this subsection is explained how, given a set of $\rho$ regions $R$ containing each one a subset of $s$ observable cells, the entropy is used to calculate the probabilities of each region $R_r$ of being picked (in the intervals chosen by Algorithm 2) by the entropy-based spatial policy for data gathering purposes. As opposed to the approach presented for deciding when to explore, in this case, the temporal entropy evolution is not taken into account. Instead the entropy is calculated from all the accumulated people detections gathered in the past. In order to calculate the probabilities for each $R_r$ the steps proposed are the following:

**I)** First, the entropy of each region $R_r$ is computed as the sum of the entropy of all the cells that are observable ($c_r$) at $R_i$ as

$$H_{R_r} = \sum_{i=1}^{s_r} H_{cell_i}[P(X)], \quad r \in 1, 2, ..., \rho, \tag{6.8}$$

where $H_{cell}[P(X)]$ is given by Equation 6.4 from all the detections seen in the past distributed in the $k$ number of bins.

For example, Figures 6.4 and 6.5 show the occurrences for 2 different cells ($a$ and $b$) using $k = 8$ discrete orientations in 1 hour time intervals and their corresponding cumulative distributions. The cell $a$ in Figure 6.4 shows a distribution with two clear peaks corresponding to the two dominant orientations of human motion, corresponding to a low entropy value ($H_{cell_a} = 1.58$). By contrast, Figure 6.5 illustrates a cell $b$ in another part of the environment where each one of the $k = 8$ orientations obtains a similar number of person detections, corresponding to a more unpredictable behaviour, obtaining a flatter distribution, and hence a higher entropy value ($H_{cell_b} = 2.76$).

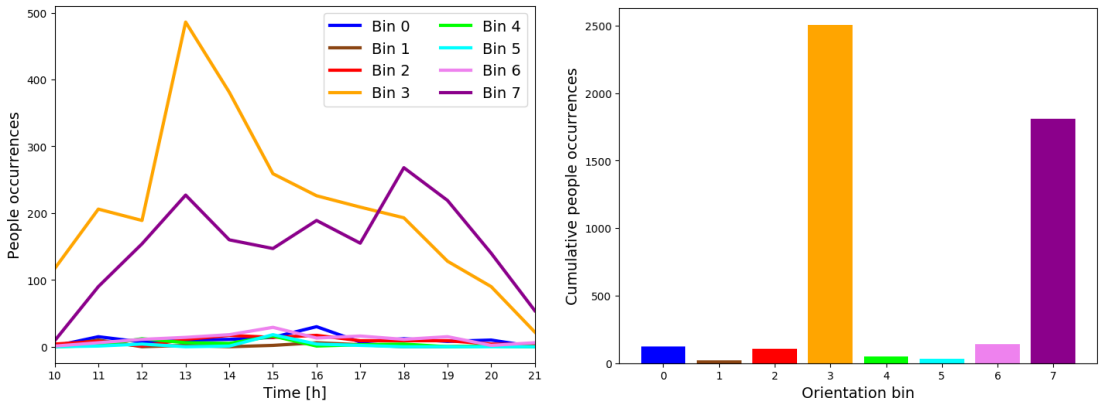


Figure 6.4: Pedestrian counts in each direction over a day and the cumulative distribution for the cell $a$ with low entropy.

**II)** Second, the probabilities that define the chances of each regions $R_i$ to be chosen to explore are calculated as

$$P(R_r) = 1/\frac{H_{R_r}}{\sum_{j=1}^{\rho} H_{R_j}}, \quad r \in 1, 2, ..., \rho. \tag{6.9}$$

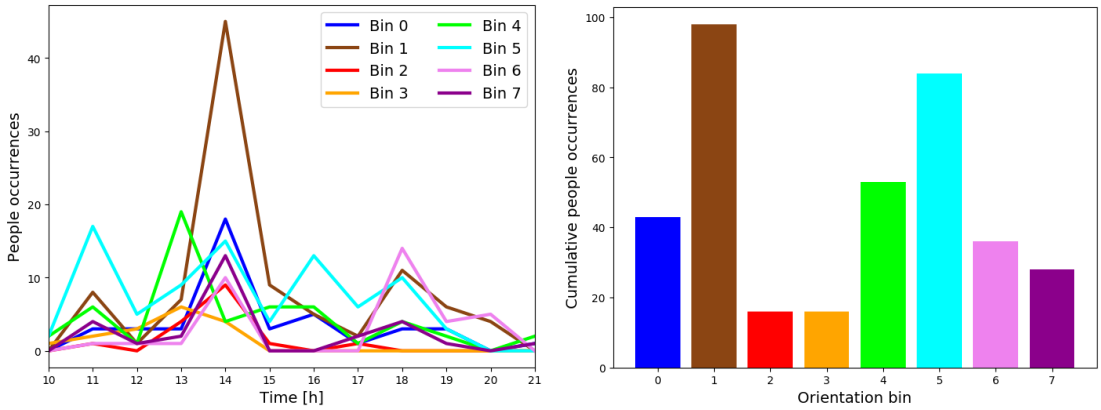


Figure 6.5: Pedestrian counts in each direction over a day and the cumulative distribution for the cell $b$ with high entropy.

So that every time a certain interval is chosen to be explored, the region where the robot will travel to obtain information about the human motion has to be defined. Similar to the approach presented for the intervals in Algorithm 2, this decision is chosen randomly, but the probability of selecting a given region $R_r$ is proportional to $P(R_r)$.

For example, let us take an environment with just two regions and each region containing just one cell. $R_1$ has only the cell $a$ from Figure 6.4 and $R_2$ has only the cell $b$ from Figure 6.5. After gathering the information shown in Figures 6.4 and 6.5, the associated normalised probabilities in this case would be $P(R_1) = 0.64$ and $P(R_2) = 0.36$.

## 6.3 Evaluation

### 6.3.1 Experimental scenarios

In the experimental section, three exploration policies are tested (Entropy, Random and Round Robin), which define the set of rules to create the exploration sequence both in time and space.

- **Entropy (E)** policy: the regions/intervals are chosen following the schemes presented in the previous section. The recalculation of the entropy levels is

done at the end of each day of exploration using all the data gathered on that day.

For the two uninformed cases implemented, the environment dynamics are not taken into account. These strategies calculate the sequence of visits simply from the number of intervals $\tau$, the number of regions $\rho$ and the ratio $e$.

- **Random (R)** policy: as its name indicates, the regions and intervals for exploration are chosen in a uniformly random way. Namely, all the $\tau$ intervals and all the $\rho$ regions have the same probability of being chosen.
- **Round Robin (B)** policy: all the areas/time intervals of the environment are visited with the same frequency, interleaving the observations so that the exploration ratio $e$ is satisfied.

In initial comparisons, a **Greedy (G)** algorithm was also implemented (Sutton et al., 2018). This always looks for the intervals/regions with the highest probability defined by Equation 6.7 and 6.9 respectively. However, in all the experiments this method performed poorly compared to the other three policies aforementioned. For that reason, the results for this approach are only presented in Figure 6.10 but not in the rest of the figures containing the box-plots. This might seem a bit counter-intuitive, but the fact that the robot always goes to the area with the lowest entropy is not always the best option, as there is no chance for the other parts to be explored. This is due to the fact that in this experimental scenario, observing a cell does not imply a change in its entropy after the measurement.

The Entropy, Random and Round Robin exploration policies are compared using the 9 different spatio-temporal combinations: R-R, B-R, E-R, R-B, B-B, E-B, R-E, B-E and E-E, where the first letter indicates the policy for choosing the location and the second letter indicates the one in charge of deciding when to explore. So, for example, in the case of R-B, the region to explore is chosen in a random way, while the time to explore is deterministic.

Regarding the temporal aspect, three different exploration ratios are used: $e =$

0.5, 0.25, 0.125. This percentage defines the number of time intervals that the robot will devote to gathering data from the total number of intervals available.

### 6.3.2 Datasets

The datasets used in the evaluation part are the same three (ATC, Corridor and Office) that were described in Chapter 3 and used in Chapter 4 for explaining the STeF-map contribution.

### 6.3.3 Model parameters

The space is discretised into $1 \times 1$ m cells for all environments, resulting in a total of $C = 1248$ , $C = 117$ and $C = 126$ active cells, respectively. The number of bins chosen to discretise the orientations in all three cases is $k = 8$, distributed as previously shown in Figure 4.6.

In the experiments it is considered that it is not possible to observe the state of the whole environment at once, so instead a set of observable regions for each dataset are defined. During exploration, only the people passing within the boundaries of the cell belonging to the chosen region are taken into account to update the spatio-temporal model at a given interval in time, while the rest of the environment remains unseen. The division is done into 24 regions for the ATC dataset, 6 for the corridor, and 7 for the office environment, giving an average of 52, 19 and 18 observable $m^2$ per region, respectively. The 3D lidar human detector used for the creation of datasets achieves good performance up to around 10 meters, which translates to an area of roughly 300 $m^2$. However, this is in an ideal scenario with open space and no occlusions, which is usually not the case. Therefore, for the ATC dataset it has been chosen to have full 360-degree coverage with a down-scaled radius of 4 m, corresponding to an area of $\sim$50 $m^2$. Using this same 50 $m^2$ for the smaller corridor and office datasets would mean having only 2 regions, so to make it more interesting instead an area was chosen in the order of the typical coverage of a depth camera (6 meters range and 60 degrees of horizontal field of view, corresponding to $\sim$19 $m^2$). In order to partition each environment into spatial regions, the $k$-means algorithm is used (Lloyd, 1982),

optimising such that all regions should contain the same or a very similar number of active cells. The summary of the parameters used in each data set can be seen in Table 6.1 and the environmental area division in Figure 6.6.

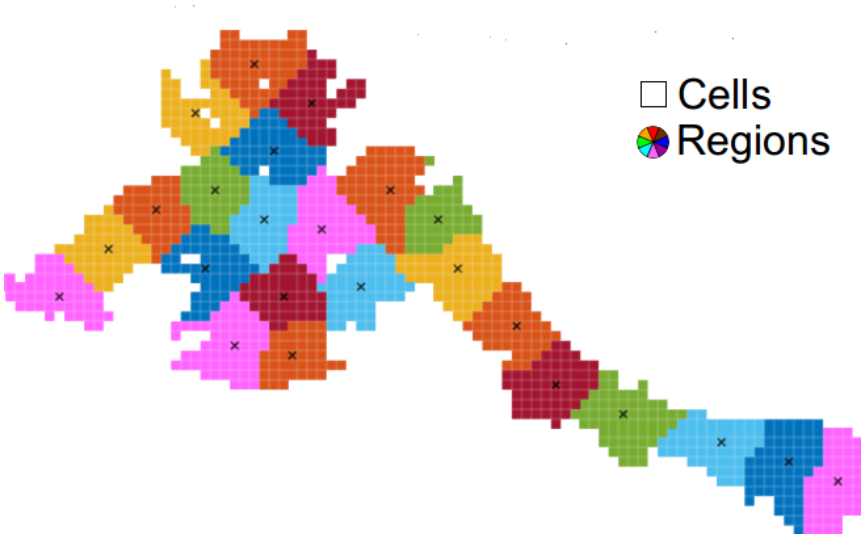


(a) ATC

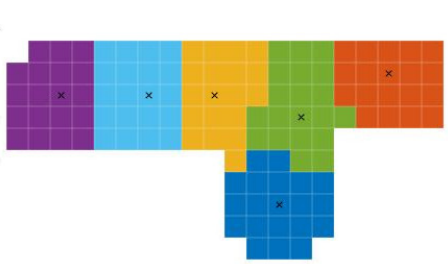

(b) Corridor

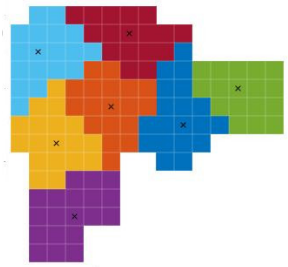

(c) Office

Figure 6.6: Spatial division in observable regions for each environment map.

Regarding time, the same parameters are used for all three datasets. The interval for creating the histograms employed as the input for the STeF-map model creation is set to 10 min. The same interval is used to provide a single observation, i.e. every 10 minutes the exploration strategy can decide whether the robot should stay in the same region or instead move to a different one. If the robot has to move to another regions, the path from the centroid (marked with crosses in Figure 6.6) of the current region to the centroid of the goal region is computed by means of the A* algorithm (Hart et al., 1968). During the travelling phase, a constant robot speed of 1 m/s is assumed (also assuming that there is no interaction with the people moving around),

and that the robot is only able to see what happens inside the region currently being traversed at each instant of time.

For each environment, the total available time for exploring in each day used is 12h (the active hours), corresponding to $\tau = 72$ time intervals (10 minutes each). For the ATC dataset the starting time is 09:00, and for the corridor and office the starting time is 08:00. The rest of the time, the environment is inactive/empty and all the cells in the environment are set to 0. From these 72 time intervals available, data gathering only happens in a certain number of time intervals, which is proportional to the exploration ratio set in each case (e.g. if the ratio is 25%, only 18 of the 72 intervals are used for exploration, while the rest remain unused).

The recalculation of the entropies for both the temporal and spatial domains are done at the end of each explored day, also at midnight the spatial-temporal schedule for the following day is created.

| **Dataset** | **Train** | **Validate** | **Test** | **Regions** | **Region size** | **Cell size** | **Cells** |
|---|---|---|---|---|---|---|---|
| ATC | 42 days | 2 days | 2 days | 24 | $\sim 52$ m$^2$ | 1×1 m | 1248 |
| Corridor | 10 days | 2 days | 2 days | 6 | $\sim 19.5$ m$^2$ | 1×1 m | 117 |
| Office | 18 days | 2 days | 2 days | 7 | $\sim 18$ m$^2$ | 1×1 m | 126 |

Table 6.1: Summary of the spatial and temporal parameters used in each data set

Every cell in the map can present different periodicities corresponding to different human activity patterns. So, in the experiments, each cell's entropy is calculated with either 1 or 2 periodicities, which is usually enough to represent the environment dynamics (Krajník et al., 2017). Using the validation days, the best number of spectral components for each cell is chosen with the corresponding frequencies, magnitude and phase shifts. These are used later to compute the model predictions and loss in model quality over the testing days.

### 6.3.4 Evaluation metric

In order to compare the performance of the different exploration strategies, a metric is needed that evaluates the prediction quality from the models. Following the same concept presented for the evaluation of the STeF-map in Chapter 4, in this section the

Chi-Squared ($\chi^2$) distance is used again to quantify the spatio-temporal strategies (see Section 4.2.2 and Equation 4.14 for the $\chi^2$ metric definition).

As mentioned before, this distance has no units, therefore in the results section the prediction accuracy is expressed as the percentage loss in model quality. The loss is based on how much worse the model prediction is compared to the distance obtained with a model created with full observability in time and space, i.e. with a 100% exploration ratio and always seeing all the cells in the map. The closer the value to 0, the better the predicted model and hence, the better the performance of the spatio-temporal strategy.

## 6.4 Results

In this section, the result obtained for the 3 different datasets are presented (Figs. 6.7 to 6.9). For each one, the 9 possible spatio-temporal exploration combinations are tested (R-R, B-R, E-R, R-B, B-B, E-B, R-E, B-E and E-E), with 3 different exploration ratios: 50%, 25% and 12.5%.

Since the *Random* and *Entropy* strategies produce stochastic policies, the values obtained are shown using a boxplot over 10 runs (median in yellow, interquartile in green, minimum and maximum with the dashed lines, and potential outliers in red). Even though *Round-Robin* produces a deterministic policy for visiting the areas/intervals, the results are also expressed with confidence intervals, since it has been defined that the starting region is not always the same. The values obtained are always computed at the end of the total training days corresponding to each dataset (Table 6.1). The validation days are used to decide the number of periodicities for each cell, and the testing days are used to obtain the percentage loss in model quality.

Furthermore, for the three "pure" combinations possible, namely R-R, B-B and E-E, the model quality loss at certain days during the total exploration days is computed, always using the same validation/training days (at the bottom of each Fig. 6.7, 6.8 and 6.9). As before, 10 runs per strategy are computed, plotting the results as the

mean together with a 95% confidence interval using Student's $t$-distribution, in order to assess the statistical significance of the differences between the means.

## ATC dataset

The results obtained for the ATC dataset are summarised in Fig. 6.7. As a general overview, the strategies with an entropy-based policy perform consistently better than their uninformed counterparts.

For low exploration ratios, as in the 12.5% case, E-R, E-B and E-E produce better results, showing that taking into account the entropy in the spatial domain is a key factor. However, as the available time to explore is increased, the strategies which take into account the entropy to decide when to explore (R-E, B-E, E-E) obtain better results, and the spatial domain becomes a secondary factor.

Observing the temporal evolution, the B-B exploration obtains by far the worst results, being the slowest one and only being able to "catch up" with the rest of the strategies in the period from day 35 to 42. For the 50% case, R-R and E-E perform very similarly, but for 25% and 12.5% after day 25, approximately, E-E obtain slightly but significantly better results.

## Corridor and Office datasets

For the last two datasets (Figs. 6.8 and 6.9), the results are a bit more difficult to analyse, due to the fact that the deviations on the results tend to be much bigger compared with the ATC dataset. This may be a consequence of having a much lower number of people occurrences in each day. So, sometimes, seeing a person in a certain interval of time becomes just a matter of luck.

Nevertheless, for the 25% exploration ratio in the Corridor dataset, the B-B exploration strategy obtains consistently better results, which is also confirmed by observing the temporal evolution. However, for the 50% and 12.5% exploration ratios, no meaningful conclusions can be extracted, as all of them behave similarly and there are no patterns on either the spatial or temporal side.

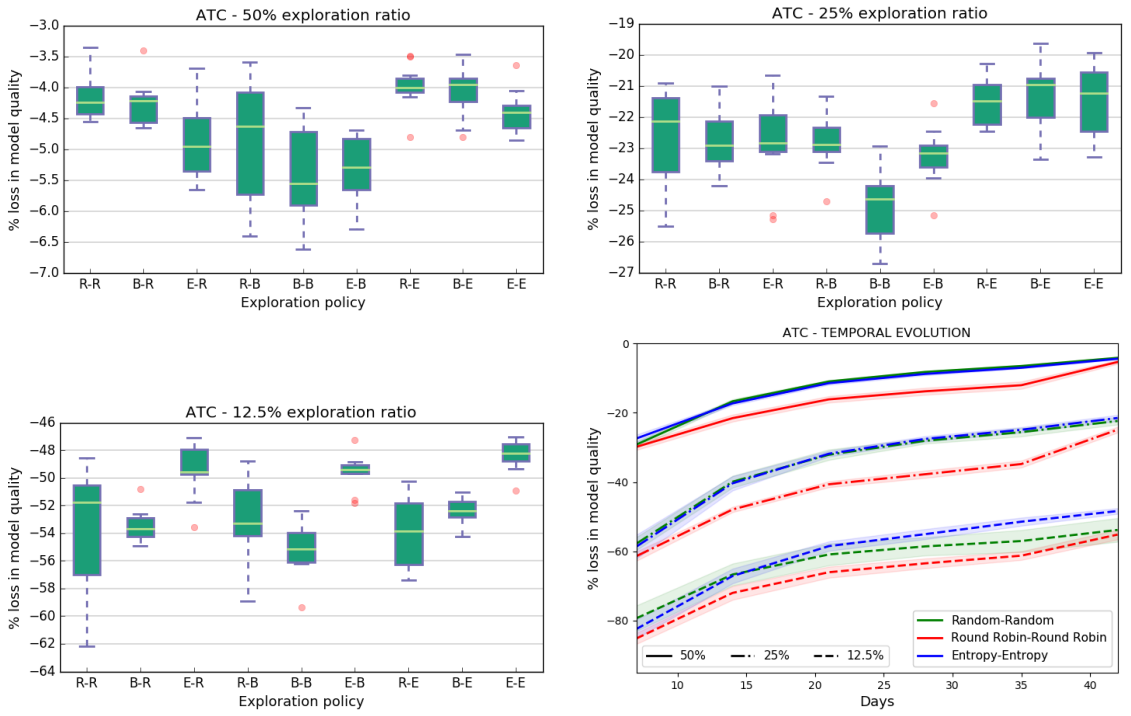


Figure 6.7: Results for the ATC dataset with 50, 25 and 12.5% exploration ratios with the 9 spatio-temporal exploration strategy combinations, and temporal evolution over the exploration days for the 3 pure combinations.

For the Office dataset, the exploration strategies which follow the *Round-Robin* policy in the temporal domain perform worse for low exploration ratios, which can also be seen in the temporal evolution plot. The major difference appreciated in this dataset comes for the 25% ratio, where the combinations sharing the entropy-based exploration in the time domain (R-E, B-E and E-E) manage to obtain consistently better results.

### 6.4.1 Discussion

The results suggest that the entropy-based exploration works well when we have an environment with a substantial number of people detections and somewhat regular flows, as in the ATC dataset. In scenarios with fewer human encounters, like the Corridor and Office environments, it would probably be necessary to further extend the days explored to several weeks to obtain statistically significantly results, or compute hundreds of runs to deal with the higher deviations obtained. Also, in the Corridor and Office environments at any point the exploration strategy in charge of

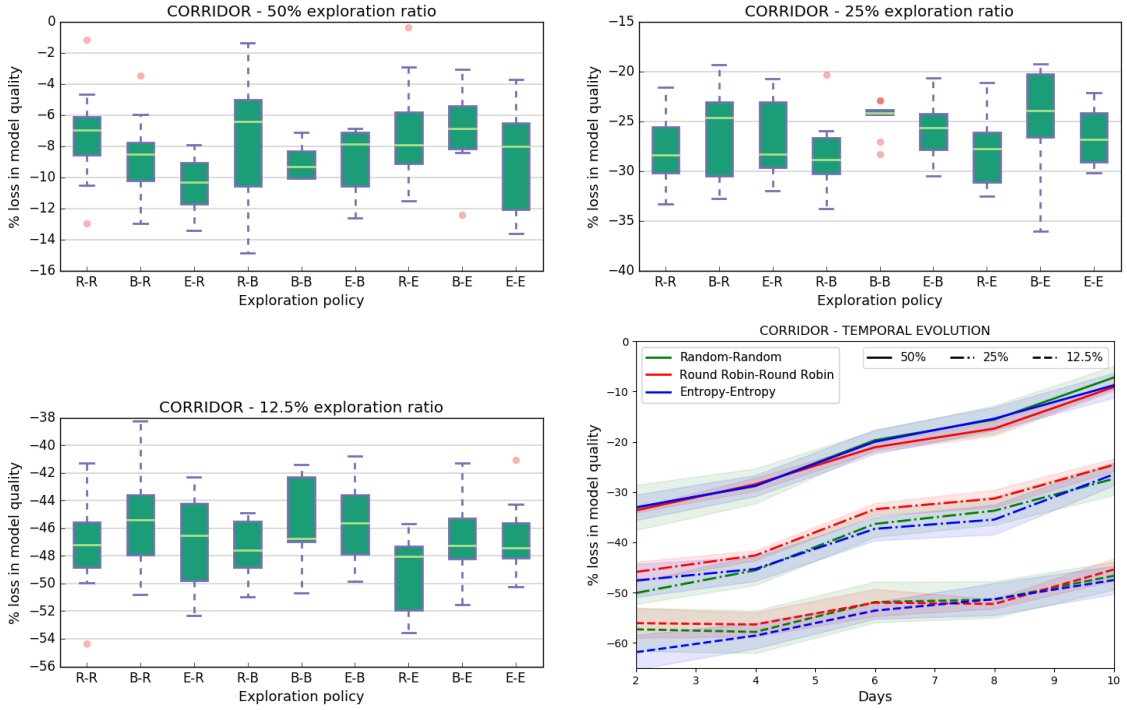


Figure 6.8: Results for the Corridor dataset with 50, 25 and 12.5% exploration ratios with the 9 spatio-temporal exploration strategy combinations, and temporal evolution over the exploration days for the 3 pure combinations.

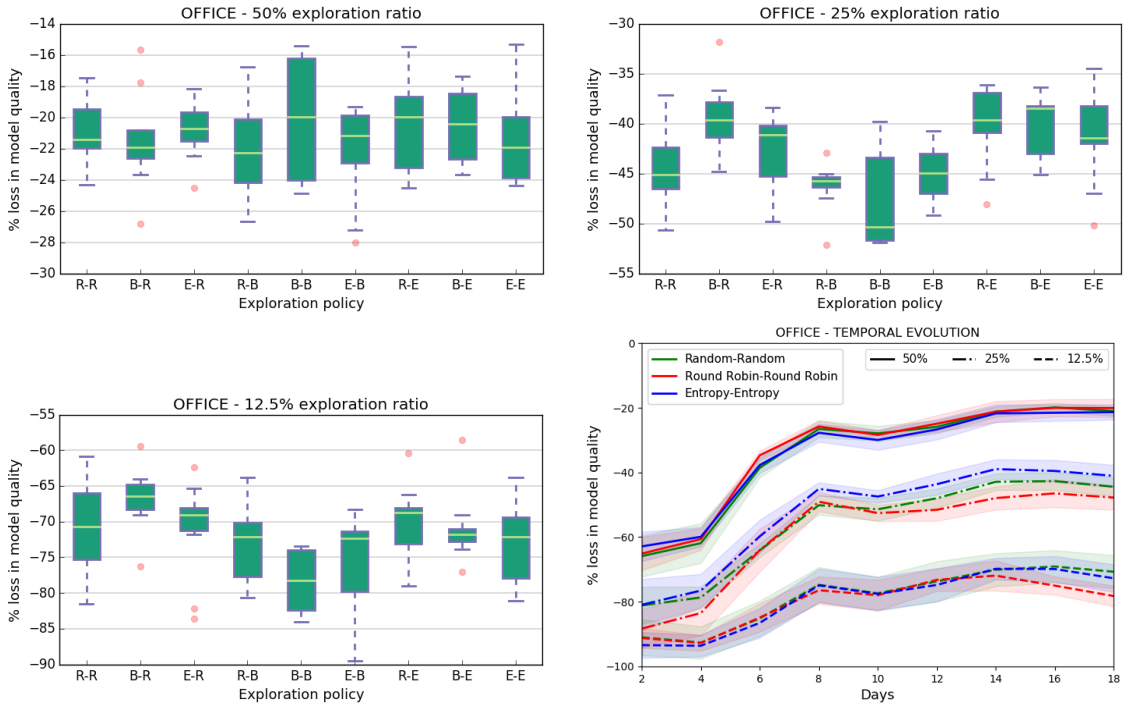


Figure 6.9: Results for the Office dataset with 50, 25 and 12.5% exploration ratios with the 9 spatio-temporal exploration strategy combinations, and temporal evolution over the exploration days for the 3 pure combinations.

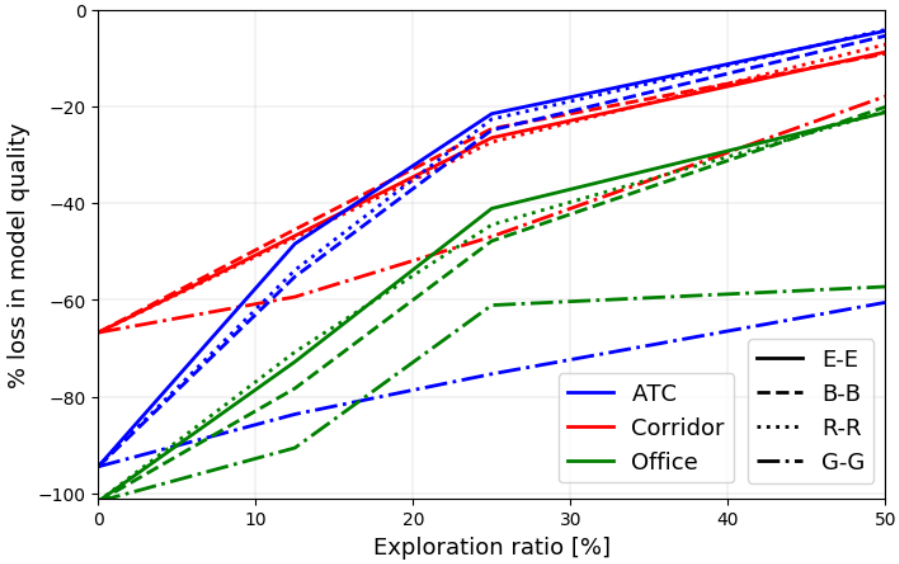


Figure 6.10: Correlation between model quality loss and exploration ratio for all datasets with the 3 pure exploration strategy combinations (E-E, B-B, R-R) and the Greedy-Greedy (G-G) approach omitted in the previous results due to poor performance compared to the rest.

scheduling the region to explore has a major impact on the final results. Probably the fact that there is a much lower number of regions to explore compared to the shopping centre makes no actual difference, as the simulated robot is able to visit them a lot more times, even for low exploration ratios.

However, taking the exploration ratio as clearly the factor that has the biggest impact on the total percentage loss in model quality during the exploration activities (which is clear to see in the temporal evolution plot in Figs. 6.7 to 6.9), we see that in all datasets this impact follows a similar trend. In Fig. 6.10 is plotted the correlation between the percentage loss in model quality and the exploration ratio for all three datasets, at the end of the corresponding exploration days for the three pure combinations (E-E, B-B, R-R). The value obtained with 0% exploration ratio corresponds to a model which has not been trained with any data, so all orientations in each cell have the same probability. The outcome shows that the loss tends to decrease exponentially as the exploration ratio is increased.

Looking at the loss in model quality also in Fig. 6.10, the Office dataset obtains noticeably worse results for all exploration ratios compared to the Corridor and ATC datasets. This may be caused by the fact that the recordings in the Office dataset

were also done during the weekends, days which present a very different behaviour (the environment is mostly empty) when compared to the weekdays. This increased complexity makes it more difficult for the spatio-temporal model to find the overall patterns to be modelled using only sparse partial observations. In the ATC dataset, weekends are also part of the data, but in this case, there are no major differences in human motion behaviour between the weekday and weekend recorded.

## 6.5 Summary

In this chapter, a comparison between multiple robot exploration strategies to build a spatio-temporal model of human motion in a given environment is presented. Moreover, it is proposed to use the data already gathered by the robot to determine where and when to perform future observations, based on the entropy levels in the model, which are computed from the distributions of pedestrian motion direction.

The results show that the entropy-driven policy improves the results obtained by the uninformed exploration strategies in scenarios with a substantial degree of human presence and rhythmic patterns of activity.

Furthermore, it has been demonstrated that the exploration ratio is the key factor affecting the model prediction quality and that similar trends in the correlation between model quality loss and the exploration ratio are obtained. This is interesting, considering that all three datasets tested in the experiments contain a different number of exploration days and a different number of regions to explore.

### 6.5.1 Limitations

The simulation experiments tried to mimic a real mobile robot exploring the environment using pre-recorded datasets of pedestrian activities. However, the results have been obtained using certain simplifications, including no noise/occlusions in the perception and perfect navigation without any physical interaction with people. These aspects would play an important role when the experiments are carried out with real mobile robots. Nevertheless, the current work is considered necessary, as

having ground truth data (having an "overhead" sensor/sensors capable of seeing the whole environment all the time) is essential to compare the exploration strategies. Using datasets that are collected by mobile robots would mean that the model can only be updated from locations where the robot was actually present during the real-life recordings, which would not allow us to compare exploration strategies in the spatial domain. Also, the ability to place the simulated robot at any time in the past to start the exploration with the same human behaviour over and over again, and that it is possible to simulate the exploration days in a much smaller fraction of time, would be difficult if not impossible to reproduce for real-world experiments. Moreover, in the experiments done here, the temporal strategies were free to choose any time interval during the available time as long as the total number of intervals chosen met the exploration ratio constraints. In a real environment, the available time can differ from day to day due to the other main tasks in the robot's schedule, which adds further complexity to the system.

# Chapter 7

# Conclusions and Future Work

The overarching idea behind the work presented in this thesis is to investigate the introduction of temporal dynamics into mapping and exploration activities, in order to model pedestrian flow patterns from a mobile robot's perspective. The motivation comes from the belief that robots should take into account the expected flow of people at a given time to plan their trajectories, in an attempt to improve their behaviour and navigate in a more socially compliant way.

The discussion in Chapter 2 indicates that much of the related work to date has been focused only on spatial reasoning, rather than spatio-temporal reasoning, as in this thesis. However, introducing mobile robots into tasks requiring long-term autonomy introduces several challenges, as the environmental models have to handle temporal changes, and the robot's exploration strategy should also account for those, thus becoming a never-ending task.

## 7.1 Summary of contributions

Following the aforementioned concepts, this thesis presented the following contributions.

**STeF-map.** In Chapter 4, a grid-based representation of human flows called a Spatio-Temporal Flow Map, or STeF-map, was introduced. In contrast to similar approaches reviewed in Section 2.1.2, STeF-map captures temporal flow changes in the cells composing the map. Assuming that people tend to follow cyclic patterns of activity, the model is able to learn the different temporal periodicities (hours to weeks) by a set of harmonic functions associated to discrete orientations in each grid cell. This allows us to make probabilistic predictions at any point in time about the

expected human motion distributions. The approach has been evaluated in three real long-term pedestrian datasets, showing that the introduction of temporal dynamics to model people flows results in improved prediction accuracy. The ROS implementation of STeF-map is publicly available and can be found in *LCAS - Software and Datasets* 2020.

**Experimental comparison.** In Chapter 5, the STeF-map representation introduced in the previous chapter is compared against other state-of-the-art pattern-based approaches for modelling human motion in two different ways. The first comparison evaluates the prediction quality of future human flows after some days of training the models. For that purpose, two different metrics are used, the Chi-squared ($\chi^2$) distance between predicted and ground truth human motion discrete distributions and the root mean square error. The second comparison focuses on the model's impact from a social perspective, evaluating the utility of the predictions for assisting mobile robot navigation tasks in human-shared environments. The output from both comparisons shows that STeF-map manages to outperform the rest of the approaches for prediction capabilities using the $\chi^2$ distance and also in the social cost-based evaluation.

**Spatio-temporal robotic exploration.** Understanding how people are likely to move is key to an efficient and safe robot navigation in human environments. However, mobile robots can only observe a fraction of the environment at a time, while the activity patterns of people may also change at different times. Therefore in Chapter 6, the spatio-temporal robot constraints were addressed by the introduction of a new methodology for mobile robot exploration to maximise the knowledge of human activity patterns, by deciding where and when to collect observations. The thesis presented an exploration policy driven by the entropy levels from the previously gathered data, together with a comparison between multiple spatio-temporal exploration strategies, including both informed and uninformed approaches. The evaluation was performed by simulating mobile robot exploration using real sensory data from the three long-term pedestrian datasets. The results suggest that for cer-

tain scenarios, the proposed exploration system can better predict the flow patterns than the uninformed strategies considered.

**Pedestrian datasets.** And last, but not least, the literature review in Chapter 3 showed that there was a lack of long-term pedestrian datasets available for research, as most of the existing ones have relatively short recording times. Hence, during the development of the thesis, two new datasets were introduced, one containing 14 days of people motions in a corridor and the other 22 consecutive days recorded in an office environment. These datasets provide complex spatio-temporal human motion patterns to support the evaluation and analysis in Chapters 4, 5 and 6. These datasets are also made publicly available for benchmarking and result comparison by the wider research community. They can be found in *LCAS - Software and Datasets* 2020.

## 7.2 Future research directions

### 7.2.1 Spatio-Temporal Flow map

Besides the specific improvements to the model, such as adding the speed in the prediction or keeping the human flow intensity/density values described in more detail in Section 4.4, from a higher-level point-of-view, there are two areas of application which could benefit the most from the STeF-map representation and present interesting further research paths: planning and navigation, and motion prediction.

**Planning and navigation.** The increase in prediction accuracy from the introduction of the temporal dynamics means that a robot has a better understanding of how the people will behave, hence enabling the robot to plan its activities around humans in a more optimal way (Palmieri et al., 2017; Swaminathan et al., 2018).

The benefits of this technology should extend to a wide range of applications where socially compliant navigation is needed. Possible use cases include transport and delivery applications in crowded environments, where the robot should move with the direction of pedestrian flows in order to minimise the possibility of head-on

collisions, for example, in shopping malls (Brscic et al., 2013), airports (Triebel et al., 2016b), and museums (Duchetto et al., 2019). In service robotics, the approach could be used by the robot's scheduling software to maximise and optimise encounters with selected user groups, such as providing information services to residents in care homes, or patrolling in security and surveillance applications (Hawes et al., 2017), based on the expected future locations of people. For example, a robot might move to a location where a task has to be carried out some time in advance to avoid congestion at the destination point. In safety critical applications within industrial environments, such as warehouses (Carmona et al., 2019) and farms (Das et al., 2018), the approach could be used to maintain a safe distance to the expected location of human workers, in order to minimise the probability of accidents.

Although the potential benefits and domains where this technology could be useful have been identified, there is still an ongoing need to evaluate the actual impact of the different motion models on the surrounding people in real application scenarios. Usually the metrics employed are useful to evaluate the improvement from the robot's point-of-view: navigation success ratio (Fentanes et al., 2015) or time to reach the goal and path distance (Palmieri et al., 2017), but they rarely consider the human side.

A major limitation of the current research presented in this thesis is that human-robot interaction has not been considered, because the sensory data used for the model building or the exploration simulations was obtained from pre-recorded data-sets. Hence it does not take into account that, for example, placing a real robot in the same environment that has to be modelled produces an influence on the observed motion patterns that is created by the robot itself. This human-robot interaction (HRI) or influence is extremely hard to predict and, therefore, realistic simulations do not currently exist. Considering the HRI limitations assumed in this work, a natural step forward for the research would be performing HRI studies with real robots interacting with real people. The work by Belhassein et al., 2019 proposes some checkpoints to take into account when designing HRI experiments. For example, it mentions the so-called "wow" effect that a robot causes in people who are not very accustomed to seeing robots, attracting more attention that normal, at least

during the initial deployment. Consequently, in experiments that aim at modelling human motion behaviour, this effect could cause the model to not reflect the normal behaviour of people in the long term. Also, during the evaluation it is important to understand that what can be considered as socially compliant in one country or culture may not be the same in others. For example, the study of proxemics by Sorokowska et al., 2017, on interpersonal distances in multiple countries, revealed different behaviours according to factors such as age, culture and gender.

**Adding speed values.** Besides the orientation, from the exploitation point-of-view, it could be also useful to introduce the speed in the $\langle t, x, y, \theta \rangle$ vector for every detection. A way to encode this extra variable would imply adding extra models for each cell. For example, in Figure 7.1 there is a proposal with a cell containing 16 different temporal models. In this example, adding two states for the speed (less or equal that 1m/s or greater than 1m/s) means having an extra 8 states from the original "orientation only" discretisation. The disadvantage of such an approach would be that more data would be required, in order to have sufficient detections in each cell to populate all 16 states in each interval in a meaningful way.

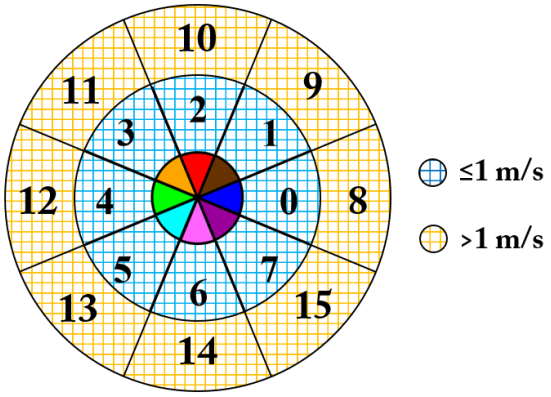


Figure 7.1: Proposal of cell discretisation for adding the motion speed into the model.

**Motion prediction.** Another research direction is to investigate the applicability of the introduced spatio-temporal flow map for improving the prediction of the expected motion of an individual person (instance) observed in the environment. As presented in Section 2.1, besides the pattern-based human motion approaches (such as STeF-map), there are physics-based and planning-based approaches that

apply the predictions for each moving entity in the map. They attempt to recreate the expected human motion in the immediate future (a couple of seconds) mainly for safety purposes, and from a slightly longer-term perspective (several seconds) for trajectory prediction inside the whole environment. Using as a prior the STeFmap spatio-temporal generalisation capabilities, in combination with the physics and planning-based approaches, might lead to improved human trajectory prediction. This leads to research works aiming at merging or combining different domain approaches for increasing the overall accuracy of human motion prediction.

### 7.2.2 Spatio-Temporal exploration

From the spatio-temporal robotic exploration work introduced in Chapter 6 stem several future research areas which could help to further improve the methodology and the conclusions extracted from the results.

**More realistic simulations.** In the simulation carried out for evaluating the multiple exploration strategies, the pedestrians and the robot were considered as 2D points moving inside a map without any form of interaction. To make the simulation more realistic it could be extended into a 3D environment. For example, a physics-based simulator like Gazebo (*Gazebo Simulator* 2020) with a standard mobile platform could be adopted, together with a pedestrian crowd simulator such as the 'PedSim' system (*PedSim ROS* 2020) developed within the SPENCER project (Triebel et al., 2016a). This would allow to recreate higher fidelity models of the sensors present in the robot such as 2D lasers, 3D lidar or RGB-D cameras and, for example, the occlusions from having multiple people surrounding the robot.

**Integration with a task scheduler.** In the experiments carried out, the locations and times to explore were planned at the beginning of each day. The scheduler had complete freedom to allocate the intervals without any temporal restriction other than to meet the specified exploration ratio. However, this scenario is not always possible. Let us take, for example, the scenario presented in the introduction chapter of a pallet truck operating in a warehouse (Section 1.2.1). In this case, it

would be interesting to investigate adding the exploration system to the warehouse management system that allocates the different tasks (moving goods, palletising, wrapping, etc.) to the robots. The exploration strategy should also take into account these non-exploration tasks in order to optimise the data gatherings during the time scheduled for additional exploration actions.

**Real robot experiments.** A clear step forward to further analyse the results obtained with different exploration strategies is to implement the same system and methodology on a real mobile robot. However, this raises some interesting questions and problems. One of the issues comes the fact that sometimes the environments that need to be modelled are not structurally static. Let us take, for example, an airport, where it is quite common to see "wet floor" signs that can modify the human motion patterns, creating a discrepancy in the model, or to find queues of people acting as a barrier, making the traversability more difficult between different areas that need to be explored. The model should account for these uncertainties, allowing a higher degree of flexibility in the system.

Another issue from experimenting in a real environment is that the robots can not travel to the past to compare different exploration behaviours with the same people occurrences. When the comparison focuses on evaluating spatial-only exploration strategies, the map that needs to be build is assumed to be static, so it does not matter that different strategies are run at different days (because the ground truth is always the same). However, exploring tasks aimed at learning models that also change over time makes the comparison a challenge, as the ground truth data is constantly changing. In order to attempt to overcome this data ground-truthing constraint some king of temporal cross validation could be used.

**Multi-robot systems.** Following works presented in the related work chapter for frontier-based or information-based exploration, the methodology presented here could also be adapted for multi-robot applications. Having more robots means more sensors able to capture the people trajectories in the environment. In theory, this would mean that the models can be updated and refined more often, obtaining better

prediction results earlier in time after deployment. With a simplified 2D simulation, the task of adding another entity sharing the same metric map and updating the same model could be a relatively straightforward task. However, moving into more realistic 3D physics-based simulations and working with real robots increases the complexity of the systems, as the robots need real-time localisation, navigation and communication between the robots, as well as planning constraints (time and spatial).

**Benchmarking of spatio-temporal exploration strategies.** The simulation environment created in Chapter 6 was developed from scratch to meet the needs of the required comparison. Further research and improvements to the simulation, such as those discussed above, could go together with a standardisation of the methodology so it can be automated. For example, in computer vision, the KITTI dataset (Geiger et al., 2012) is a widely used benchmark suite for research topics including stereo vision, optical flow, visual odometry, 3D object detection and 3D tracking. Or, in the robotic exploration domain, a guideline and framework for multi-robot frontier-based exploration benchmarking was presented by Faigl et al., 2015. The authors describe a multi-stage methodology that relies on simulation and real-world experiments in controllable environments, which enable the evaluation of the exploration strategies using different metrics including distance travelled or duration of the exploration task. Having standard benchmarks would make the comparison of different approaches by different authors easier to evaluate. So, following the same path of the two aforementioned approaches, it would be interesting to have a similar benchmark suite for evaluating multiple spatio-temporal exploration strategies to model human motion in space and time.

**Exploitation during exploration.** Another area for future work would involve exploiting the flow models obtained during exploration. Currently, the robot follows an optimal path from region A to region B, but instead the spatio-temporal model could be exploited in different ways. For example, the model could be used as a prior for path planning, so the robot can move in a more efficient way, or the entropy values

obtained from previous days could be used to bias the robot movements through certain regions to increase information gain, even if some time is lost.

**Exploration algorithm in other applications.** The experiments carried out in Chapter 6 regarding the multiple exploration strategies were performed having in mind a specific application in the mobile robots domain. However, there are other situations where this approach could also be exploited and tested. For example, let us consider a CCTV camera system in the streets aimed at learning the traffic flows patterns (C. Fox et al., 2010) which it is not capable to cover the full environment that needs to be modelled, because each camera can only cover a limited area at each point in time. This situation could be compared to having a multi-robot system, but instead of dealing with a mobile robot fleet, the system would be composed of sensors (static in the space by dynamic in orientation) that need to be controlled and redirected to learn the traffic patterns and relearn them as fast as possible if they change over time.

# References


Alahi, Alexandre, Kratarth Goel, Vignesh Ramanathan, Alexandre Robicquet, Li Fei-Fei and Silvio Savarese (2016). 'Social LSTM: Human trajectory prediction in crowded spaces'. In: *Proceedings of the IEEE conference on computer vision and pattern recognition*, pp. 961–971 (cit. on p. 14).

Amigoni, Francesco and Vincenzo Caglioti (2010). 'An information-based exploration strategy for environment mapping with mobile robots'. In: *Robotics and Autonomous Systems* 58.5, pp. 684–699. ISSN: 0921-8890. DOI: https://doi.org/10.1016/j.robot.2009.11.005. URL: http://www.sciencedirect.com/science/article/pii/S0921889009002024 (cit. on p. 24).

Aoude, Georges, Joshua Joseph, Nicholas Roy and Jonathan How (2011). 'Mobile agent trajectory prediction using Bayesian nonparametric reachability trees'. In: *Infotech@ Aerospace 2011*, p. 1512 (cit. on pp. 11, 12).

Baglietto, M, M Paolucci, L Scardovi and R Zoppoli (2002). 'Information-based multi-agent exploration'. In: *Proceedings of the Third International Workshop on Robot Motion and Control, 2002. RoMoCo'02.* IEEE, pp. 173–179 (cit. on p. 24).

Ballan, Lamberto, Francesco Castaldo, Alexandre Alahi, Francesco Palmieri and Silvio Savarese (2016). 'Knowledge transfer for scene-specific motion prediction'. In: *European Conference on Computer Vision*. Springer, pp. 697–713 (cit. on p. 13).

Barraquand, Jerome, Bruno Langlois and J-C Latombe (1992). 'Numerical potential field techniques for robot path planning'. In: *IEEE transactions on systems, man, and cybernetics* 22.2, pp. 224–241 (cit. on p. 20).

Barth, Alexander and Uwe Franke (2008). 'Where will the oncoming vehicle be the next second?' In: *2008 IEEE Intelligent Vehicles Symposium*. IEEE, pp. 1068–1073 (cit. on p. 11).

Bartoli, Federico, Giuseppe Lisanti, Lamberto Ballan and Alberto Del Bimbo (2018). 'Context-aware trajectory prediction'. In: *2018 24th International Conference on Pattern Recognition (ICPR)*. IEEE, pp. 1941–1946 (cit. on p. 14).

Belhassein, Kathleen, Guilhem Buisan, Aurélie Clodic and Rachid Alami (2019). 'Towards methodological principles for user studies in Human-Robot Interaction'. In: *Test Methods and Metrics for Effective HRI in Collaborative Human-Robot Teams Workshop, ACM/IEEE International Conference on Human-Robot Interaction* (cit. on p. 112).

Bellotto, Nicola and Huosheng Hu (2010). 'Computationally efficient solutions for tracking people with a mobile robot: an experimental evaluation of Bayesian filters'. In: *Autonomous Robots* 28.4, pp. 425–438 (cit. on pp. 33, 34).

Belongie, Serge, Jitendra Malik and Jan Puzicha (2002). 'Shape matching and object recognition using shape contexts'. In: *IEEE transactions on pattern analysis and machine intelligence* 24.4, pp. 509–522 (cit. on p. 52).

Benfold, Ben and Ian Reid (2011). 'Stable multi-target tracking in real-time surveillance video'. In: *CVPR 2011*. IEEE, pp. 3457–3464 (cit. on p. 29).

Benkrid, Abdenour, Abdelaziz Benallegue and Noura Achour (2019). 'Multi-robot Coordination for Energy-Efficient Exploration'. In: *Journal of Control, Automation and Electrical Systems* 30.6, pp. 911–920 (cit. on p. 22).

Bennewitz, Maren, Wolfram Burgard, Grzegorz Cielniak and Sebastian Thrun (2005). 'Learning motion patterns of people for compliant robot motion'. In: *The International Journal of Robotics Research* 24.1, pp. 31–48 (cit. on p. 14).

Bennewitz, Maren, Wolfram Burgard and Sebastian Thrun (2002). 'Using EM to learn motion behaviors of persons with mobile robots'. In: *IEEE/RSJ International Conference on Intelligent Robots and Systems*. Vol. 1. IEEE, pp. 502–507 (cit. on p. 14).

Best, Robert A and JP Norton (1997). 'A new model and efficient tracker for a target with curvilinear motion'. In: *IEEE Transactions on Aerospace and Electronic Systems* 33.3, pp. 1030–1037 (cit. on p. 11).

Biber, P. and T. Duckett (2009). 'Experimental analysis of sample-based maps for long-term SLAM'. In: *International Journal of Robotics Research* (cit. on pp. 17, 25).

Biswas, Joydeep and Manuela Veloso (2016). 'The 1,000-km challenge: Insights and quantitative and qualitative results'. In: *IEEE Intelligent Systems* 31.3, pp. 86–96 (cit. on p. 27).

Bourgault, Frederic, Alexei A Makarenko, Stefan B Williams, Ben Grocholsky and Hugh F Durrant-Whyte (2002). 'Information based adaptive robotic exploration'. In: *IEEE/RSJ international conference on intelligent robots and systems*. Vol. 1. IEEE, pp. 540–545 (cit. on p. 23).

Bracewell, Ronald Newbold and RN Bracewell (1986). *The Fourier transform and its applications*. Vol. 31999. McGraw-Hill New York (cit. on p. 40).

Brscic, D., T. Kanda, T. Ikeda and T. T. Miyashita (2013). 'Person position and body direction tracking in large public spaces using 3D range sensors'. In: *IEEE Transactions on Human-Machine Systems* 43.6, pp. 522–534 (cit. on pp. 29–31, 38, 112).

Burgard, Wolfram, Mark Moors, Dieter Fox, Reid Simmons and Sebastian Thrun (2000). 'Collaborative multi-robot exploration'. In: *Proceedings 2000 ICRA. Millennium Conference. IEEE International Conference on Robotics and Automation. Symposia Proceedings (Cat. No. 00CH37065)*. Vol. 1. IEEE, pp. 476–481 (cit. on p. 22).

Burgard, Wolfram, Mark Moors, Cyrill Stachniss and Frank E Schneider (2005). 'Coordinated multi-robot exploration'. In: *IEEE Transactions on robotics* 21.3, pp. 376–386 (cit. on p. 24).

Camara, Fanta, Nicola Bellotto, Serhan Cosar, Dimitris Nathanael, Matthias Althoff, Jingyuan Wu, Johannes Ruenz, André Dietrich and Charles W Fox (2020a). 'Pedestrian Models for Autonomous Driving Part I: low level models, from sensing to tracking'. In: *IEEE Transactions on Intelligent Transportation Systems* (cit. on p. 10).

Camara, Fanta, Nicola Bellotto, Serhan Cosar, Florian Weber, Dimitris Nathanael, Matthias Althoff, Jingyuan Wu, Johannes Ruenz, André Dietrich, Gustav Markkula et al. (2020b). 'Pedestrian Models for Autonomous Driving Part II: High-Level Models of Human Behavior'. In: *IEEE Transactions on Intelligent Transportation Systems* (cit. on p. 10).

Camplani, Massimo, Adeline Paiement, Majid Mirmehdi, Dima Damen, Sion Hannuna, Tilo Burghardt and Lili Tao (2016). 'Multiple human tracking in RGB-depth data: a survey'. In: *IET computer vision* 11.4, pp. 265–285 (cit. on p. 32).

Carmona, Manuel Fernandez, Tejas Parekh and Marc Hanheide (2019). 'Making the Case for Human-Aware Navigation in Warehouses'. In: *Towards Autonomous Robotic Systems*. Springer International Publishing, pp. 449–453. DOI: 10.1007/978-3-030-25332-5_38. URL: https://doi.org/10.1007/978-3-030-25332-5_38 (cit. on p. 112).

Carrillo, Henry, Philip Dames, Vijay Kumar and Jose Castellanos (2015). 'Autonomous robotic exploration using occupancy grid maps and graph slam based on shannon and Renyi entropy'. In: *2015 IEEE international conference on robotics and automation (ICRA)*. IEEE, pp. 487–494 (cit. on p. 23).

Carrillo, Henry, Philip Dames, Vijay Kumar and José A Castellanos (2018). 'Autonomous robotic exploration using a utility function based on Rényi's general theory of entropy'. In: *Autonomous Robots* 42.2, pp. 235–256 (cit. on p. 23).

Chang, Chih-Chung and Chih-Jen Lin (2011). 'LIBSVM: A library for support vector machines'. In: *ACM transactions on intelligent systems and technology (TIST)* 2.3, pp. 1–27 (cit. on p. 34).

Cheng, Yizong (1995). 'Mean shift, mode seeking, and clustering'. In: *IEEE transactions on pattern analysis and machine intelligence* 17.8, pp. 790–799 (cit. on p. 71).

Chevalier, Guillaume (2018). *The LSTM cell*. [Online; accessed 07-08-2020]. URL: https://commons.wikimedia.org/w/index.php?curid=71836793 (cit. on p. 72).

Chinellato, Eris, Kanti V Mardia, David C Hogg and Anthony G Cohn (2017). 'An incremental von mises mixture framework for modelling human activity streaming data'. In: *Proceedings ITISE 2017* (cit. on p. 18).

Churchill, Winston S. and Paul Newman (2013). 'Experience-based navigation for long-term localisation'. In: *IJRR*. DOI: 10.1177/0278364913499193. eprint: http://ijr.sagepub.com/content/early/2013/09/16/0278364913499193.full.pdf+html (cit. on pp. 17, 25).

Cielniak, Grzegorz, Maren Bennewitz and Wolfram Burgard (2003). 'Where is...? learning and utilizing motion patterns of persons with mobile robots'. In: *IJCAI*. Vol. 25, pp. 909–914 (cit. on p. 14).

Cochran, WG (1952). 'The chi-square test of goodness of fit'. In: *Ann. Math. Statist* 23, pp. 315–345 (cit. on p. 52).

Cooley, J, P Lewis and P Welch (1969). 'The finite Fourier transform'. In: *IEEE Transactions on audio and electroacoustics* 17.2, pp. 77–85 (cit. on p. 43).

Cortes, Corinna and Vladimir Vapnik (1995). 'Support-vector networks'. In: *Machine learning* 20.3, pp. 273–297 (cit. on p. 34).

Coscia, Pasquale, Francesco Castaldo, Francesco AN Palmieri, Alexandre Alahi, Silvio Savarese and Lamberto Ballan (2018). 'Long-term path prediction in urban scenarios using circular distributions'. In: *Image and Vision Computing* 69, pp. 81–91 (cit. on pp. 11, 12).

Cula, Oana G and Kristin J Dana (2004). '3D texture recognition using bidirectional feature histograms'. In: *International Journal of Computer Vision* 59.1, pp. 33–60 (cit. on p. 52).

Daily, Robert and David M Bevly (2008). 'Harmonic potential field path planning for high speed vehicles'. In: *2008 American Control Conference*. IEEE, pp. 4609–4614 (cit. on p. 20).

Das, Gautham, Grzegorz Cielniak, Pal From and Marc Hanheide (May 2018). 'Discrete Event Simulations for Scalability Analysis of Robotic In-Field Logistics in Agriculture - A Case Study'. In: *IEEE International Conference on Robotics and Automation, Workshop on Robotic Vision and Action in Agriculture*. URL: http://eprints.lincoln.ac.uk/id/eprint/32170/ (cit. on p. 112).

Dayoub, Feras and Tom Duckett (2008). 'An adaptive appearance-based map for long-term topological localization of mobile robots'. In: *Proc. of Int. Conference on Intelligent Robots and Systems (IROS)* (cit. on pp. 17, 25).

Dempster, Arthur P (2008). 'Upper and lower probabilities induced by a multivalued mapping'. In: *Classic works of the Dempster-Shafer theory of belief functions*. Springer, pp. 57–72 (cit. on p. 92).

Dhillon, Inderjit S and Suvrit Sra (2003). *Modeling data using directional distributions*. Tech. rep. Technical Report TR-03-06, Department of Computer Sciences, The University ... (cit. on pp. 69, 71).

Duchetto, Francesco Del, Paul Baxter and Marc Hanheide (Oct. 2019). 'Lindsey the Tour Guide Robot - Usage Patterns in a Museum Long-Term Deployment'. In: *2019 28th IEEE International Conference on Robot and Human Interactive Communication (RO-MAN)*. IEEE. DOI: 10.1109/ro-man46459.2019.8956329. URL: https://doi.org/10.1109/ro-man46459.2019.8956329 (cit. on p. 112).

Duckett, Tom and Ulrich Nehmzow (1999). 'Exploration of unknown environments using a compass, topological map and neural network'. In: *Proceedings 1999 IEEE International Symposium on Computational Intelligence in Robotics and Automation. CIRA'99 (Cat. No. 99EX375)*. IEEE, pp. 312–317 (cit. on p. 19).

Dudek, Gregory, Michael Jenkin, Evangelos Milios and David Wilkes (1978). 'Robotic exploration as graph construction'. In: *J. Comput., vol* 7.3 (cit. on p. 19).

Elnagar, Ashraf (2001). 'Prediction of moving objects in dynamic environments using Kalman Filters'. In: *Proceedings 2001 IEEE International Symposium on Computational Intelligence in Robotics and Automation (Cat. No. 01EX515)*. IEEE, pp. 414–419 (cit. on p. 11).

Ester, Martin, Hans-Peter Kriegel, Jörg Sander, Xiaowei Xu et al. (1996). 'A density-based algorithm for discovering clusters in large spatial databases with noise.' In: *Kdd*. Vol. 96. 34, pp. 226–231 (cit. on p. 69).

Everingham, Mark, Luc Van Gool, Christopher KI Williams, John Winn and Andrew Zisserman (2010). 'The pascal visual object classes (voc) challenge'. In: *International journal of computer vision* 88.2, pp. 303–338 (cit. on p. 34).

Faigl, Jan and Miroslav Kulich (2015). 'On benchmarking of frontier-based multi-robot exploration strategies'. In: *2015 european conference on mobile robots (ECMR)*. IEEE, pp. 1–8 (cit. on p. 116).

Fentanes, Jaime Pulido, Amir Badiee, Tom Duckett, Jonathan Evans, Simon Pearson and Grzegorz Cielniak (2018). 'Kriging-Based Robotic Exploration for Soil Moisture Mapping Using a Cosmic-Ray Sensor'. In: *arXiv preprint arXiv:1811.05384* (cit. on p. 24).

Fentanes, Jaime Pulido, Bruno Lacerda, Tomas Krajnik, Nick Hawes and Marc Hanheide (2015). 'Now or later? predicting and maximising success of navigation actions from long-term experience'. In: *2015 IEEE international conference on robotics and automation (ICRA)*. IEEE, pp. 1112–1117 (cit. on pp. 25, 112).

Fermin-Leon, Leonardo, José Neira and José A Castellanos (2017). 'TIGRE: Topological graph based robotic exploration'. In: *2017 European Conference on Mobile Robots (ECMR)*. IEEE, pp. 1–6 (cit. on p. 20).

Forssén, Per-Erik and David G Lowe (2007). 'Shape descriptors for maximally stable extremal regions'. In: *2007 IEEE 11th International Conference on Computer Vision*. IEEE, pp. 1–8 (cit. on p. 52).

Fox, Charles (2013). 'Where wall-following works: case study of simple heuristics vs. optimal exploratory behaviour'. In: *Conference on Biomimetic and Biohybrid Systems*. Springer, pp. 108–118 (cit. on p. 24).

Fox, Charles, Peter Billington, Dominic Paulo and Clive Cooper (2010). 'Origin Destination Analysis on the London Orbital Automated Number Plate Recognition Network'. In: *European Transport Conference, 2010*. Leeds (cit. on p. 117).

Fox, Dieter, Jonathan Ko, Kurt Konolige, Benson Limketkai, Dirk Schulz and Benjamin Stewart (2006). 'Distributed multirobot exploration and mapping'. In: *Proceedings of the IEEE* 94.7, pp. 1325–1339 (cit. on p. 22).

Fraundorfer, Friedrich, Christopher Engels and David Nistér (2007). 'Topological mapping, localization and navigation using image collections'. In: *2007 IEEE/RSJ International Conference on Intelligent Robots and Systems*. IEEE, pp. 3872–3877 (cit. on p. 20).

*Gazebo Simulator* (2020). URL: `http://gazebosim.org/` (visited on 1st June 2020) (cit. on p. 114).

Ge, Shuzhi Sam and Yun J Cui (2002). 'Dynamic motion planning for mobile robots using potential field method'. In: *Autonomous robots* 13.3, pp. 207–222 (cit. on p. 20).

Geiger, Andreas, Philip Lenz and Raquel Urtasun (2012). 'Are we ready for autonomous driving? the kitti vision benchmark suite'. In: *2012 IEEE Conference on Computer Vision and Pattern Recognition*. IEEE, pp. 3354–3361 (cit. on pp. 29, 116).

Gers, Felix A and E Schmidhuber (2001). 'LSTM recurrent networks learn simple context-free and context-sensitive languages'. In: *IEEE Transactions on Neural Networks* 12.6, pp. 1333–1340 (cit. on p. 73).

Gers, Felix A, Jürgen Schmidhuber and Fred Cummins (1999). 'Learning to forget: Continual prediction with LSTM'. In: (cit. on p. 72).

Gers, Felix A, Nicol N Schraudolph and Jürgen Schmidhuber (2002). 'Learning precise timing with LSTM recurrent networks'. In: *Journal of machine learning research* 3.Aug, pp. 115–143 (cit. on p. 73).

*gmapping* (2020). URL: `http://wiki.ros.org/gmapping` (visited on 1st June 2020) (cit. on p. 36).

Gnanadesikan, Ramanathan and John R Kettenring (1972). 'Robust estimates, residuals, and outlier detection with multiresponse data'. In: *Biometrics*, pp. 81–124 (cit. on p. 68).

Gong, Haifeng, Jack Sim, Maxim Likhachev and Jianbo Shi (2011). 'Multi-hypothesis motion planning for visual object tracking'. In: *2011 International Conference on Computer Vision*. IEEE, pp. 619–626 (cit. on p. 16).

González-Banos, Héctor H and Jean-Claude Latombe (2002). 'Navigation strategies for exploring indoor environments'. In: *The International Journal of Robotics Research* 21.10-11, pp. 829–848 (cit. on p. 24).

Graves, Alex, Navdeep Jaitly and Abdel-rahman Mohamed (2013). 'Hybrid speech recognition with deep bidirectional LSTM'. In: *2013 IEEE workshop on automatic speech recognition and understanding*. IEEE, pp. 273–278 (cit. on p. 76).

Hart, Peter E, Nils J Nilsson and Bertram Raphael (1968). 'A formal basis for the heuristic determination of minimum cost paths'. In: *IEEE transactions on Systems Science and Cybernetics* 4.2, pp. 100–107 (cit. on p. 100).

Hawes, Nick, Christopher Burbridge, Ferdian Jovan, Lars Kunze, Bruno Lacerda, Lenka Mudrova, Jay Young, Jeremy Wyatt, Denise Hebesberger, Tobias Kortner, Rares Ambrus, Nils Bore, John Folkesson, Patric Jensfelt, Lucas Beyer, Alexander Hermans, Bastian Leibe, Aitor Aldoma, Thomas Faulhammer, Michael Zillich, Markus Vincze, Eris Chinellato, Muhannad Al-Omari, Paul Duckworth, Yiannis Gatsoulis, David C. Hogg, Anthony G. Cohn, Christian Dondrup, Jaime Pulido Fentanes, Tomas Krajnik, Joao M. Santos, Tom Duckett and Marc Hanheide (Sept. 2017). 'The STRANDS Project: Long-Term Autonomy in Everyday Environments'. In: *IEEE Robotics & Automation Magazine* 24.3, pp. 146–156. DOI: 10.1109/mra.2016.2636359. URL: https://doi.org/10.1109/mra.2016.2636359 (cit. on pp. 25, 27, 112).

Helbing, Dirk and Peter Molnar (1995). 'Social force model for pedestrian dynamics'. In: *Physical review E* 51.5, p. 4282 (cit. on p. 12).

Hochreiter, Sepp and Jürgen Schmidhuber (1997). 'Long short-term memory'. In: *Neural computation* 9.8, pp. 1735–1780 (cit. on pp. 65, 71, 72, 76).

Holz, D., N. Basilico, F. Amigoni and S. Behnke (2010). 'Evaluating the Efficiency of Frontier-based Exploration Strategies'. In: *ISR 2010 (41st International Symposium on Robotics) and ROBOTIK 2010 (6th German Conference on Robotics)*, pp. 1–8 (cit. on pp. 21, 22).

Hwang, Yong Koo, Narendra Ahuja et al. (1992). 'A potential field approach to path planning.' In: *IEEE Transactions on Robotics and Automation* 8.1, pp. 23–32 (cit. on p. 20).

Hyndman, Rob J and George Athanasopoulos (2018). *Forecasting: principles and practice*. OTexts (cit. on p. 78).

Hyndman, Rob J and Anne B Koehler (2006). 'Another look at measures of forecast accuracy'. In: *International journal of forecasting* 22.4, pp. 679–688 (cit. on p. 78).

Joseph, Joshua, Finale Doshi-Velez, Albert S Huang and Nicholas Roy (2011). 'A Bayesian nonparametric approach to modeling motion patterns'. In: *Autonomous Robots* 31.4, p. 383 (cit. on p. 14).

Jovan, Ferdian, Jeremy Wyatt, Nick Hawes and Tomáš Krajnık (2016). 'A Poisson-spectral model for modelling temporal patterns in human data observed by a robot'. In: *2016 IEEE/RSJ International Conference on Intelligent Robots and Systems (IROS)*. IEEE, pp. 4013–4018 (cit. on p. 17).

Juliá, Miguel, Arturo Gil, Luis Payá and Oscar Reinoso (2008). 'Potential Field based Integrated Exploration for Multi-robot Teams.' In: *ICINCO-RA (2)*, pp. 308–314 (cit. on p. 21).

Jumel, Fabrice, Jacques Saraydaryan and Olivier Simonin (2017). 'Mapping likelihood of encountering humans: application to path planning in crowded environment'. In: *2017 European Conference on Mobile Robots (ECMR)*. IEEE, pp. 1–7 (cit. on p. 2).

Jung, David and Alexander Zelinsky (1996). 'Whisker based mobile robot navigation'. In: *Proceedings of IEEE/RSJ International Conference on Intelligent Robots and Systems. IROS'96*. Vol. 2. IEEE, pp. 497–504 (cit. on p. 19).

Karasev, Vasiliy, Alper Ayvaci, Bernd Heisele and Stefano Soatto (2016). 'Intent-aware long-term prediction of pedestrian motion'. In: *2016 IEEE International Conference on Robotics and Automation (ICRA)*. IEEE, pp. 2543–2549 (cit. on p. 16).

*Keras* (2020). URL: `https://keras.io/api/` (visited on 4th Aug. 2020) (cit. on p. 73).

*Kinect v2* (2020). URL: `https://docs.depthkit.tv/docs/kinect-for-windows-v2` (visited on 4th Aug. 2020) (cit. on p. 31).

Kingma, Diederik P and Jimmy Ba (2014). 'Adam: A method for stochastic optimization'. In: *arXiv preprint arXiv:1412.6980* (cit. on p. 73).

Kolmogorov, Andrey N (1950). 'Foundations of the Theory of Probability, 1933'. In: *English translation: Chelsea, New York* (cit. on p. 42).

Krajník, Tomáš, Jaime Pulido Fentanes, João Santos and Tom Duckett (2017). 'FreMEn: Frequency Map Enhancement for Long-Term Mobile Robot Autonomy in Changing Environments'. In: *IEEE Transactions on Robotics* (cit. on pp. 2, 17, 18, 39, 66, 101).

Krajnik, Tomas, Miroslav Kulich, Lenka Mudrova, Rares Ambrus and Tom Duckett (2015). 'Where's Waldo at time t? using spatio-temporal models for mobile robot search'. In: *2015 IEEE International Conference on Robotics and Automation (ICRA)*. IEEE, pp. 2140–2146 (cit. on p. 25).

Krajnik, Tomas, Tomas Vintr, Sergi Molina, Jaime P Fentanes, Grzegorz Cielniak and Tom Duckett (2018). 'Warped Hypertime Representations for Long-term Autonomy of Mobile Robots'. In: *arXiv preprint arXiv:1810.04285* (cit. on p. 17).

Krajnik, Tomas, Tomas Vintr, Sergi Molina, Jaime Pulido Fentanes, Grzegorz Cielniak, Oscar Martinez Mozos, George Broughton and Tom Duckett (2019). 'Warped hypertime representations for long-term autonomy of mobile robots'. In: *IEEE Robotics and Automation Letters* 4.4, pp. 3310–3317 (cit. on pp. 7, 64, 65, 76).

Kruse, Eckhard and Friedrich M Wahl (1998). 'Camera-based observation of obstacle motions to derive statistical data for mobile robot motion planning'. In: *Proceedings. 1998 IEEE International Conference on Robotics and Automation (Cat. No. 98CH36146)*. Vol. 1. IEEE, pp. 662–667 (cit. on p. 13).

Kucner, Tomasz Piotr (2018). 'Probabilistic Mapping of Spatial Motion Patterns for Mobile Robots'. PhD thesis. Orebro University (cit. on p. 1).

Kucner, Tomasz Piotr, Martin Magnusson, Erik Schaffernicht, Victor Hernandez Bennetts and Achim J Lilienthal (2017). 'Enabling flow awareness for mobile robots in partially observable environments'. In: *IEEE Robotics and Automation Letters* 2.2, pp. 1093–1100 (cit. on pp. 2, 14, 18, 64, 70, 76).

Kucner, Tomasz Piotr, Jari Saarinen, Martin Magnusson and Achim J Lilienthal (2013). 'Conditional transition maps: Learning motion patterns in dynamic environments'. In: *2013 IEEE/RSJ International Conference on Intelligent Robots and Systems*. IEEE, pp. 1196–1201 (cit. on p. 13).

Kumar, Neerendra, Zoltán Vámossy and Zsolt Miklós Szabó-Resch (2016). 'Robot obstacle avoidance using bumper event'. In: *2016 IEEE 11th International Symposium on Applied Computational Intelligence and Informatics (SACI)*. IEEE, pp. 485–490 (cit. on p. 19).

Kunze, Lars, Nick Hawes, Tom Duckett, Marc Hanheide and Tomáš Krajnık (2018). 'Artificial intelligence for long-term robot autonomy: A survey'. In: *IEEE Robotics and Automation Letters* 3.4, pp. 4023–4030 (cit. on pp. 1, 25).

Landa, Yanina, David Galkowski, Yuan R Huang, Abhijeet Joshi, Christine Lee, Kevin K Leung, Gitendra Malla, Jennifer Treanor, Vlad Voroninski, Andrea L Bertozzi et al. (2007). 'Robotic path planning and visibility with limited sensor data'. In: *2007 American Control Conference*. IEEE, pp. 5425–5430 (cit. on p. 22).

Lauri, Mikko and Risto Ritala (2016). 'Planning for robotic exploration based on forward simulation'. In: *Robotics and Autonomous Systems* 83, pp. 15–31 (cit. on p. 24).

LaValle, Steven M (2006). *Planning algorithms*. Cambridge University Press (cit. on p. 22).

*LCAS - Software and Datasets* (2020). URL: `https://lcas.lincoln.ac.uk/wp/research/data-sets-software/` (visited on 1st June 2020) (cit. on pp. 34, 110, 111).

Lerner, Alon, Yiorgos Chrysanthou and Dani Lischinski (2007). 'Crowds by example'. In: *Computer graphics forum*. Vol. 26. 3. Wiley Online Library, pp. 655–664 (cit. on p. 29).

Limosani, Raffaele, L Yoichi Morales, Jani Even, Florent Ferreri, Atsushi Watanabe, Filippo Cavallo, Paolo Dario and Norihiro Hagita (2015). 'Long-term human affordance maps'. In: *2015 IEEE/RSJ International Conference on Intelligent Robots and Systems (IROS)*. IEEE, pp. 5748–5754 (cit. on p. 9).

Ling, Haibin and David W Jacobs (2007). 'Shape classification using the inner-distance'. In: *IEEE transactions on pattern analysis and machine intelligence* 29.2, pp. 286–299 (cit. on p. 52).

Lloyd, Stuart (1982). 'Least squares quantization in PCM'. In: *IEEE transactions on information theory* 28.2, pp. 129–137 (cit. on p. 99).

Luber, Matthias, Luciano Spinello, Jens Silva and Kai O Arras (2012). 'Socially-aware robot navigation: A learning approach'. In: *2012 IEEE/RSJ International Conference on Intelligent Robots and Systems*. IEEE, pp. 902–907 (cit. on p. 15).

Luber, Matthias, Johannes A Stork, Gian Diego Tipaldi and Kai O Arras (2010). 'People tracking with human motion predictions from social forces'. In: *2010 IEEE International Conference on Robotics and Automation*. IEEE, pp. 464–469 (cit. on p. 12).

Machado dos Santos, Joao Pedro et al. (2017). 'Lifelong information-driven exploration for mobile robots to complete and Refine spatio-temporal maps in changing environments'. PhD thesis. University of Lincoln (cit. on pp. 18, 24).

Majecka, Barbara (2009). 'Statistical models of pedestrian behaviour in the forum'. In: *Master's thesis, School of Informatics, University of Edinburgh* (cit. on pp. 29, 71).

Manning, James (Oct. 2018). *www.timeout.com*. `https://www.timeout.com/london/news/dont-forget-the-clocks-go-back-this-weekend-102518` (cit. on p. 2).

Marchant, R. and F. Ramos (2012). 'Bayesian optimisation for Intelligent Environmental Monitoring'. In: *2012 IEEE/RSJ International Conference on Intelligent Robots and Systems*, pp. 2242–2249. DOI: 10.1109/IROS.2012.6385653 (cit. on pp. 25, 92).

Martin, Roberto, Hamid Rezatofighi, Abhijeet Shenoi, Mihir Patel, JunYoung Gwak, Nathan Dass, Alan Federman, Patrick Goebel and Silvio Savarese (2019). 'JRDB: A Dataset and Benchmark for Visual Perception for Navigation in Human Environments'. In: *arXiv preprint arXiv:1910.11792* (cit. on p. 29).

Martin, Steven and Peter Corke (2014). 'Long-term exploration & tours for energy constrained robots with online proprioceptive traversability estimation'. In:

*2014 IEEE International Conference on Robotics and Automation (ICRA)*. IEEE, pp. 5778–5785 (cit. on p. 25).

Mei, Yongguo, Yung-Hsiang Lu, CS George Lee and Y Charlie Hu (2006). 'Energy-efficient mobile robot exploration'. In: *Proceedings 2006 IEEE International Conference on Robotics and Automation, 2006. ICRA 2006.* IEEE, pp. 505–511 (cit. on p. 22).

Miller, George A and William G Madow (1963). 'On the maximum likelihood estimate of the Shannon-Wiener measure of information'. In: *Readings in mathematical psychology* 1, pp. 448–469 (cit. on p. 91).

Mises, Richard von (1981). 'Uber die" Ganzzahligkeit" der Atomgewicht und verwandte Fragen'. In: *Physikal. Z.* 19, pp. 490–500 (cit. on p. 69).

Molina, Sergi, G. Cielniak, T. Krajnik and T. Duckett (2017). 'Modelling and Predicting Rhythmic Flow Patterns in Dynamics Environments'. In: *Robotics and Autonomous Systems: Robots Working for and Among Us.* (Cit. on p. 5).

Molina, Sergi, Grzegorz Cielniak and Tom Duckett (2019). 'Go with the Flow: Exploration and Mapping of Pedestrian Flow Patterns from Partial Observation'. In: *IEEE International Conference on Robotics and Automation (ICRA)* (cit. on pp. 6, 87).

Molina, Sergi, G.Cielniak and T. Duckett (2018). 'Modelling and Predicting Rhythmic Flow Patterns in Dynamic Environments'. In: *Towards Autonomous Robotic Systems (TAROS)*. Vol. 10965, pp. 135–146 (cit. on pp. 3, 76).

Morris, Aaron, David Silver, David Ferguson and Scott Thayer (2005). 'Towards topological exploration of abandoned mines'. In: *Proceedings of the 2005 IEEE International Conference on Robotics and Automation*. IEEE, pp. 2117–2123 (cit. on p. 19).

Muench, Christian and Dariu M Gavrila (2019). 'Composable Q-Functions for Pedestrian Car Interactions'. In: *2019 IEEE Intelligent Vehicles Symposium (IV)*. IEEE, pp. 905–912 (cit. on p. 16).

Neubert, Peer, Niko Sunderhauf and Peter Protzel (2015). 'Superpixel-based appearance change prediction for long-term navigation across seasons'. In: *Robotics and Autonomous Systems* 69, pp. 15–27 (cit. on p. 25).

O'Callaghan, Simon T and Fabio T Ramos (2012). 'Gaussian process occupancy maps'. In: *The International Journal of Robotics Research* 31.1, pp. 42–62 (cit. on p. 77).

Oh, Sangmin, Anthony Hoogs, Amitha Perera, Naresh Cuntoor, Chia-Chih Chen, Jong Taek Lee, Saurajit Mukherjee, JK Aggarwal, Hyungtae Lee, Larry Davis et al. (2011). 'A large-scale benchmark dataset for event recognition in surveillance video'. In: *CVPR 2011*. IEEE, pp. 3153–3160 (cit. on p. 29).

Oliveira, Mariana, Luıs Torgo and Vıtor Santos Costa (2018). 'Evaluation procedures for forecasting with spatio-temporal data'. In: *Joint European Conference on Machine Learning and Knowledge Discovery in Databases*. Springer, pp. 703–718 (cit. on p. 77).

Ordóñez, Francisco Javier and Daniel Roggen (2016). 'Deep convolutional and LSTM recurrent neural networks for multimodal wearable activity recognition'. In: *Sensors* 16.1, p. 115 (cit. on p. 76).

Palmieri, Luigi, Tomasz Piotr Kucner, Martin Magnusson, Achim J Lilienthal and Kai O Arras (2017). 'Kinodynamic motion planning on Gaussian mixture fields'. In: *2017 IEEE International Conference on Robotics and Automation (ICRA)*. IEEE, pp. 6176–6181 (cit. on pp. 2, 82, 111, 112).

Panda, Satchidananda, John B Hogenesch and Steve A Kay (2002). 'Circadian rhythms from flies to human'. In: *Nature* 417.6886, pp. 329–335 (cit. on p. 45).

Paninski, Liam (2003). 'Estimation of entropy and mutual information'. In: *Neural computation* 15.6, pp. 1191–1253 (cit. on p. 91).

*PedSim ROS* (2020). URL: `https://github.com/srl-freiburg/pedsim_ros` (visited on 1st June 2020) (cit. on p. 114).

Pele, Ofir and Michael Werman (2010). 'The quadratic-chi histogram distance family'. In: *European conference on computer vision*. Springer, pp. 749–762 (cit. on p. 52).

Pellegrini, S., A. Ess, K. Schindler and L. Van Gool (2009). 'You'll never walk alone: Modeling social behavior for multi-target tracking'. In: *2009 IEEE 12th International Conference on Computer Vision*. IEEE, pp. 261–268 (cit. on pp. 12, 29).

Renzaglia, Alessandro and Agostino Martinelli (2010). 'Potential field based approach for coordinate exploration with a multi-robot team'. In: *2010 IEEE Safety Security and Rescue Robotics*. IEEE, pp. 1–6 (cit. on p. 21).

Robicquet, Alexandre, Amir Sadeghian, Alexandre Alahi and Silvio Savarese (2016). 'Learning social etiquette: Human trajectory understanding in crowded scenes'. In: *European conference on computer vision*. Springer, pp. 549–565 (cit. on p. 29).

Roth, Peter M., Sabine Sternig, Helmut Grabner and Horst Bischof (2009). 'Classifier Grids for Robust Adaptive Object Detection'. In: *Proc. IEEE Conference on Computer Vision and Pattern Recognition (CVPR)* (cit. on p. 29).

Roy, Anandarup, Swapan K Parui and Utpal Roy (2016). 'SWGMM: a semi-wrapped Gaussian mixture model for clustering of circular–linear data'. In: *Pattern Analysis and Applications* 19.3, pp. 631–645 (cit. on p. 70).

Rudenko, Andrey, Luigi Palmieri and Kai O. Arras (2018). 'Joint Long-Term Prediction of Human Motion Using a Planning-Based Social Force Approach'. In: *IEEE International Conference on Robotics and Automation (ICRA)* (cit. on p. 16).

Rudenko, Andrey, Luigi Palmieri, Michael Herman, Kris M Kitani, Dariu M Gavrila and Kai O Arras (2019). 'Human motion trajectory prediction: A survey'. In: *arXiv preprint arXiv:1905.06113* (cit. on pp. 10, 26).

Saarinen, Jari, Henrik Andreasson and Achim J Lilienthal (2012). 'Independent Markov chain occupancy grid maps for representation of dynamic environment'. In: *IEEE Intelligent Robots and Systems*. IEEE, pp. 3489–3495 (cit. on p. 10).

Santos, João Machado, Tomáš Krajník and Tom Duckett (2017). 'Spatio-temporal exploration strategies for long-term autonomy of mobile robots'. In: *Robotics and Autonomous Systems* 88, pp. 116–126. ISSN: 0921-8890. DOI: https://doi.org/10.1016/j.robot.2016.11.016. URL: http://www.sciencedirect.com/science/article/pii/S092188901630690X (cit. on pp. 26, 44, 92).

Schneider, Nicolas and Dariu M Gavrila (2013). 'Pedestrian path prediction with recursive bayesian filters: A comparative study'. In: *German Conference on Pattern Recognition*. Springer, pp. 174–183 (cit. on p. 29).

Schürmann, Thomas (2004). 'Bias analysis in entropy estimation'. In: *Journal of Physics A: Mathematical and General* 37.27, p. L295 (cit. on p. 91).

Senanayake, Ransalu and Fabio Ramos (2018). 'Directional grid maps: modeling multimodal angular uncertainty in dynamic environments'. In: *IEEE/RSJ Int. Conference on Intelligent Robots and Systems (IROS)* (cit. on pp. 2, 14, 64, 69, 70, 76).

Shade, Robbie (2011). 'Choosing where to go: mobile robot exploration'. PhD thesis. Oxford University (cit. on pp. 18, 20).

Shafer, Glenn (1976). *A mathematical theory of evidence*. Vol. 42. Princeton university press (cit. on p. 92).

Shannon, Claude Elwood (1948). 'A mathematical theory of communication'. In: *Bell system technical journal* 27.3, pp. 379–423 (cit. on pp. 89, 90).

Silva Jr, Edson Prestes e, Paulo M Engel, Marcelo Trevisan and Marco AP Idiart (2002). 'Exploration method using harmonic functions'. In: *Robotics and Autonomous Systems* 40.1, pp. 25–42 (cit. on p. 20).

Sim, Robert and Gregory Dudek (2003). 'Effective exploration strategies for the construction of visual maps'. In: *Proceedings 2003 IEEE/RSJ International Conference on Intelligent Robots and Systems (IROS 2003)(Cat. No. 03Ch37453)*. Vol. 4. IEEE, pp. 3224–3231 (cit. on p. 18).

Simmons, Reid, David Apfelbaum, Wolfram Burgard, Dieter Fox, Mark Moors, Sebastian Thrun and Håkan Younes (2000). 'Coordination for multi-robot exploration and mapping'. In: *Aaai/Iaai*, pp. 852–858 (cit. on p. 22).

Singh, A., F. Ramos, H. D. Whyte and W. J. Kaiser (2010). 'Modeling and decision making in spatio-temporal processes for environmental surveillance'. In:

*2010 IEEE International Conference on Robotics and Automation*, pp. 5490–5497. DOI: 10.1109/ROBOT.2010.5509934 (cit. on p. 25).

Smaldino, Paul E (2013). 'Measures of individual uncertainty for ecological models: Variance and entropy'. In: *Ecological modelling* 254, pp. 50–53 (cit. on p. 89).

Sorokowska, Agnieszka, Piotr Sorokowski, Peter Hilpert, Katarzyna Cantarero, Tomasz Frackowiak, Khodabakhsh Ahmadi, Ahmad M Alghraibeh, Richmond Aryeetey, Anna Bertoni, Karim Bettache et al. (2017). 'Preferred interpersonal distances: a global comparison'. In: *Journal of Cross-Cultural Psychology* 48.4, pp. 577–592 (cit. on p. 113).

Stachniss, Cyrill, O Martinez Mozos and Wolfram Burgard (2006). 'Speeding-up multi-robot exploration by considering semantic place information'. In: *Proceedings 2006 IEEE International Conference on Robotics and Automation, 2006. ICRA 2006.* IEEE, pp. 1692–1697 (cit. on p. 25).

Sujan, Vivek A, Marco A Meggiolaro and Felipe AW Belo (2006). 'Information based indoor environment robotic exploration and modeling using 2-D images and graphs'. In: *Autonomous Robots* 21.1, pp. 15–28 (cit. on p. 23).

Sun, Li, Zhi Yan, Sergi Molina, Marc Hanheide and Tom Duckett (2018). '3DOF Pedestrian Trajectory Prediction Learned from Long-Term Autonomous Mobile Robot Deployment Data'. In: *IEEE International Conference on Robotics and Automation* (cit. on pp. 1, 14, 15).

Sutton, Richard S and Andrew G Barto (2018). *Reinforcement learning: An introduction*. MIT press (cit. on p. 98).

Swaminathan, Chittaranjan Srinivas, Tomasz Piotr Kucner, Martin Magnusson, Luigi Palmieri and Achim J Lilienthal (2018). 'Down The CLiFF: Flow-aware Trajectory Planning under Motion Pattern Uncertainty'. In: *2018 IEEE/RSJ International Conference on Intelligent Robots and Systems (IROS)*. IEEE, pp. 7403–7409 (cit. on p. 111).

Tao, Tong, Yalou Huang, Fengchi Sun and Tingting Wang (2007). 'Motion planning for SLAM based on frontier exploration'. In: *2007 International Conference on Mechatronics and Automation*. IEEE, pp. 2120–2125 (cit. on p. 22).

Tay, Meng Keat Christopher and Christian Laugier (2008). 'Modelling smooth paths using Gaussian processes'. In: *Field and Service Robotics*. Springer, pp. 381–390 (cit. on p. 15).

Taylor, Sean J and Benjamin Letham (2018). 'Forecasting at scale'. In: *The American Statistician* 72.1, pp. 37–45 (cit. on p. 80).

*TensorFlow* (2020). URL: https://www.tensorflow.org/ (visited on 4th Aug. 2020) (cit. on p. 73).

Thompson, Simon, Takehiro Horiuchi and Satoshi Kagami (2009). 'A probabilistic model of human motion and navigation intent for mobile robot path planning'. In: *2009 4th International Conference on Autonomous Robots and Agents*. IEEE, pp. 663–668 (cit. on p. 13).

*TIAGo Robot* (2020). URL: http://pal-robotics.com/robots/tiago/ (visited on 1st June 2020) (cit. on p. 37).

Tipaldi, Gian Diego and Kai O Arras (2011). 'I want my coffee hot! Learning to find people under spatio-temporal constraints'. In: *2011 IEEE International Conference on Robotics and Automation*. IEEE, pp. 1217–1222 (cit. on pp. 10, 63).

Tipaldi, Gian Diego, Daniel Meyer-Delius and Wolfram Burgard (2013). 'Lifelong localization in changing environments'. In: *IJRR*. DOI: 10.1177/0278364913502830. eprint: http://ijr.sagepub.com/content/early/2013/10/21/0278364913502830.full.pdf+html (cit. on pp. 17, 25).

Tovar, Benjamın, Luis Guilamo and Steven M LaValle (2004). 'Gap navigation trees: Minimal representation for visibility-based tasks'. In: *Algorithmic Foundations of Robotics VI*. Springer, pp. 425–440 (cit. on pp. 22, 23).

Triebel, Rudolph, Kai Arras, Rachid Alami, Lucas Beyer, Stefan Breuers, Raja Chatila, Mohamed Chetouani, Daniel Cremers, Vanessa Evers, Michelangelo Fiore et al. (2016a). 'Spencer: A socially aware service robot for passenger guidance and help in busy airports'. In: *Field and service robotics*. Springer, pp. 607–622 (cit. on p. 114).

Triebel, Rudolph, Kai Arras, Rachid Alami, Lucas Beyer, Stefan Breuers, Raja Chatila, Mohamed Chetouani, Daniel Cremers, Vanessa Evers, Michelangelo Fiore, Hayley Hung, Omar A. Islas Ramırez, Michiel Joosse, Harmish Khambhaita, Tomasz Kucner, Bastian Leibe, Achim J. Lilienthal, Timm Linder, Manja Lohse, Martin Magnusson, Billy Okal, Luigi Palmieri, Umer Rafi, Marieke van Rooij and Lu Zhang (2016b). 'SPENCER: A Socially Aware Service Robot for Passenger Guidance and Help in Busy Airports'. In: *Springer Tracts in Advanced Robotics*. Springer International Publishing, pp. 607–622. DOI: 10.1007/978-3-319-27702-8_40. URL: https://doi.org/10.1007/978-3-319-27702-8_40 (cit. on p. 112).

Vallvé, J. and J. Andrade-Cetto (2014). 'Dense entropy decrease estimation for mobile robot exploration'. In: *2014 IEEE International Conference on Robotics and Automation (ICRA)*, pp. 6083–6089. DOI: 10.1109/ICRA.2014.6907755 (cit. on p. 20).

Varma, Manik and Andrew Zisserman (2008). 'A statistical approach to material classification using image patch exemplars'. In: *IEEE transactions on pattern analysis and machine intelligence* 31.11, pp. 2032–2047 (cit. on p. 52).

Vasishta, Pavan, Dominique Vaufreydaz and Anne Spalanzani (2017). 'Natural vision based method for predicting pedestrian behaviour in urban environments'. In:

*2017 IEEE 20th International Conference on Intelligent Transportation Systems (ITSC)*. IEEE, pp. 1–6 (cit. on p. 16).

Vintr, Tomas, Kerem Eyisoy and Tomas Krajnik (2018). 'A Practical Representation of Time for the Human Behaviour Modelling'. In: *Forum Statisticum Slovacum* 14, pp. 61–75. ISSN: 1336-7420 (cit. on p. 76).

Vintr, Tomas, Sergi Molina, Ransalu Senanayake, George Broughton, Zhi Yan, Jiří Ulrich, Tomasz Piotr Kucner, Chittaranjan Srinivas Swaminathan, Filip Majer, Mária Stachová, Achim J. Lilienthal and Tomáš Krajník (2019). 'Time-varying Pedestrian Flow Models for Service Robots'. In: *European Conference on Mobile Robotics*. Accepted (cit. on p. 7).

Vintr, Tomas, Zhi Yan, Kerem Eyisoy, Filip Kubis, Jan Blaha, Jiri Ulrich, Chittaranjan Swaminathan, Sergi Molina, Tomasz Piotr Kucner, Martin Magnusson, Gregorz Cielniak, Jan Faigl, Tom Duckett, Achim Lilienthal and Tomas Krajnik (2020). 'Natural Criteria for Comparison of Pedestrian Flow Forecasting Models'. In: *International Conference on Intelligent Robots and Systems*. IEEE (cit. on pp. 81, 84).

*VLP-16* (2020). URL: `https://velodynelidar.com/products/puck/` (visited on 4th Aug. 2020) (cit. on p. 31).

Wada, Tetsuya, Zhidong Wang, Yuji Ogawa, Yasuhisa Hirata and Kazuhiro Kosuge (2012). 'Incremental human motion map system and human walking behavior representation in indoor environment'. In: *2012 IEEE International Conference on Robotics and Biomimetics (ROBIO)*. IEEE, pp. 747–752 (cit. on p. 18).

Wang, Yunfeng and Gregory S Chirikjian (2000). 'A new potential field method for robot path planning'. In: *Proceedings 2000 ICRA. Millennium Conference. IEEE International Conference on Robotics and Automation. Symposia Proceedings (Cat. No. 00CH37065)*. Vol. 2. IEEE, pp. 977–982 (cit. on p. 20).

Wang, Zhan, Patric Jensfelt and John Folkesson (2015). 'Multi-scale conditional transition map: Modeling spatial-temporal dynamics of human movements with local and long-term correlations'. In: *2015 IEEE/RSJ International Conference on Intelligent Robots and Systems (IROS)*. IEEE, pp. 6244–6251 (cit. on p. 13).

Wettach, Jens and Karsten Berns (2010). 'Dynamic frontier based exploration with a mobile indoor robot'. In: *ISR 2010 (41st International Symposium on Robotics) and ROBOTIK 2010 (6th German Conference on Robotics)*. VDE, pp. 1–8 (cit. on p. 22).

Wirth, Stephan and Johannes Pellenz (2007). 'Exploration transform: A stable exploring algorithm for robots in rescue environments'. In: *2007 IEEE International Workshop on Safety, Security and Rescue Robotics*. IEEE, pp. 1–5 (cit. on p. 22).

Wurm, Kai M, Cyrill Stachniss and Wolfram Burgard (2008). 'Coordinated multi-robot exploration using a segmentation of the environment'. In: *2008 IEEE/RSJ*

*International Conference on Intelligent Robots and Systems*. IEEE, pp. 1160–1165 (cit. on p. 22).

Xiao, Shuang, Zhan Wang and John Folkesson (2015). 'Unsupervised robot learning to predict person motion'. In: *2015 IEEE International Conference on Robotics and Automation (ICRA)*. IEEE, pp. 691–696 (cit. on p. 15).

Xie, Dan, Sinisa Todorovic and Song-Chun Zhu (2013). 'Inferring "dark matter" and "dark energy" from videos'. In: *Proceedings of the IEEE International Conference on Computer Vision*, pp. 2224–2231 (cit. on p. 15).

*Xtion* (2020). URL: `https://www.asus.com/3D-Sensor/Xtion/` (visited on 4th Aug. 2020) (cit. on p. 31).

Xu, Dong, Tat Jen Cham, Shuicheng Yan, Lixin Duan and Shih-Fu Chang (2010). 'Near duplicate identification with spatially aligned pyramid matching'. In: *IEEE Transactions on Circuits and Systems for Video Technology* 20.8, pp. 1068–1079 (cit. on p. 52).

Yamaguchi, Kota, Alexander C Berg, Luis E Ortiz and Tamara L Berg (2011). 'Who are you with and where are you going?' In: *CVPR 2011*. IEEE, pp. 1345–1352 (cit. on p. 12).

Yamauchi, Brian (1998). 'Frontier-based exploration using multiple robots'. In: *Proceedings of the second international conference on Autonomous agents*, pp. 47–53 (cit. on pp. 21, 22).

Yan, Xu, Ioannis A Kakadiaris and Shishir K Shah (2014). 'Modeling local behavior for predicting social interactions towards human tracking'. In: *Pattern recognition* 47.4, pp. 1626–1641 (cit. on p. 12).

Yan, Zhi, Tom Duckett and Nicola Bellotto (2017). 'Online learning for human classification in 3d lidar-based tracking'. In: *2017 IEEE/RSJ International Conference on Intelligent Robots and Systems (IROS)*. IEEE, pp. 864–871 (cit. on pp. 29, 32, 34, 35).

Zapf, Marc Patrick, Motoaki Kawanabe and Luis Yoichi Morales Saiki (2019). 'Pedestrian Density Prediction for Efficient Mobile Robot Exploration'. In: *2019 IEEE/RSJ International Conference on Intelligent Robots and Systems (IROS)*. IEEE, pp. 4615–4622 (cit. on p. 10).

Zhang, Jianguo, Marcin Marszałek, Svetlana Lazebnik and Cordelia Schmid (2007). 'Local features and kernels for classification of texture and object categories: A comprehensive study'. In: *International journal of computer vision* 73.2, pp. 213–238 (cit. on p. 52).

Zhao, Zheng, Weihai Chen, Xingming Wu, Peter CY Chen and Jingmeng Liu (2017). 'LSTM network: a deep learning approach for short-term traffic forecast'. In: *IET Intelligent Transport Systems* 11.2, pp. 68–75 (cit. on p. 76).

Zhou, Bolei, Xiaogang Wang and Xiaoou Tang (2012). 'Understanding collective crowd behaviors: Learning a mixture model of dynamic pedestrian-agents'. In: *2012 IEEE Conference on Computer Vision and Pattern Recognition*. IEEE, pp. 2871–2878 (cit. on p. 29).

Zreda, M., W. J. Shuttleworth, X. Zeng, C. Zweck, D. Desilets, T. Franz and R. Rosolem (2012). 'COSMOS: the COsmic-ray Soil Moisture Observing System'. In: *Hydrology and Earth System Sciences* 16.11, pp. 4079–4099. DOI: 10.5194/hess-16-4079-2012. URL: https://www.hydrol-earth-syst-sci.net/16/4079/2012/ (cit. on p. 24).